Kinetic and structural characterization of the self-labeling protein tags HaloTag7, SNAP-tag and CLIP-tag

Jonas Wilhelm[1,9], Stefanie Kühn[1,9], Miroslaw Tarnawski[2], Guillaume Gotthard[3,7], Jana Tünnermann[1], Timo Tänzer[4], Julie Karpenko[4,8], Nicole Mertes[1], Lin Xue[1], Ulrike Uhrig[5], Jochen Reinstein[6], Julien Hiblot[1,4,10]* and Kai Johnsson[1,4,10]*.

[1]Department of Chemical Biology, Max Planck Institute for Medical Research, Heidelberg, Germany.
[2]Protein Expression and Characterization Facility, Max Planck Institute for Medical Research, Heidelberg, Germany.
[3]Structural Biology Group, European Synchrotron Radiation Facility (ESRF), Grenoble, France.
[4]Institute of Chemical Sciences and Engineering, École Polytechnique Fédérale de Lausanne (EPFL), Lausanne, Switzerland.
[5]Chemical Biology Core Facility, European Molecular Biology Laboratory, Heidelberg, Germany.
[6]Department of Biomolecular Mechanisms, Max Planck Institute for Medical Research, Heidelberg, Germany.
[7]Present addresses: Division of Biology and Chemistry–Laboratory for Biomolecular Research, Paul Scherrer Institute, Villigen, Switzerland. Department of Biology, Institute of Molecular Biology and Biophysics, ETH Zürich, Zürich, Switzerland.
[8]Present address: Laboratoire d'Innovation Thérapeutique, UMR7200 CNRS/Université de Strasbourg, Strasbourg Drug Discovery and Development Institute (IMS), Illkirch-Graffenstaden, France.
[9]These authors contributed equally: Jonas Wilhelm, Stefanie Kühn.
[10]These authors contributed equally: Julien Hiblot, Kai Johnsson.
* e-mail: julien.hiblot@mr.mpg.de; johnsson@mr.mpg.de.

Abstract

The self-labeling protein tags (SLPs) HaloTag7, SNAP-tag and CLIP-tag allow the covalent labeling of fusion proteins with synthetic molecules for applications in bioimaging and biotechnology. To guide the selection of an SLP-substrate pair and provide guidelines for the design of substrates, we report a systematic and comparative study on the labeling kinetics and substrate specificities of HaloTag7, SNAP-tag and CLIP-tag. HaloTag7 reaches almost diffusion-limited labeling rates with certain rhodamine substrates, which are more than two orders of magnitude higher than those of SNAP-tag for the corresponding substrates. SNAP-tag labeling rates however are less affected by the structure of the label than those of HaloTag7, which vary over six orders of magnitude for commonly employed substrates. Solving the crystal structures of HaloTag7 and SNAP-tag labeled with fluorescent substrates allowed us to rationalize their substrate preferences. We also demonstrate how these insights can be exploited to design substrates with improved labeling kinetics.

Introduction

Modern high-resolution fluorescence imaging techniques require the specific labeling of proteins with appropriate fluorescent probes. Self-labeling protein tags (SLPs) have been shown to offer a straightforward way to achieve this goal as they undergo a specific and irreversible reaction with synthetic substrates such as fluorophores (1). SLPs are furthermore employed in various other applications such as *in vitro* biophysical studies (2, 3), the generation of semisynthetic biosensors (4-7) and yeast three-hybrid screenings (8). The three most popular SLPs are HaloTag7 (HT7) (9), SNAP-tag (SNAP) (10) and CLIP-tag (CLIP) (11) (**Fig. 1**).

HT7 was engineered from a bacterial dehalogenase (DhaA from *Rhodococcus sp.*), an enzyme able to hydrolyze halogenated alkanes (12). Inactivating the second catalytic step of its enzymatic reaction (mutation H272N in HT7) abolished the hydrolysis of the ester formed with an active site aspartate residue and created an SLP. HT7 reacts specifically with chloroalkane-PEG (CA) molecules resulting in covalent bonding of the alkane chain to the catalytic aspartate and release of a chloride ion (**Fig. 1A**). HT7 was further engineered for increased stability and efficient labeling kinetics toward CA-fluorophore substrates (13).

SNAP was engineered from the human O^6-alkylguanine-DNA alkyltransferase (hAGT), a protein involved in the repair of alkylated DNA by transferring alkyl moieties to its reactive cysteine (14). SNAP was engineered to efficiently react with benzylguanine (BG) derivatives as substrates (**Fig. 1B**) and to reduce its DNA binding properties (10). SNAP irreversibly transfers the benzyl moiety of the substrate to its reactive cysteine, leading to the release of guanine. SNAP also accepts substrates in which the guanine is replaced by a chloropyrimidine (CP) (**Fig. 1B**), reported to possess higher cell permeability (15). Later, CLIP was engineered from SNAP as an orthogonal SLP system, accepting benzylcytosine (BC) derivatives as substrates (11) (**Fig. 1B**).

Even though it has become clear over the last years that the nature of the transferred label can have a significant impact on the reaction kinetics (9, 16, 17), no systematic study has been reported so far that addresses the influence of the transferred label on the SLP labeling kinetics. The structural reasons for the differences in labeling rates are poorly understood. Furthermore, the reaction kinetics of SLPs are usually characterized as a single step-reaction under pseudo-first order reaction conditions, *i.e.* in large excess of one of the reactants (Model 1, **Fig. 1C**). However, the reaction mechanism of SLPs is more complex and should be characterized by a multi-step kinetic model comprising reversible substrate binding (k_1), unbinding (k_{-1}) and irreversible covalent reaction (k_2) (Model 2, **Fig. 1C**). Here, we report an in-depth characterization of the reaction kinetics of HT7, SNAP and CLIP with different substrates, identifying those structural fea-

tures of labels that control labeling rates for the different tags. We complement these kinetic studies by reporting crystal structures of HT7 and SNAP covalently labeled with rhodamine-based fluorophores, providing a detailed understanding of their substrate preferences. Our results will (i) facilitate the use of SLPs in various applications, (ii) aid in the SLP engineering and (iii) help in the design of improved labeling substrates.

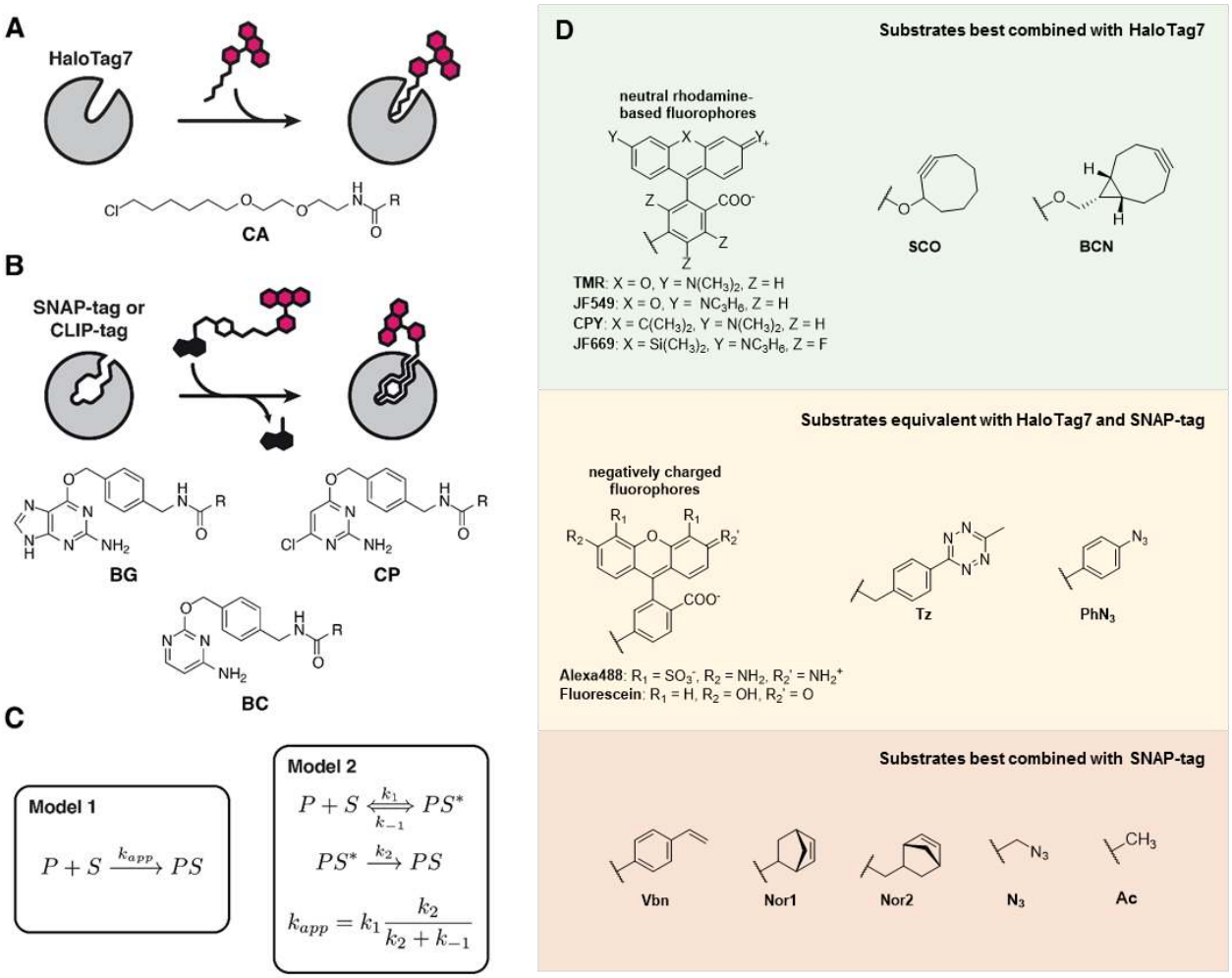

Figure 1: Self-labeling reaction, substrates and kinetic models.

A. Scheme of HT7 labeling reaction with fluorophore substrates. The chemical structure of HT7 substrates (CA) is depicted below. R represents the functional moiety to be linked to HT7. **B.** Scheme of SNAP(f) / CLIP(f) labeling reaction with fluorophore substrates. The chemical structures of SNAP/CLIP substrates (BG/CP/BC) are depicted bellow. R represents the functional moiety to be linked to the SLP. **C**. Models employed to describe the SLP kinetics in this study. **D.** Chemical structure of different SLP substrate substituents. Substrates are organized by their preferential use with HT7 or SNAP.

Results

HaloTag7 kinetic characterization. Fluorophores represent the most popular class of labels employed with SLPs. We characterized HT7 labeling kinetics with different CA-fluorophore substrates, namely CA-TMR, CA-JF549, CA-LIVE580, CA-CPY, CA-JF669 and CA-Alexa488 (**Fig. 1D & S1**) by tracking fluorescence anisotropy change over time at different reactant concentrations. The very high labeling speed of HT7 towards most rhodamine-based CA substrates required a stopped-flow setup to precisely measure the labeling kinetics. Data were fitted to the kinetic model 2 (**Fig. 1C**), which described the reaction kinetics of most rhodamine-based HT7 substrates and allowed to determine the three kinetic parameters (k_1, k_{-1} & k_2) independently (**Fig. 2A-C, S2 & Table S1**). Data fitted to the simplified model 1 resulted in a poorer fit, since curves show a clear biphasic character, indicating that model 2 should be preferred to describe these fast labeling kinetics (**Fig. S3**). It should be noted that fitting the data for the faster reacting substrates to model 1 would lead to a significant overestimation of the labeling speed (**Fig. S4 & Table S2**). The slower labeling reaction with CA-Alexa488 allowed to perform measurements in a microplate reader. However, fitting model 2 to this data does not allow to determine the kinetic parameters (k_1, k_{-1} & k_2) independently. Hence the data was fitted using the kinetic model 1 (**Fig. S5**). The kinetic model 1 yields the apparent second-order rate constant k_{app} which describes the labeling reaction at reactant concentrations far below the K_d at which the substrate binding site is not saturated and the labeling rate depends linearly on the reactant concentrations. To compare the labeling rate constants of substrates analyzed through different kinetic models (**Fig. 2D & Table 1**), k_{app} can also be calculated from the individual rate constants obtained with kinetic model 2 (**Fig. 1C**).

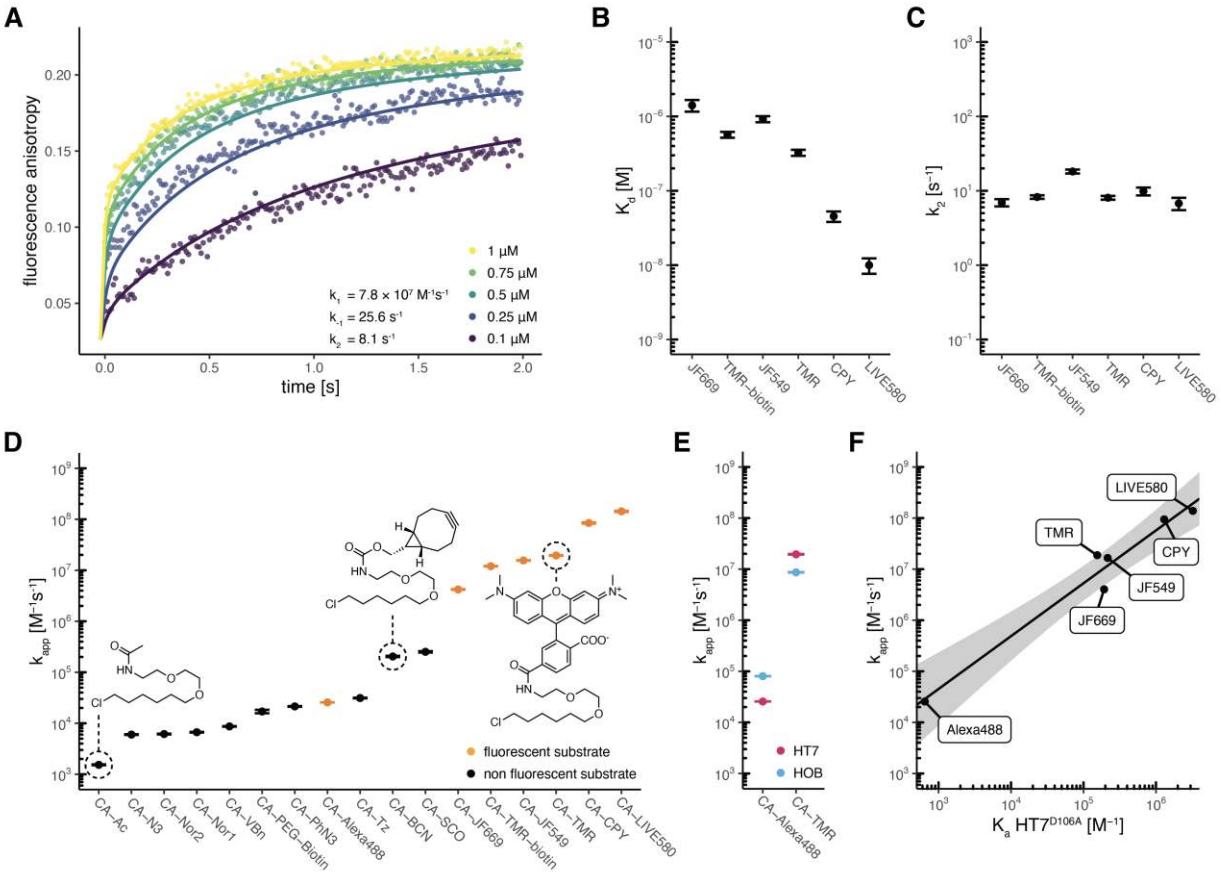

Figure 2: Characterization of HaloTag7 labeling kinetics.

A. Fluorescence anisotropy traces (points) and fitted curves of HT7 labeling with CA-TMR in 1:1 stoichiometry at the indicated concentrations. Kinetics were recorded by following fluorescence anisotropy over time using a stopped flow device. Reactions were started by mixing equal volumes of HT7 and CA-TMR. Data were fitted to the kinetic model 2 (lines). **B**. HT7 affinities (K_d) for different fluorophore substrates calculated from the kinetic parameters (k_{-1}/k_1). **C**. HT7 reactivity (k_2) for different fluorophore substrates obtained from fluorescence anisotropy kinetics. The minimal differences in k_2 illustrate that labeling kinetics are mostly influenced by differences in K_d. **D**. Apparent second order labeling rate constants (k_{app}) of HT7 with different substrates. Rate constants span over six order of magnitude. Non-negatively charged fluorophore substrates reach the fastest labeling kinetics. **E**. Comparison of k_{app} between HT7 and HOB for CA-TMR and CA-Alexa488 labeling highlighting the preference of HOB for the negatively charged substrate CA-Alexa488. **F**. Correlation between HT7 apparent second order rate constant (k_{app}) and affinity ($K_a = 1/K_d$) for different fluorophore substrates. Affinities were obtained with the catalytically inactive variant $HT7^{D106A}$. Log transformed values were fitted to a linear model (black line, $\log(k_{app}) = \log(K_a) \times 1.042 + 1.544$). The grey area represents the 95% confidence bands (the area in which the true regression line lies with 95% confidence).

HaloTag7 reaches fast kinetics with fluorophore substrates. Among the tested fluorophore substrates, CA-LIVE580 turned out to be the fastest substrate for HT7 with a k_{app} of 1.39 ± 0.03 $\times 10^8$ $M^{-1}s^{-1}$, reaching an almost diffusion-limited labeling rate, and a calculated K_d (= k_{-1}/k_1) of 9.99 nM (7.64 to 12.35 nM 95% CI). All other rhodamine-based substrates showed efficient labeling kinetics as well ($10^6 < k_{app} < 10^9$ $M^{-1}s^{-1}$) with the exception of the negatively charged CA-Alexa488 (k_{app} = 2.57 ± 0.01 × 10^4 $M^{-1}s^{-1}$) (**Table 1 & Fig. 2D**). The HT7 variant HOB (halo-based oligonucleotide binder) (18) features several positively charged surface mutations close to the substrate

binding site, which were introduced to increase the labeling rates with chloroalkanes attached to oligonucleotides. We hypothesized that HOB may have increased labeling kinetics with the negatively charged CA-Alexa488. Indeed, HOB shows a 3.13 ± 0.01 fold increase in k_{app} compared to HT7 with CA-Alexa488, while a decrease in k_{app} was observed with CA-TMR (2.09 ± 0.01 fold) (**Fig. 1E, S5 & Table S3**). This suggests that kinetics of negatively charged substrates might suffer from charge repulsions at the HT7 surface.

Table 1: Apparent labeling rate constants (k_{app}) for different HT7, SNAP and CLIP substrates.

k_{app} [$M^{-1}s^{-1}$] (value | s.d.)

		Halo	SNAP		CLIP
		CA	BG	CP	BC
Fluorescent	Alexa488	2.57 (± 0.01) × 10^4	1.22 (± 0.01) × 10^4	3.12 (± 0.01) × 10^3	1.26 (± 0.01) × 10^3
	Fluorescein	-	1.17 (± 0.01) × 10^5	*1.42 (± 0.01) × 10^4	4.36 (± 0.01) × 10^3
	JF669	#4.03 (± 0.02) × 10^6	-	-	-
	TMR-biotin	#1.04 (± 0.01) × 10^7	-	-	-
	JF549	#1.66 (± 0.01) × 10^7	-	-	-
	TMR	#1.88 (± 0.01) × 10^7	4.29 (± 0.01) × 10^5	7.69 (± 0.01) × 10^4	1.85 (± 0.01) × 10^4
	CPY	#9.44 (± 0.18) × 10^7	2.17 (± 0.01) × 10^5	*1.59 (± 0.01) × 10^4	*2.65 (± 0.01) × 10^4
	Live580	#1.39 (± 0.03) × 10^8	-	-	-
Non-fluorescent	Ac	1.53 (± 0.02) × 10^3	1.48 (± 0.05) × 10^4	3.45 (± 0.38) × 10^3	
	-	-	1.87 (± 0.05) × 10^4	4.15 (± 0.62) × 10^3	
	N_3	6.00 (± 0.06) × 10^3	3.70 (± 0.09) × 10^4	6.36 (± 0.41) × 10^3	
	Nor2	6.15 (± 0.07) × 10^3	-	-	
	Nor1	6.68 (± 0.06) × 10^3	7.34 (± 0.01) × 10^4	1.77 (± 0.04) × 10^4	
	Vbn	8.68 (± 0.07) × 10^3	3.84 (± 0.07) × 10^4	5.50 (± 0.45) × 10^3	
	PEG-biotin	1.70 (± 0.08) × 10^4	-	-	
	PhN_3	2.14 (± 0.02) × 10^4	4.78 (± 0.09) × 10^4	2.91 (± 0.40) × 10^3	
	Tz	3.13 (± 0.03) × 10^4	3.94 (± 0.08) × 10^4	-	
	BCN	2.04 (± 0.03) × 10^5	3.88 (± 0.07) × 10^4	3.34 (± 0.31) × 10^3	
	SCO	2.52 (± 0.05) × 10^5	3.75 (± 0.06) × 10^4	4.22 (± 0.61) × 10^3	

Rate constants were obtained by fitting the data to kinetic model 1 or 2 (#). For some SNAP/CLIP substrates, a third kinetic model was used which included a slow aging event of the labeled species (*), see Table S5.

HaloTag7 labeling kinetics correlate with substrate affinity. For the substrates whose labeling kinetics followed model 2, we observed that k_1 and k_2 values were rather constant among the different HT7 fluorophore substrates, while larger differences were observed for the dissociation

rate constant k_{-1} (**Fig. S6 & Table S1**). The substrate preference of HT7 seems therefore mainly driven by the substrate affinity ($K_d^{kinetic} = k_{-1}/k_1$) (**Fig. 2B**). After binding, the deeply buried CA moiety might adapt a similar conformation for all substrates, potentially explaining the minor effects of the substituent on the catalytic step (k_2) (**Fig. 2C**). The trend observed for the K_d values calculated from the kinetic parameters was confirmed by measuring the affinity of the catalytically dead variant $HT7^{D106A}$ for the same CA-fluorophore substrates using fluorescence polarization (**Fig. S6F & S7**). The $K_d^{kinetic}$ correlates with K_d^{D106A} (**Fig. S6E**) and as a consequence the association constant K_a^{D106A} (= $1/K_d$) correlates with k_{app} (**Fig. 2F**). Hence, the K_a^{D106A} can be used to estimate the k_{app} for fluorescent HT7 substrates.

HaloTag7 reacts slower with non-fluorophore substrates. In order to determine k_{app} for non-fluorescent CA substrates, we developed a competitive kinetic assay in which the non-fluorescent CA substrates compete with CA-Alexa488 for protein labeling. Non-fluorescent substrates were significantly slower than zwitterionic rhodamine substrates ($10^3 < k_{app} < 10^6$ $M^{-1}s^{-1}$), highlighting the strong preference of HT7 for the rhodamine core structure. Larger alkynes (*e.g.* SCO, BCN) and aromatic structures (*e.g.* Tz, PhN_3, VBn) were preferred over alkenes (Nor) and small moieties (Ac, N_3) (**Fig. 2D, S8 & Table 1**).

HaloTag7 substrate design. Overall, HT7 can reach labeling kinetics near the diffusion limit but its apparent rate constants span over six orders of magnitude, depending on the nature of the label (**Fig. 2D**). HT7 exhibits a strong preference for rhodamine derivatives, with the exception of negatively charged rhodamines. It is noteworthy that the substrate with the slowest labeling rate carries the smallest label, *i.e.* an acetate group (CA-Ac). The preference for rhodamines can be exploited to increase labeling rates of poor substrates. As an example, the commercially available CA-PEG-biotin substrate presents slow reaction kinetics ($k_{app} = 1.70 \pm 0.08 \times 10^4$ $M^{-1}s^{-1}$, **Table 1 & Fig. S8**), but synthesizing a CA-TMR-biotin ligand led to an over 500 fold increase in labeling kinetics ($k_{app} = 1.04 \pm 0.01 \times 10^7$ $M^{-1}s^{-1}$, **Table 1, S1 & Fig. S2**), greatly facilitating biotinylation of HT7 fusion proteins. This strategy to improve labeling rates of HT7 ligands should be applicable to various other labels.

Structural analysis of rhodamine-bound HaloTag. In order to better understand the substrate preference of HT7 for rhodamine-based CA substrates, we solved the X-ray structure of TMR- (PDB ID 6Y7A) and CPY-bound HT7 (PDB ID 6Y7B) at 1.4 Å and 3.1 Å resolution, respectively (**Fig. 3A, 3C, S9 & Table S4**). Additionally, the TMR-bound structure of HOB was obtained at 1.5

Å resolution (PDB ID 6ZCC) (**Fig. 3H, S9 & Table S4**). These structures present the same α/β hydrolase fold of the superfamily with minimal deviation from already available HT7 X-ray structures (19-22) (**Fig. S9C**). In addition to the conventional α/β hydrolase topology, HT7 features an extra capping domain made of six α-helices (Hlx4 to 9) which partially cover the catalytic site and form an entry channel for the CA substrate. After reaction, the PEG-alkane ligand is buried in the protein, while the xanthene moiety of the dye lays on the distorted α-helix 8 (Hlx8) in a conformation partially constrained by the crystal packing (**Fig. 3A, 3C & S9D**). A recently published HT7-TMR X-ray structure (PDB ID 6U32) shows the fluorophore bound in two alternative conformations (23). In one conformation, the fluorophore lays on Hlx8 similar to what we report here and in the other, it lays on the Hlx7-turn-Hlx8 motif (**Fig. S10**). This second conformation is incompatible with our HT7-TMR structure due to steric clashes caused by the crystal packing. The alkane-fluorophore is positioned by the Hlx6-turn-Hlx7-turn-Hlx8 motif of the HT7 capping domain from which $T172^{Hlx8}$ and, to a lesser extent, $T148^{Hlx6}$ form hydrogen bonds with the oxygen and the nitrogen of the amide bond linking PEG-alkane and fluorophore (**Fig. 3A & 3C**). CA-TMR and CA-CPY have similar conformations in both structures (**Fig. S11A**) with only minor differences in their torsion angles (**Fig. 3E**). In comparison to TMR, one of the additional methyl groups of CPY is forming van-der-Waals interactions at the protein surface, potentially explaining the increased affinity of CA-CPY relative to CA-TMR.

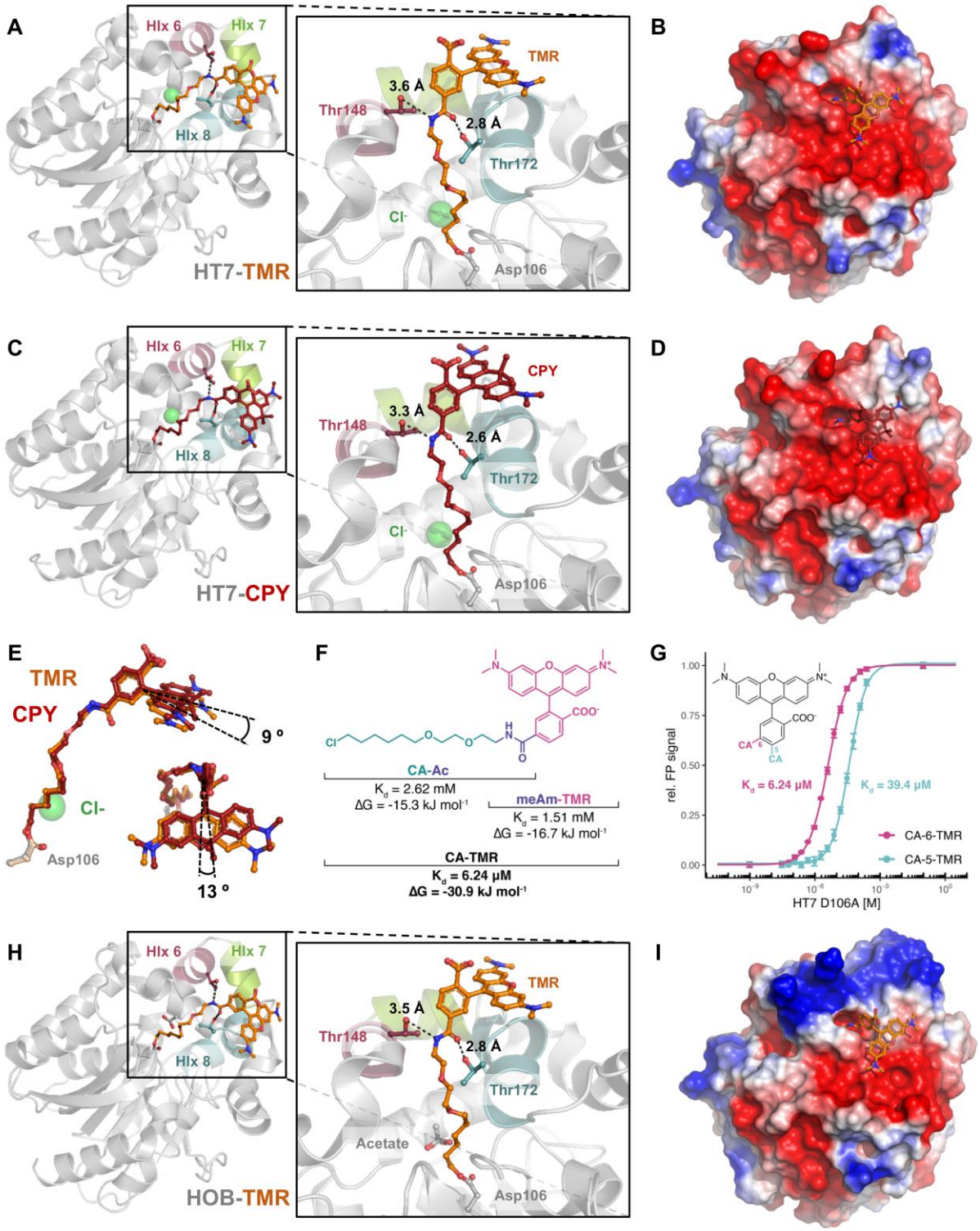

Figure 3: Structure-function analysis of HaloTag7 substrate interactions.

Crystal structures of HT7-TMR (PDB ID 6Y7A, **A**), HT7-CPY (PDB ID 6Y7B, chain A, **C**) and HOB-TMR (PDB ID 6ZCC, **H**). Proteins are represented as grey cartoons, the fluorophore substrates and residues as sticks. Putative hydrogen bonds are represented as black dashed lines with annotated distances. Electrostatic potentials at protein surfaces (**B**, **D** & **I**, respectively) are drawn at -2.0 (red) to 2.0 (blue) kJ/mol/e and were obtained using the APBS software with standard parameters. **E**. Comparison of the TMR and CPY conformation on HT7. **F**. HT7 affinities (K_d) and free binding energies (ΔG) for different TMR substrate substructures. **G**. Comparison of HT7 affinity for CA-6-TMR and CA-5-TMR.

Fluorophore and CA core contribute both to HaloTag7 substrate affinity. To characterize the contributions of rhodamine structures and the CA core to the overall affinity of HT7 substrates, we measured affinities of the catalytically dead variant HT7^{D106A} for the acetylated chloroalkane (CA-Ac) and *N*-methylamide-fluorophores (meAm-TMR/CPY). Although the acetylated chloroalkane should form hydrogen bonds to the protein (via T148/T172) and is well buried in the cavity, we observed a rather low affinity (K_d) of 2.62 mM (2.44 to 2.72 mM CI 95%, **Fig. 3F & S12**), which is consistent with the low apparent labeling rate constant of CA-Ac (**Fig. 2D**). The protein binds the meAm-TMR fluorophore with a slightly higher affinity (K_d = 1.51 mM, 1.40 to 1.64 mM CI 95%) (**Fig. 3F & S12**). The free binding energies for both fragments calculated from the K_d values (CA-Ac: -15.3 kJ.mol^{-1} and meAm-TMR: -16.7 kJ.mol^{-1}) are thus comparable and almost sum up to the calculated free binding energy of the full CA-TMR substrate (30.9 kJ mol^{-1}, K_d = 6.24 µM), *i.e.* no synergistic effect in binding is observed (24). Similar results were obtained for meAm-CPY (**Fig. S12**). The CA-fluorophore binding is thus driven by interactions with both the CA core and the fluorophore, explaining the high impact of fluorophore structure changes on the overall labeling kinetics.

The importance of substrate geometry was interrogated by synthesizing CA-fluorophore substrates linked via the 5 position of the rhodamine benzyl ring instead of the usual 6 position (**Fig. 3G**). According to the observed conformations in the presented crystal structures, these 5-substrates should not be able to interact with Hlx8 after HT7 binding since the xanthene would be turned 60º away from the protein surface. HT7^{D106A} showed reduced affinities towards these substrates compared to the 6-substituted rhodamine substrates (6.31 fold and 22.7 fold decrease for CA-TMR and CA-CPY, respectively) (**Fig. 3G**). This result emphasizes the importance of the interaction between the xanthene ring and the Hlx8.

HaloTag7 surface charge impacts substrate recognition. HOB comprises four surface mutations compared to HT7 close to the substrate entry channel but opposite to the TMR binding site (**Fig. S11B**). These mutations lead to faster labeling rates with negatively charged CA substrates relative to HT7. Only minor differences can be observed between the crystal structures of HOB and HT7 labeled with CA-TMR (**Fig. 3H & S11B**). Since the HOB mutations replace mostly negative by positively charged residues, we analyzed the electrostatic potential of both proteins. While HT7 features an overall negatively charged surface around the substrate entry channel (**Fig. 3B & 3D**), HOB shows a positively charged patch opposite to the fluorophore binding site (**Fig. 3I**). Hence, a putative electrostatic steering effect (25) could explain the altered substrate preference of HOB despite that its positive charges are on the opposite side of the fluorophore binding site.

Kinetic characterization of SNAP-tag. SNAP labeling kinetics were characterized for both BG- and CP-fluorophore substrates (*i.e.* TMR, CPY, Alexa488 and Fluorescein) (**Fig. 1D & S1**), by following fluorescence polarization changes during the labeling reaction at different protein concentrations in a plate reader assay. The kinetic model 2 did not allow to determine the kinetic parameters (k_1, k_{-1} & k_2) independently. Hence, data were fitted to model 1 in order to obtain apparent second order rate constants (k_{app}) of the labeling reactions (**Table 1 & Fig. S13**). SNAP's apparent labeling rate constants are ranging between 10^4 and 10^6 $M^{-1}s^{-1}$ for BG-fluorophore substrates (**Fig. 4A**), among which BG-TMR presents the fastest labeling rate (k_{app} = 4.29 ± 0.01 × 10^5 $M^{-1}s^{-1}$) (**Table 1**). CP substrates show 4 – 14 times slower reaction kinetics than the corresponding BG substrates ($10^3 < k_{app} < 10^5$ $M^{-1}s^{-1}$) (**Fig. 4A**). Some CP substrates (CPY and Fluorescein) exhibit a slow additional phase of fluorescence polarization increase or decrease after labeling that might be due to a slow conformational change of the labeled protein. In order to fit these traces, the kinetic model 1 was extended by adding a step that occurs after labeling. The rate constants of this additional process (k_3) ranged between 10^{-2} and 10^{-3} s^{-1} (**Fig. S13 & Table S5**). SNAP labeling with BG-TMR and CP-TMR was further investigated by measuring stopped flow fluorescence anisotropy kinetics at higher protein concentrations (**Fig. S14 & Table S6**). Fitting the data to the kinetic model 2 allowed to estimate the kinetic parameters k_1, k_{-1} and k_2 independently and to calculate K_d values (**Fig. S14C**). The calculated k_{app} for both substrates were similar to the k_{app} determined via the plate reader assay using model 1 (**Fig. S14C**). CP-TMR presents similar k_1 and k_2 as BG-TMR, while k_{-1} is significantly higher for CP-TMR (8.8 fold), indicating that both substrates feature the same chemical reactivity but differ in their affinity towards SNAP.

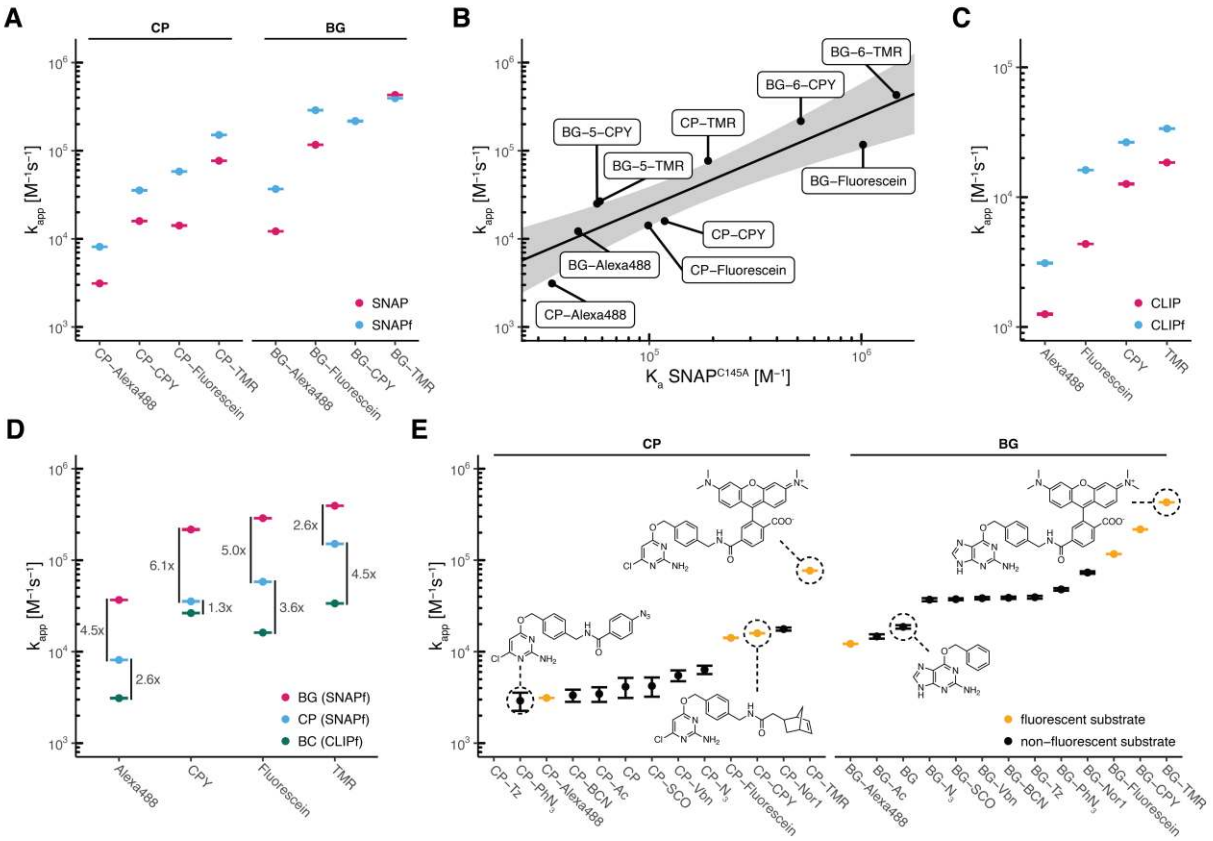

Figure 4: Characterization of SNAP- and CLIP-tag labeling kinetics.

A. Comparison of labeling kinetics (k_{app}) between SNAP and SNAPf. **B**. Correlation between SNAP apparent second order rate constant (k_{app}) and affinity ($K_a = 1/K_d$) for different fluorophore substrates. Affinities were obtained for the catalytically inactive variant $SNAP^{C145A}$. Log transformed values were fitted to a linear model (black line, $\log(k_{app}) = \log(K_a) * 1.0217 - 0.7407$). The grey area represents the 95% confidence bands (the area in which the true regression line lies with 95% confidence). **C**. Comparison of labeling kinetics (k_{app}) between CLIP and CLIPf. **D**. Comparison of labeling kinetics (k_{app}) between SNAPf and CLIPf. **E**. Apparent second order labeling rate constants (k_{app}) of SNAP with different substrates. Kinetics span over three orders of magnitude (two orders of magnitude within each substrate class BG/CP). BG-based, non-negatively charged fluorophore substrates reach the fastest labeling kinetics.

SNAP-tag labeling kinetics correlate with substrate affinity. To confirm the previous finding, affinities for different fluorescent substrates were measured using the catalytically inactive mutant $SNAP^{C145A}$ (**Fig. S15**). A strong preference for BG-TMR over CP-TMR was observed with almost one order of magnitude difference in K_d^{C145A}. $SNAP^{C145A}$ presents a 3 fold lower K_d^{C145A} for BG-TMR (0.68 µM; 0.63 to 0.75 µM CI 95%) than calculated from stopped-flow experiments using active SNAP. $SNAP^{C145A}$ showed similar affinities as for BG-TMR towards various xanthene-based fluorophores such as BG-MaP555, BG-JF549 and BG-fluorescein (**Fig. S15**), indicating that modifications of the rhodamine structure seem not to affect the affinity of the protein as much as observed for HT7 substrates. However, $SNAP^{C145A}$ has very low affinity for sulfonated fluorophore substrates such as BG-Alexa488 (21.6 µM; 20.5 to 22.9 µM CI 95%) or BG-sulfo-Cy3/5 (Cy3, 68.1

µM; 63.8 to 72.7 µM CI 95%) (**Fig. S15**). A good correlation between K_d^{C145A} and k_{app} was observed for the tested fluorophore substrates (**Fig. 4B**), highlighting again the importance of high affinity for a quick labeling reaction. As for HT7, we attempt to decipher SNAP substrate recognition by measuring its affinity towards BG-Ac and meAm-TMR. While no affinity could be measured for meAm-TMR, $SNAP^{C145A}$ presented a relatively high affinity for BG-Ac (88.0 µM; 88.6 to 91.5 µM CI 95%) and CP-Ac (201 µM; 192 to 212 µM CI 95%) compared to HT7 affinity for CA-Ac (**Fig. S16**), which could explain the promiscuity of SNAP.

Kinetic characterization of CLIP-tag and SNAP-tag variants. The mutant SNAPf ($SNAP^{E30R}$) is a SNAP variant with faster labeling rates for BG-Alexa488, BG-TMR, BG-Atto549 and BG-AlexaFluor647 (26) (**Fig. 4A**, **Fig. S17**). Fluorescence polarization kinetics of SNAPf revealed a 2 to 4 fold k_{app} increase compared to SNAP for most BG- and CP-fluorophore substrates (**Fig. 4A, S7, S18 & Table S7**). Nevertheless, no increase in labeling kinetics was observed for the best SNAP substrates BG-TMR and BG-CPY (**Fig. 4A**). CLIP (11) and CLIPf ($CLIP^{E30R}$) (26) are orthogonal variants of SNAP accepting BC instead of BG substrates (**Fig. S17**). Labeling kinetics of CLIP and CLIPf (**Table S7 & Fig. S19**) yielded apparent second order rate constants (k_{app}) ranging from 10^3 to 10^5 $M^{-1}s^{-1}$ with a 2 to 4 fold increase for CLIPf compared to CLIP (**Fig. 4C**). The fastest labeling kinetics were achieved with CLIPf and BC-TMR showing a k_{app} of $3.37 \pm 0.01 \times 10^4$ $M^{-1}s^{-1}$. However, CLIPf is significantly slower than SNAPf (**Fig. 4D**).

Cross-reactivity of SNAP- and CLIP-tag substrates. SNAP and CLIP originate from hAGT (10, 11) (**Fig. S17**), which can potentially react with SNAP and CLIP substrates. We therefore measured the labeling activity of hAGT for the corresponding TMR-based substrates (**Fig. S20**). BG/CP-TMR labeling of hAGT is 130 / 20 times slower than the labeling of SNAP ($k_{app}^{BG\text{-}TMR} = 3.38 \pm 0.01 \times 10^3$ $M^{-1}s^{-1}$; $k_{app}^{CP\text{-}TMR} = 3.13 \pm 0.01 \times 10^3$ $M^{-1}s^{-1}$) (**Table 2**). Interestingly, hAGT shows no preference for BG over CP substrates. BC-TMR reaction with hAGT is 25'000 times slower than with CLIP ($k_{app} = 0.70 \pm 0.01$ $M^{-1}s^{-1}$) (**Table 2**). Our results suggest that CLIP should be preferred over SNAP in cases where cross-reactivity of substrates with endogenous hAGT is a concern.

CLIP development was motivated by the perspective to use both SLPs together for multicolor labeling. However, the cross-reactivities of the fastest reacting SNAP and CLIP rhodamine substrates have not yet been determined. Hence, we measured cross-reactivity of BG/CP-TMR with CLIP and BC-TMR with SNAP (**Table 2**). SNAP reacts more than 1000 times slower with BC-TMR (SNAP $k_{app}^{BC\text{-}TMR} = 3.20 \pm 0.02 \times 10^2$ $M^{-1}s^{-1}$) than with BG-TMR despite the noticeable affinity of

SNAP^{C145A} for BC-Ac (416 µM, 408 to 421 µM CI 95%) which is only 5 times lower than for BG-Ac (**Fig. S16**). On the other hand, CLIP reacts 100 times slower with BG-TMR (CLIP $k_{app}^{BG\text{-}TMR}$ = 8.26 ± 0.05 x 10^1 $M^{-1}s^{-1}$) than with BC-TMR. These data are in agreement with values previously reported for fluorescein substrates (11). Since both proteins show residual reactivity towards their non-respective substrates, simultaneous co-labeling of both proteins or prior SNAP labeling is advisable to minimize cross-reactions.

Table 2: Labeling kinetics (k_{app}) of hAGT, SNAP and CLIP with TMR substrates.

k_{app} [$M^{-1}s^{-1}$] (value | s.d.)

	hAGT		SNAP		CLIP	
BG-TMR	3.38 (± 0.01)	× 10^3	4.29 (± 0.01)	× 10^5	8.26 (± 0.05)	× 10^1
CP-TMR	3.13 (± 0.01)	× 10^3	7.69 (± 0.01)	× 10^4	7.22 (± 0.04)	× 10^0
BC-TMR	6.25 (± 0.01)	× 10^{-1}	3.20 (± 0.02)	× 10^2	1.85 (± 0.01)	× 10^4

SNAP-tag is a promiscuous SLP. Labeling kinetics of non-fluorescent SNAP substrates were characterized by competition kinetics against BG-Alexa488 (**Fig. S21**). Non-fluorescent BG substrates ($10^4 < k_{app} < 10^5$ $M^{-1}s^{-1}$) were preferred over CP substrates ($10^3 < k_{app} < 10^4$ $M^{-1}s^{-1}$) (**Fig. 4E & Table 1**). In general, SNAP kinetics with non-fluorescent substrates were slower than with fluorescent substrates with the exception of the negatively charged Alexa488. However, in comparison to HT7, the labeling rates of SNAP show much less dependence on the nature of the label (**Fig. 4E & Table 1)**.

Structural analysis of TMR-bound SNAP-tag. To better understand the preference of SNAP for TMR substrates, the X-ray structure of SNAP labeled with TMR was solved at 2.3 Å resolution (PDB ID 6Y8P) (**Fig. 5A, S22 & Table S4**). The structure shows the same α/β topology with two domains as observed for hAGT and other SNAP structures (27, 28). The active site is very similar to the benzylated SNAP structure (PDB ID 3L00) (28), despite the presence of an alternative cysteine conformation (**Fig. S22C**). The TMR moiety strongly participates in the crystal packing, engaging in interactions with the neighboring xanthene ring and protein in a sandwich-like topology (**Fig. S22D**). As a consequence, and in contrast to HT7-TMR, SNAP does not interact with the bound fluorophore in the present X-ray structure.

We next evaluated the relative preference for 6- versus 5-carboxy isomers of TMR and CPY substrates by studying their labeling rates (**Fig. S23 & Table S8**) and affinities (**Fig. S15**) for SNAP, SNAPf and their dead variants. SNAP and SNAPf showed 10 times slower reaction rates with 5-

fluorophores ($k_{app} \approx 10^4 – 10^5$ $M^{-1}s^{-1}$) compared to the corresponding 6-fluorophores ($k_{app} \geq 10^5$ $M^{-1}s^{-1}$). These differences were even more pronounced for the affinities, which were up to 25 fold higher for the 6-carboxy isomers.

In the crystal structure of TMR-labeled SNAP, a structural ethylene glycol forms hydrogen bonds with both the backbone carbonyl oxygen of I31 and the carbonyl oxygen of the amide linking the benzyl to the fluorophore (**Fig. 5A**). This benzyl-fluorophore amide is also forming a hydrogen bond to the backbone carbonyl oxygen of the catalytically important E159 residue via its Nα atom. Comparison with the BG-bound $SNAP^{C145A}$ structure (PDB ID 3KZZ, **Fig. 5B**) suggests that, after catalytic reaction, the E159 side chain flips inside the BG binding cavity, resulting in a reorientation of its backbone carbonyl oxygen that can then interact with the amide of the substrate (**Fig. 5B**).

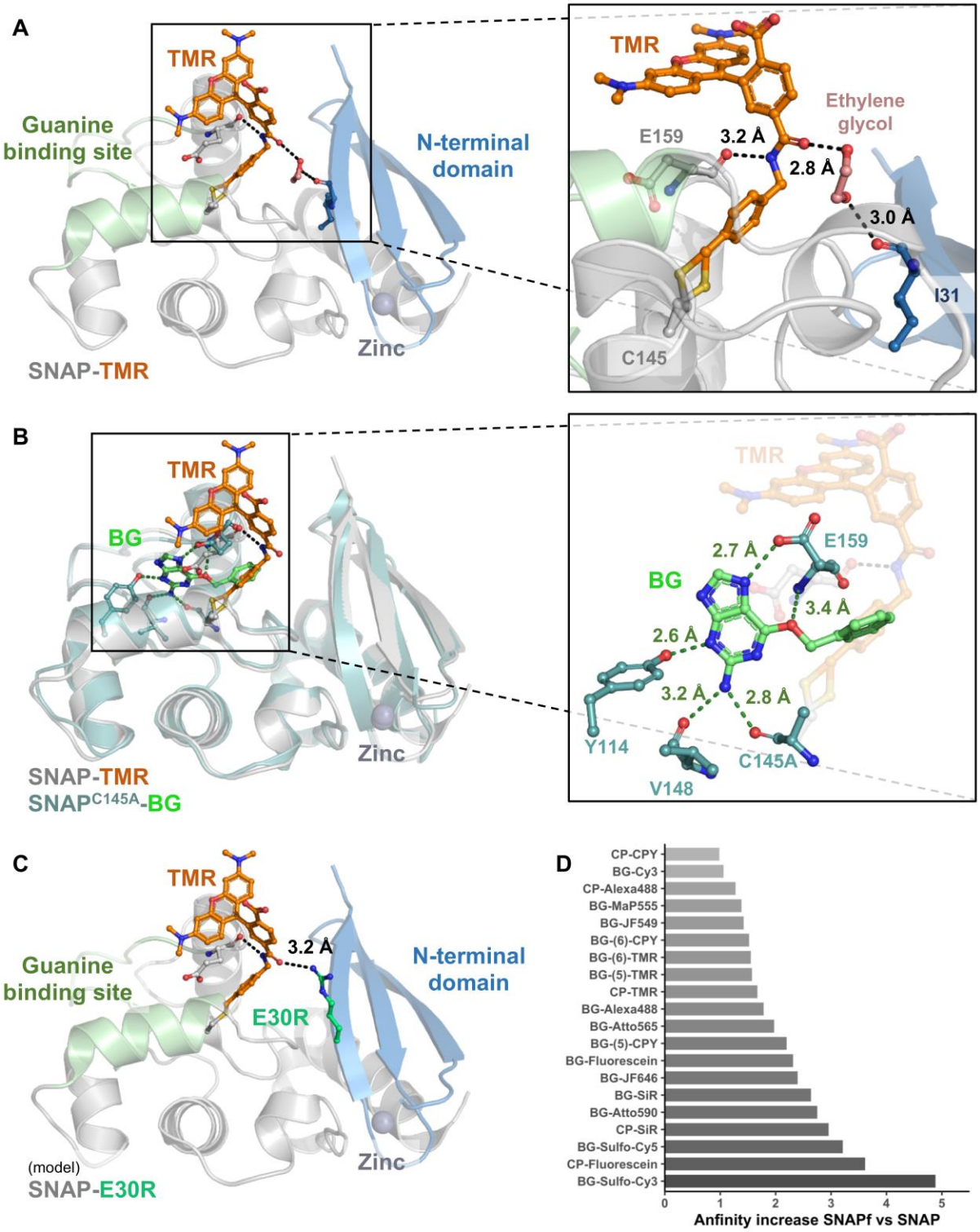

Figure 5: Structure-function analysis of SNAP-tag fluorophore substrate interactions.

A. Crystal structure of SNAP labeled with a TMR substrate. **B**. Structural comparison between SNAP-TMR and the BG bound variant of SNAP^{C145A}. **C**. Modeling of the E30R mutation in the SNAP-TMR crystal structure. SNAP is represented as cartoon, the fluorophore substrate and residues as sticks. Putative hydrogen bonds and corresponding distances are indicated by black dashes. **D**. Affinity increase between SNAP^{C145A} and SNAPf^{C145A} for different fluorophore substrates. Number in brackets indicate different linkage of the fluorophore benzyl group to BG.

SNAPf has a higher affinity for its substrates. We modeled the SNAPf mutation E30R in the structure of TMR-labeled SNAP to gain a better understanding of how it affects the labeling kinetics (**Fig. 5C**). Results suggest that an arginine in position 30 could interact with the carbonyl oxygen of the amide group in the label via a moderate hydrogen bond (3.2 Å), replacing the hydrogen bond observed with the ethylene glycol in the crystal structure. This could lead to an increased affinity for the substrate or a better substrate positioning resulting in a quicker labeling. To probe this hypothesis, the affinities of SNAP^{C145A} and SNAPf^{C145A} were compared side by side for various fluorophore substrates (**Fig S16**). Among the 21 fluorophore substrates tested, only five did not show a significant increase in affinity (*i.e.* above 50%) and nine showed more than a 2 fold affinity increase (**Fig. 5D**). As observed for SNAP, SNAPf^{C145A} substrate affinities correlate well with the corresponding k_{app} values for SNAPf (**Fig. S24**). It is noteworthy to mention that negatively charged substrates such as BG-sulfo-Cy3 show the strongest increase in the protein affinities and labeling rates when comparing SNAP to SNAPf. This could be due to the exchange of the negatively charged glutamic acid by a positively charged arginine resulting in a potential electrostatic steering effect as mentioned for HT7 (25).

Comparison between SNAP-tag and SsOGT-H^5. Recently, an homologue of hAGT from an extremophile archaea was converted to an SLP (*Ss*OGT-H^5) by introducing mutations that have been shown to increase the reactivity of SNAP (29). Its crystal structure labeled with SNAP-Vista Green® (SVG, *i.e.* BG-5-fluorescein) (30) shows a different fluorophore conformation, constrained by the crystal packing (**Fig. S25**). Interestingly, the *Ss*OGT-H^5-SVG structure was obtained with a fluorophore connected via the 5-carboxy isomer of the fluorophore and presents a substrate conformation that could not exist in the SNAP structure due to steric clashes (**Fig. S25A**). We compared the kinetics of SNAP and *Ss*OGT-H^5 (**Fig. S26 & Table S9**) toward the substrates BG-TMR (5- and 6-substituted) and BG-6-Alexa488 at 37°C. In contrast to SNAP, *Ss*OGT-H^5 showed a preference for BG-5-TMR (k_{app} = 1.45 ± 0.92 x 10^2 $M^{-1}s^{-1}$) over BG-6-TMR (k_{app} = 6.78 ± 0.67 x 10^1 $M^{-1}s^{-1}$). Furthermore, the negatively charged BG-6-Alexa488 (k_{app} = 1.24 ± 0.01 x 10^2 $M^{-1}s^{-1}$) presents kinetics in the same range as BG-5-TMR, highlighting a different substrate preference between SNAP and *Ss*OGT-H^5. For all substrates, *Ss*OGT-H^5 presents kinetics 100 times slower than SNAP or CLIP, making it less suitable for labeling applications at physiological temperatures.

Discussion

We provide here a systematic comparison of the labeling kinetics of HT7, SNAP and CLIP towards a large panel of substrates. A structure-function relationship analysis complements this comparison, thereby yielding insights into the origins of the different substrate specificities of HT7 and SNAP. The data should assist scientists in choosing SLP-substrate pairs for specific purposes.

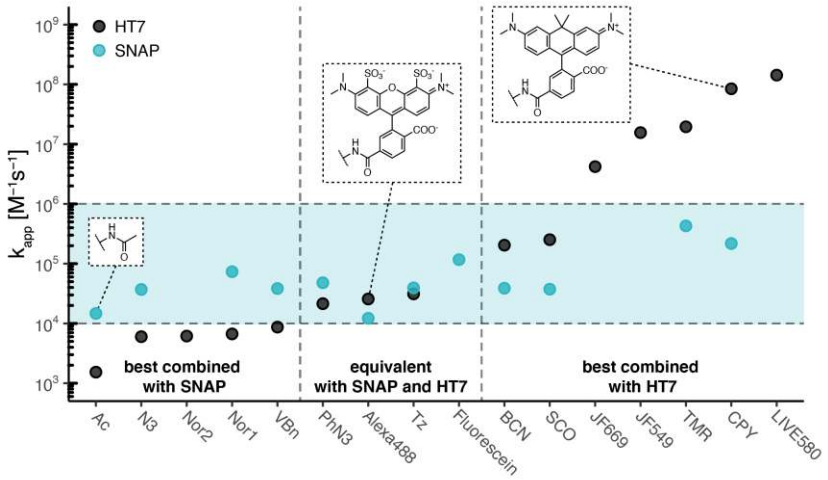

Figure 6: Labeling kinetics comparison between SNAP-tag and HaloTag7.

Apparent labeling rate constants (k_{app}) of HT7 span over six orders of magnitude while rate constants of SNAP span only over two orders of magnitude (BG-substrates). The blue area highlights the span of SNAP apparent labeling rate constants. Depending on the application, some substrates should preferentially be employed with HT7 or SNAP to ensure quick labeling.

The direct comparison of SNAP and HT7 reveals that HT7 features significantly higher labeling rates with various fluorescent rhodamine derivatives (**Fig 6 & Table 1**). These differences in reactivity can be explained by specific interactions of the rhodamine's xanthene ring with selected surface residues of HT7. The high reactivity of HT7 towards rhodamines is important as rhodamines up to now represent the most relevant class of cell-permeable fluorophores for live-cell imaging. The interactions between rhodamines and HT7 also help to explain why some rhodamine-based HT7 substrates tend to have improved spectroscopic properties and are more fluorogenic than the corresponding SNAP or CLIP substrates (16). Most rhodamine-based fluorophores exist in an equilibrium between spirocyclic non-fluorescent and zwitterionic fluorescent forms. While in solution the spirocyclic form might be favored, labeling reaction with an SLP switches this equilibrium toward the zwitterionic form, leading to a fluorescence intensity increase (31). This property is of particular interest in wash-free live-cell fluorescence microscopy since it leads to higher signal over background (26, 32-35) and can also be exploited for sensor design (23, 36). Furthermore, the dynamic equilibrium between the spirocyclic non-fluorescent and zwitterionic fluorescent form is crucial for cell permeability (33). The mechanism underlying the equilibrium

shift from the spirocyclic non-fluorescent to the zwitterionic fluorescent form is not fully understood yet but our results indicate that the planar, zwitterionic form of rhodamines (*e.g.* TMR and CPY) features energetically favorable interactions with HT7 surface, thus potentially favoring this state of the fluorophore when labeled to the protein.

While HT7 reacts quicker with most rhodamine-based fluorophore substrates than SNAP, the differences become much less pronounced or reversed for negatively charged substrates. For example, SNAP reacts faster with Alexa488 than HT7 and the reactivity for most other non-fluorescent substrates tends to be higher for SNAP as well (**Fig 6 & Table 1**). It is interesting to hypothesize about the origin of the substrate specificity differences between SNAP and HT7. Most likely, these differences are, at a least partially, a consequence of the substrates used in the engineering of the tags. For HT7, TMR was used in most screening assays (9, 13) and, as a result, HT7 shows a specificity for zwitterionic rhodamines. In contrast, different substrates such as BG-fluorescein (37), BG-Cy3 (38) as well as affinity reagents such as BG-biotin (37) were used in SNAP screening and selection assays. As a consequence, SNAP is more promiscuous than HT7. Differences in labeling speed of both SLPs are mostly driven by differences in substrate affinity: an overall correlation between affinity and rate constants was observed for both proteins that was more pronounced for HT7. Indeed, HT7 presents a very low affinity toward the *e.g.* unsubstituted CA-Ac substrate highlighting that HT7 affinity toward substrates is highly driven by the substituent and so are the kinetics. We show here how the low reactivity of HT7, for example towards CA-PEG-biotin, can be overcome by designing substrates in which the label of interest is attached to a CA-TMR core and anticipate that such strategy could be expanded to other substituents.

A key property of SLP substrates for live-cell applications that we have not addressed in this study is their cell permeability. Generally speaking, the CA core is less polar than BG, CP and BC. The permeability of HT7 substrates therefore can be expected to be higher than the corresponding SNAP-tag substrates. However, this question will have to be more systematically addressed in future studies.

For future engineering of SLPs, it would be particularly interesting to increase the affinity of SNAP and CLIP towards rhodamine-based substrates. Given the importance of these fluorophores for live-cell fluorescence (super-resolution) microscopy (1), additional tags that display labeling kinetics towards rhodamines similar to those of HT7 would be highly welcomed. Our results suggest that increasing the reactivity towards these dyes might come with the risk of reducing the activity

towards other substrates, thereby limiting the flexibility of such tags. However, given the importance of SLPs and rhodamine-based probes for live-cell imaging, the generation of such specialized tags is warranted.

Materials and Methods

Labeling substrates and chemical synthesis. Labeling substrates for HaloTag, SNAP-tag and CLIP-tag were synthesized according to literature procedures (10, 11, 15, 32-34, 39-45); purchased from Promega Corp. (Madison, WI, USA), Abberior GmbH (Göttingen, Germany), Santa Cruz Biotechnology Inc. (Dallas, TX, USA) and NEB Inc. (Ipswitch, MA, USA); were kind gifts from Dr. L. Lavis (Janelia research campus, USA) and Dr. A.D.N. Butkevich (MPI for Medical Research, Germany) or were synthesized according to the procedure available in the supplementary information.

Cloning, protein expression and purification. SNAP, SNAPf, SNAP^{cx}, CLIP, CLIPf, HT7 and HOB were cloned in a pET51b(+) vector (Novagen) for production in *Escherichia coli*, featuring an N-terminal His_{10} tag and a Tobacco Etch Virus (TEV) cleavage site. *Ss*OGT-H[5] and hAGT were cloned in the same plasmid featuring an N-terminal StrepTag-II and an enterokinase cleavage site together with a C-terminal His_{10} tag. Cloning was performed by Gibson assembly (46) using E.cloni 10G cells (Lucigen) and point mutations were performed using the Q5 site-directed mutagenesis kit (NEB). Proteins were expressed in *E. coli* strain BL21(DE3)-pLysS (Novagen). Lysogeny broth (LB) (47) cultures were grown at 37°C to optical density at 600 nm (OD_{600nm}) of 0.8. Transgene expression was induced by the addition of 0.5 mM isopropyl-β-D-thiogalactopyranoside (IPTG) and cells were grown at 17°C overnight in the presence of 1 mM $MgCl_2$. Cells were harvested by centrifugation and lysed by sonication.

For N-terminally His-tagged proteins, the cell lysate was cleared by centrifugation (75 000g, 4º C, 10 min) before affinity-tag purification using a HisTrap FF crude column (Cytiva, Marlborough, MA, USA) and an ÄktaPure FPLC (Cytiva). Buffer was exchanged using a HiPrep 26/10 Desalting column (Cytiva) to HEPES 50 mM, NaCl 50 mM pH 7.3 (*i.e.* activity buffer). Proteins were concentrated using Ultra-15 mL centrifugal filter devices (Amicon, Merck KGaA, Darmstadt, Germany) with a molecular weight cut-off (MWCO) smaller than the protein size to a final concentration of 500 µM. Proteins were aliquoted and stored at -80°C after flash freezing in liquid nitrogen. Double-tagged proteins, after similar cell lysis and clearing, were purified using HisPur Ni-NTA Superflow Agarose (Thermo Fisher Scientific, Waltham, MA, USA) by batch incubation followed by washing and elution steps on a polypropylene column (Qiagen). Proteins were subsequently purified using a StrepTrap HP column (Cytiva) on an ÄktaPure FPLC. Proteins were then concentrated using Ultra-5 mL centrifugal filter devices with a MWCO smaller than the protein size and conserved in glycerol 45 % (w/v) at -20°C.

Correct size and purity of proteins were assessed by SDS-PAGE and liquid chromatography-mass spectrometry (LC-MS) analysis.

Affinity of HT7 and HOB towards CA substrates. Binding affinities of $HT7^{D106A}$ or HOB^{D106A} to chloroalkane (CA) substrates were determined by fluorescence polarization (FP, equation **1**) measurements using a microplate reader (Spark20M®, Tecan Group AG, Männedorf, Switzerland). The fluorescent substrates (10 nM) were titrated against different protein concentrations (0 – 250 µM) in activity buffer supplemented with 0.5 g/L BSA. Assays were performed in black low-volume non-binding 384-well plates (Corning Inc., Corning, NY, USA) with a final volume of 20 µL. All measurements were performed in triplicates at 37°C, filter settings are listed in **Table 3**. Obtained FP values were averaged and fitted to a single site binding model (equation **2**) to estimate K_d values for each fluorescent substrate. The FP value of each dye fully reacted with the native HT7 was used to improve fitting of the curves upper plateau by adding an extra data point at protein concentration of 0.1 M.

$$FP = \frac{I_{\parallel} - I_{\perp} * G}{I_{\parallel} + I_{\perp} * G} \quad \textbf{(1)}$$

with FP: fluorescence polarization, $I_{\parallel}$: fluorescence intensity parallel to the excitation light polarization, $I_{\perp}$: fluorescence intensity perpendicular to the excitation light polarization and G: grating factor ($G = I_{\parallel}/I_{\perp}$).

$$FP = FP_{min} + \frac{FP_{max} - FP_{min}}{1 + \frac{K_d}{[prot]}} \quad \textbf{(2)}$$

with FP_{min}: fluorescence polarization of the free fluorophore (lower plateau), FP_{max}: maximal fluorescence polarization of fully bound fluorophore (upper plateau), K_d: dissociation constant and [prot] = protein concentration.

Affinity of SNAP and SNAPf towards BG and CP substrates. Binding affinities of $SNAP^{C145A}$ and $SNAPf^{C145A}$ toward BG-Alexa488, CP-Alexa488, BG-Fluorescein, CP-Fluorescein, BG-MAP555, BG-JF549, BG-TMR(6), BG-TMR(5), CP-TMR, BG-CPY(6), BG-CPY(5), CP-CPY, BG-SiR, CP-SiR, BG-JF646, BG-Atto565, BG-Atto590, BG-sulfo-Cy3, BG-Cy3, BG-sulfo-Cy5, BG-Cy5 were determined by fluorescence polarization analogous to HT7 affinities towards CA substrates described above with the following changes: fluorescent substrates were titrated at a final concentration of 50 nM against protein concentrations ranging from (0 – 250 µM) at room temperature using 0.1 g/L BSA and 1 mM DTT (SNAP-FP buffer). The FP value of each dye fully reacted with the native SNAP/SNAPf was used to improve fitting of the upper plateau of the curves by adding an extra data point at protein concentration of 0.005 M.

Table 3: Filter settings used in FP measurements.

Fluorophore	Excitation filter (BW)	Emission filter (BW)
Alexa488, Fluorescein, Oregon green, JF503, 500R	485 (20) nm	535 (25) nm
TMR, JF549, JF525, TMR-az-F2, TMR-CN, TMR-SCH3, TMR-SNH2, MaP555, 510R, 515R, 580CP, Atto565, Atto590, (sulfo-)Cy3	535 (25) nm	595 (35) nm
CPY, SiR, LIVE580, JF608, JF646, JF669, (sulfo-)Cy5	620 (20) nm	680 (30) nm

Affinity of HT7 towards methyl-amide fluorophores. Binding affinities of HT7 towards methyl-amide fluorophores were determined by fluorescence polarization analogous to CA substrates described above with following changes: fluorescent substrates were used at a final concentration of 50 nM and measurements were performed at room temperature.

Affinity of HT7^{D106A} towards CA-Ac via FP competition assay. Binding affinity of HT7^{D106A} towards CA-Ac was determined by a fluorescence polarization competition assay against CA-TMR. 5 µM protein and 50 nM CA-TMR were titrated against CA-Ac concentrations ranging from 80 µM to 10 mM in activity buffer supplemented with 0.5 g/L BSA. Assays were performed in low-volume non-binding black 384-well plates (Corning Inc.) with a final volume of 20 µL using a microplate reader (Spark20M®, Tecan). All measurements were performed in triplicates at 37°C, filter settings are listed in **Table 3**. Obtained FP values were averaged and fitted to a 4 parameter logistic curve (equation **3**) to estimate the I_{50} value. The lower plateau was fixed to the measured FP value of the free dye to improve the fit. The dissociation constant of CA-Ac was calculated as described by Rossi and Taylor (2011) (48).

$$FP = FP_{max} + \frac{FP_{min} - FP_{max}}{1 + (\frac{I_{50}}{[ligand]})^{HillSlope}} \quad \textbf{(3)}$$

with FP_{min}: fluorescence polarization of the free fluorophore (lower plateau), FP_{max}: maximal fluorescence polarization of fully bound fluorophore (upper plateau), I_{50}: half maximal effective concentration, HillSlope: hill slope and [ligand]: ligand concentration.

Affinity of SNAP^{C145A} towards non-fluorescent substrates via FP competition assay. Binding affinities of SNAP^{C145A} towards BG, CP, BG-Ac, CP-Ac and BC-Ac to were obtained as previously described for HT7 by titrating 5 µM protein and 50 nM CP-TMR against non-fluorescent substrate concentrations ranging from 150 nM to 1.5 mM. Experimental conditions and data analysis were

identical despite that 1 mM DTT was added to the buffer and the assay was performed at room temperature.

Calculation of free binding energy from K_d. Free binding energies were calculated from K_d values according to equation 4:

$$\Delta G = -RT * ln\left(\frac{1}{K_d}\right) \quad \textbf{(4)}$$

with ΔG: free binding energy, R: universal gas constant, T: temperature and K_d: dissociation constant.

HT7 and HOB labeling kinetics via stopped-flow. Labeling kinetics of HT7 with CA-TMR, CA-JF549, CA-CPY, CA-LIVE580 and CA-JF669 and labeling kinetics of HOB with CA-TMR were measured by recording fluorescence anisotropy changes over time using a BioLogic SFM-400 stopped-flow instrument (BioLogic Science Instruments, Claix, France) in single mixing configuration at 37°C. Monochromator wavelengths for excitation and long pass filters used for detection are listed in **Table 4**. HT7 protein and substrates in activity buffer were mixed in a 1:1 stoichiometry in order to reach recordable speed of these fast reactions and increase information content of the traces. Concentrations were varied from 0.125 µM to 1 µM. The anisotropy of the free substrate was measured to obtain a baseline.

The dead time of the instrument was measured according to the manufacturer protocol (BioLogic Technical note #53) by recording the fluorescence decay during the pseudo-first order reaction of *N*-acetyl-L-tryptophanamide with a large excess of *N*-bromosuccinimide and fitting the data to the first order reaction rate law.

Table 4: Monochromator excitation wavelengths and filters used for stopped-flow measurements

Fluorophore	Excitation wavelength [nm]	Emission filter [nm]
TMR / JF549	555	570 Long Path
CPY	610	630 Long Path
LIVE580	603	630 Long Path
JF669	669	690 Long Path

SNAP labeling kinetics via stopped-flow. Labeling kinetics of SNAP with BG-TMR were measured via stopped-flow analogous to HT7 kinetics described above but final substrate concentration was fixed at 2 µM and the protein concentration was varied from 1.875 µM to 50 µM. The activity buffer was supplemented with 1 mM DTT.

HT7 and HOB labeling kinetics via microplate reader. Labeling kinetics of HT7 and HOB with CA-Alexa488 were measured by recording FP over time using a microplate reader (Spark20M®,

Tecan). The final concentration of fluorophore substrate remained constant (50 nM) with varying protein concentrations (200 nM – 256 µM) in activity buffer supplemented with 0.5 g/L of BSA. Labeling reactions were started by adding the fluorophore substrate using either multichannel pipets or the injector module of the plate reader. Assays were performed in black non-binding flat bottom 96-well plates (Corning Inc.) with a final reaction volume of 200 µL. All measurements were performed in triplicates at 37°C with filter settings listed in **Table 3**. The FP of the free substrate was measured to obtain a baseline.

HT7-tag competitive labeling kinetics. Competitive kinetics were measured by recording FP over time using a microplate reader (Spark20M®, Tecan). The final concentration of CA-Alexa488 (50 nM) and HT7 protein (200 nM) remained constant with varying concentrations of non-fluorescent substrates (0 – 1 µM) in activity buffer supplemented with 0.5 g/L of BSA. Assays were performed in black non-binding flat bottom 96-well plates with a final reaction volume of 200 µL. Labeling reactions were started by adding the HT7 protein to wells containing CA-Alexa488 and non-fluorescent substrates using an electronic 96 channel pipettor (Integra Bioscience Corp., Hudson, NH, USA). All measurements were performed in triplicates at 37°C with filter settings listed in **Table 3**. The FP of free CA-Alexa488 was measured to obtain a baseline.

SNAP and CLIP labeling kinetics via microplate reader. Labeling kinetics of SNAP and CLIP substrates were measured by recording FP over time using a microplate reader analogously to HT7 labeling kinetics described above with the following changes: fluorescent substrate concentration was fixed to 20 nM and protein concentrations were varied from 15 nM to 900 nM. Measurements were performed in SNAP-FP buffer. Kinetics with substrates that showed adsorption to plastic were recorded in a black quartz 96-well plate (Hellma GmbH, Müllheim, Germany).

SNAP competitive labeling kinetics. Competitive kinetics were measured by recording FP over time using a microplate reader analogous to HT7 competition kinetics described above using 100 nM of BG-Alexa488 as fluorescent substrate in SNAP-FP buffer.

Analysis of stopped-flow data. Kinetic stopped-flow data was pre-processed using a custom R script (49, 50). Recorded pre-trigger time points were removed and time points were adjusted to start at t = 0. Values from replicates were averaged. The anisotropy of the free dye was calculated by averaging anisotropy values of the baseline measurements. Pre-processed data was fit to a kinetic model (**5, 6**) described by the differential equations **7-10** using the DynaFit software (51). The anisotropy of the free dye and the mixing delay of the stopped-flow machine were set as fixed offset and delay parameters in DynaFit. It was assumed that the protein substrate complex and

the reacted product are contributing equally to the anisotropy signal. Hence, the response for both species was set equal in DynaFit and fitted together with the kinetic constants. Standard deviations (normal distribution verified) and confidence intervals of fitted parameters were estimated with the Monte Carlo method (52) with standard settings ($N = 1000$, 5% worst fits discarded). In case of SNAP kinetics with BG-TMR, the substrate concentration was fitted by DynaFit in order to rule out quantification errors of the BG quenched fluorophore. Accurate fitting of the concentration was ensured by including conditions in which protein is limiting and no maximum FP value was reached. Data points and predictions based on the fitted models were plotted using R. Fluorescence intensity changes upon protein binding were verified to be minimal (< 12 %) and hence not noticeably biasing the fluorescence anisotropy.

$$P + S \underset{k_{-1}}{\overset{k_1}{\rightleftharpoons}} PS^* \quad \textbf{(5)}$$

$$PS^* \xrightarrow{k_2} PS \quad \textbf{(6)}$$

with P: SLP protein, S: SLP substrate, PS*: protein substrate complex and PS: protein substrate conjugate.

$$\frac{d[P]}{dt} = -k_1[P][S] + k_{-1}[PS^*] \quad \textbf{(7)}$$

$$\frac{d[S]}{dt} = -k_1[P][S] + k_{-1}[PS^*] \quad \textbf{(8)}$$

$$\frac{d[PS^*]}{dt} = +k_1[P] - k_{-1}[PS^*] - k_2[PS^*] \quad \textbf{(9)}$$

$$\frac{d[PS]}{dt} = +k_2[PS^*] \quad \textbf{(10)}$$

The derived parameters K_d (dissociation constant) and k_{app} (apparent first order reaction rate) were calculated using the following equations:

$$K_d = \frac{k_{-1}}{k_1} \quad \textbf{(11)}$$

$$k_{app} = k_1 \frac{k_2}{k_2 + k_{-1}} \quad \textbf{(12)}$$

Analysis of kinetic microplate reader data. Kinetic data from microplate reader assays was fitted to a simplified kinetic model (**13**) described by the differential equations **14-16** using DynaFit. Dead time of the measurements and baseline FP value were put in as fixed parameters. Standard deviations (normal distribution verified) and confidence intervals of fitted parameters were estimated with the Monte Carlo method with standard settings ($N = 1000$, 5% worst fits discarded). In case of BG, CP and BC kinetics, the substrate concentration was fitted by DynaFit in order to rule out quantification errors of the BG, CP or BC fluorophores. Accurate fitting of the concentration

was ensured by including conditions in which protein is limiting and no maximum FP value was reached. Data points and predictions based on the fitted models were plotted using R.

$$P + S \xrightarrow{k_{app}} PS \quad \textbf{(13)}$$

with P: SLP protein, S: SLP substrate and PS: protein substrate conjugate.

$$\frac{d[P]}{dt} = -k_{app}[P][S] \quad \textbf{(14)}$$

$$\frac{d[S]}{dt} = -k_{app}[P][S] \quad \textbf{(15)}$$

$$\frac{d[PS]}{dt} = +k_{app}[P][S] \quad \textbf{(16)}$$

In some cases, a slow second phase (k_3) was observed in the kinetic data that could not be described by the simplified model **13**. This data was fit to an expanded model that includes a potential conformational change in a second step (**17, 18**).

$$P + S \xrightarrow{k_{app}} PS_a \quad \textbf{(17)}$$

$$PS_a \xrightarrow{k_3} PS_b \quad \textbf{(18)}$$

with P: SLP protein, S: SLP substrate, PS_a: protein substrate conjugate state A and PS_b: protein substrate conjugate state B.

Analysis of competition kinetics. Data was fitted to a simplified kinetic competition model (**19, 20**) described by the differential equations **21-25** using DynaFit. Dead time of the measurements and baseline FP value were put in as fixed parameters. Standard deviations (normal distribution verified) and confidence intervals of fitted parameters were estimated with the Monte Carlo method with standard settings ($N = 1000$, 5% worst fits discarded).

$$P + S \xrightarrow{k_{S_{app}}} PS \quad \textbf{(19)}$$

$$P + I \xrightarrow{k_{I_{app}}} PI \quad \textbf{(20)}$$

with P: SLP protein, S: fluorescent SLP substrate, I: non-fluorescent SLP substrate (inhibitor), PS: protein fluorescent substrate conjugate and PI: protein non-fluorescent substrate conjugate.

$$\frac{d[P]}{dt} = -k_{S_{app}}[P][S] - k_{I_{app}}[P][I] \quad \textbf{(21)}$$

$$\frac{d[S]}{dt} = -k_{S_{app}}[P][S] \quad \textbf{(22)}$$

$$\frac{d[I]}{dt} = -k_{I_{app}}[P][I] \quad \textbf{(23)}$$

$$\frac{d[PS]}{dt} = +k_{S_{app}}[P][S] \quad \textbf{(24)}$$

$$\frac{d[PI]}{dt} = +k_{I_{app}}[P][I] \quad \textbf{(25)}$$

Protein crystallization. For crystallization trials, protein purification tags were removed by overnight cleavage with TEV protease at 30°C as previously described (53). Cleaved proteins were purified by affinity-tag purification using a HisTrap FF crude column (Cytiva) on an ÄktäPure FPLC, collecting the flow-through. Proteins were further separated by size exclusion chromatography (HiLoad 26/600 Superdex 75, Cytiva) and concentrated using Ultra-4 or 15 mL centrifugal filter devices (Amicon, Merck). Correct size and high purity were verified via SDS-PAGE and LC-MS analysis. Protein labeling was performed in activity buffer, overnight at RT using fluorophore substrates at 10 µM (CA-TMR/CA-CPY and BG-TMR for HT7/HOB and SNAP, respectively) in presence of 5 µM (3 mg) of protein. After concentration to about 200 µL, excess of fluorophore substrate was removed by buffer exchange using Illustra microspin G-25 columns (Cytiva) according to the manufacturer instructions. Protein labeling was verified by SDS-PAGE fluorescence scan and LC-MS analysis. Protein concentrations were adjusted between 10 and 20 mg/mL and submitted to crystallization trials using different commercial screens mixing in 200 nL final volume protein solution:crystallization solution (1:1) using a Mosquito robot (TTP Labtech).

HT7 crystal structures. Crystallization was performed at 20°C using the vapor-diffusion method. Crystals of HT7 labeled with a chloroalkane-PEG-tetramethylrhodamine (CA-TMR) fluorophore substrate were grown by mixing equal volumes of protein solution at 20 mg/ml in 50 mM HEPES pH 7.3, 50 mM sodium chloride and a reservoir solution containing 0.1 M MES pH 6.0, 1.0 M lithium chloride and 15% (m/v) PEG 6000. The crystals were briefly washed in cryoprotectant solution consisting of the reservoir solution with glycerol added to a final concentration of 20% (v/v), prior to flash-cooling in liquid nitrogen. Crystals of HT7 labeled with a chloroalkane-PEG-carbopyronine (CA-CPY) fluorophore substrate were obtained by mixing equal volumes of protein solution at 15 mg/ml in 50 mM HEPES pH 7.3, 50 mM sodium chloride and precipitant solution containing 0.1 M Bicine pH 9.0 and 1.7 M ammonium sulfate. The crystals were briefly washed in cryoprotectant solution consisting of the reservoir solution supplemented with 20% (v/v) ethylene glycol before flash-cooling in liquid nitrogen. Crystals of HT7-based Oligonucleotide Binder (HOB) labeled with a CA-TMR fluorophore substrate were grown by mixing equal volumes of protein

solution at 9.0 mg/ml in 50 mM HEPES pH 7.3, 50 mM sodium chloride and a reservoir solution composed of 0.2 M calcium acetate and 20% (m/v) PEG 3350. Prior to flash-cooling in liquid nitrogen, the crystals were stepwise transferred into a reservoir solution with PEG 3350 concentration increased to 30 and 40% (m/v).

Single crystal X-ray diffraction data was collected at 100 K on the X10SA beamline at the SLS (PSI, Villigen, Switzerland). All data were processed with XDS (54). The structures of HT7 labeled with TMR was determined by molecular replacement (MR) using Phaser (55) and PDB ID 5UY1 coordinates as a search model. The structure of HT7 labeled with CPY and HOB labeled with TMR were subsequently determined by molecular replacement using HT7-TMR as a search model. Geometrical restraints for TMR and CPY were generated using Grade server (56). The final models were optimized in iterative cycles of manual rebuilding using Coot (57) and refinement using Refmac5 (58) and phenix.refine (59). Data collection and refinement statistics are summarized in **Table S4**, model quality was validated with MolProbity (60) as implemented in PHENIX.

SNAP crystal structure. SNAP-TMR crystals were obtained on the crystallography platform of EPFL using the SNAP^{cx}-tag construct that features the sequence of SNAP identical to available SNAP crystal structures (PDB ID 3L00, 3KZZ and 3KZY). Previously crystallized SNAP features the mutation P179R involved in the crystal packing suggesting its important role for crystallization (28). Crystals were obtained in different conditions including in 100 mM Sodium HEPES pH 7.5, 25% PEG 8000 from the PEG suite screen (Qiagen) after 48 hours at 18°C. Single crystals were fished and placed in a cryoprotectant solution (containing the crystallization solution supplemented with 20% (v/v) glycerol) before being flash frozen in liquid nitrogen. Single crystal X-ray diffraction data was collected on the ID29 beamline at the ESRF (Grenoble, France). Integration, scaling, molecular replacement (using PDB ID 3L00 as starting model) and refinement were performed as explained for HT7. Refinement statistics can be found in **Table S4**.

SNAPf* in silico *modeling. The glutamic acid in position 30 of the SNAP-TMR structure (PDB ID 6Y8P) was modeled as an arginine using the mutate function using the software SYBYL-X1.3 (Tripos Int., USA). A side-chain conformation for the arginine was selected from the rotamer source library of Lovell and minimized with few steps with no steric clashes and no direct contact with another positive charges as criteria.

Data availability and analysis. Atomic coordinates and structure factors were deposited in the Protein Data Bank (PDB) under accession codes 6Y7A (HT7-TMR), 6ZCC (HOB-TMR), 6Y7B (HT7-CPY) and 6Y8P (SNAP-TMR). Analysis was conducted on PyMOL (61). OMIT maps were

generated using Phenix (62). Root mean square deviations (RMSDs) were obtained using the cealign command from PyMOL. Electrostatic potentials were generated using the adaptive poisson–boltzmann solver (APBS) (63) as PyMOL plugin including the PDB2PQR software (64). Plasmids from this study are available at Addgene (167266-167275).

Acknowledgements

The authors thank Ilme Schlichting for X-ray data collection. HaloTag diffraction data were collected at the Swiss Light Source, beamline X10SA, of the Paul Scherrer Institute, Villigen, Switzerland. The authors thank Florence Pojer for supporting the SNAP-TMR crystallization on the EPFL platform. The ESRF is acknowledged for access to beamlines and facilities for molecular biology via its in-house research programme. The authors thank Andrea Bergner (MPIMF) and Bettina Mathes (MPIMF) for providing proteins and fluorophore substrates, respectively. The authors thank Dr. L. Lavis (HHMI, Ashburn, VA, USA) and Dr. A.D.N. Butkevich (MPI-MF, Heidelberg, Germany) for providing HaloTag substrates. We thank all members of the Johnsson lab for critical discussions. This work was supported by the Ecole Polytechnique Federale de Lausanne (EPFL), the Max Planck Society and the Deutsche Forschungsgemeinschaft (DFG, German Research Foundation), SFB 1129.

Author contributions

J.W., S.K., J.R., J.H. and K.J. designed the experiments.
J.W., S.K., J.H. and J.T. performed the biochemistry experiments.
J.H., T.T., G.G. crystalized and solved the SNAP-TMR structure.
M.T. and J.H. crystalized and solved the HaloTag structures.
U.U. performed the structural modeling work.
S.K., J.W., J.K., N.M. and L.X. synthesized the compounds used in the study.
K.J., J.H., J.W. and S.K. wrote the manuscript with input from all authors.

Competing financial information

K.J. is inventor on patents filed by MPG and EPFL on fluorophores and labeling technologies.

Additional information

Further information and requests for resources and reagents should be directed to and will be fulfilled by Julien Hiblot (julien.hiblot@mr.mpg.de) and Kai Johnsson (johnsson@mr.mpg.de).

References

1. Xue L, Karpenko IA, Hiblot J, Johnsson K. Imaging and manipulating proteins in live cells through covalent labeling. Nature chemical biology. 2015;11(12):917-23.
2. England CG, Luo H, Cai W. HaloTag Technology: A Versatile Platform for Biomedical Applications. Bioconjugate Chemistry. 2015;26(6):975-86.
3. Haruki H, Gonzalez MR, Johnsson K. Exploiting ligand-protein conjugates to monitor ligand-receptor interactions. PLoS One. 2012;7(5):e37598.
4. Farrants H, Hiblot J, Griss R, Johnsson K. Rational Design and Applications of Semisynthetic Modular Biosensors: SNIFITs and LUCIDs. Methods Mol Biol. 2017;1596:101-17.
5. Sallin O, Reymond L, Gondrand C, Raith F, Koch B, Johnsson K. Semisynthetic biosensors for mapping cellular concentrations of nicotinamide adenine dinucleotides. Elife. 2018;7.
6. Yu Q, Xue L, Hiblot J, Griss R, Fabritz S, Roux C, et al. Semisynthetic sensor proteins enable metabolic assays at the point of care. Science. 2018;361(6407):1122-6.
7. Abdelfattah AS, Kawashima T, Singh A, Novak O, Liu H, Shuai Y, et al. Bright and photostable chemigenetic indicators for extended in vivo voltage imaging. Science. 2019.
8. Chidley C, Haruki H, Pedersen MG, Muller E, Johnsson K. A yeast-based screen reveals that sulfasalazine inhibits tetrahydrobiopterin biosynthesis. Nature chemical biology. 2011;7(6):375-83.
9. Los GV, Encell LP, McDougall MG, Hartzell DD, Karassina N, Zimprich C, et al. HaloTag: a novel protein labeling technology for cell imaging and protein analysis. ACS chemical biology. 2008;3(6):373-82.
10. Keppler A, Gendreizig S, Gronemeyer T, Pick H, Vogel H, Johnsson K. A general method for the covalent labeling of fusion proteins with small molecules in vivo. Nature biotechnology. 2003;21(1):86-9.
11. Gautier A, Juillerat A, Heinis C, Correa IR, Jr., Kindermann M, Beaufils F, et al. An engineered protein tag for multiprotein labeling in living cells. Chem Biol. 2008;15(2):128-36.
12. Damborský J, Koča J. Analysis of the reaction mechanism and substrate specificity of haloalkane dehalogenases by sequential and structural comparisons. Protein Engineering, Design and Selection. 1999;12(11):989-98.
13. Encell LP, Friedman Ohana R, Zimmerman K, Otto P, Vidugiris G, Wood MG, et al. Development of a dehalogenase-based protein fusion tag capable of rapid, selective and covalent attachment to customizable ligands. Curr Chem Genomics. 2012;6:55-71.
14. Pegg AE, Dolan ME, Moschel RC. Structure, Function, and Inhibition of O6-Alkylguanine-DNA Alkyltransferase. Progress in Nucleic Acid Research and Molecular Biology1995. p. 167-223.
15. Correa I, Baker B, Zhang A, Sun L, Provost C, Lukinavic.ius Gz, et al. Substrates for Improved Live-Cell Fluorescence Labeling of SNAP-tag. Current Pharmaceutical Design. 2013;19(30):5414-20.
16. Erdmann RS, Baguley SW, Richens JH, Wissner RF, Xi Z, Allgeyer ES, et al. Labeling Strategies Matter for Super-Resolution Microscopy: A Comparison between HaloTags and SNAP-tags. Cell Chem Biol. 2019;26(4):584-92 e6.
17. Jonker CTH, Deo C, Zager PJ, Tkachuk AN, Weinstein AM, Rodriguez-Boulan E, et al. Accurate measurement of fast endocytic recycling kinetics in real time. Journal of Cell Science. 2020;133(2).
18. Kossmann KJ, Ziegler C, Angelin A, Meyer R, Skoupi M, Rabe KS, et al. A Rationally Designed Connector for Assembly of Protein-Functionalized DNA Nanostructures. Chembiochem. 2016;17(12):1102-6.
19. Liu Y, Fares M, Dunham NP, Gao Z, Miao K, Jiang X, et al. AgHalo: A Facile Fluorogenic Sensor to Detect Drug-Induced Proteome Stress. Angew Chem Int Ed Engl. 2017;56(30):8672-6.
20. Liu Y, Miao K, Dunham NP, Liu H, Fares M, Boal AK, et al. The Cation-pi Interaction Enables a Halo-Tag Fluorogenic Probe for Fast No-Wash Live Cell Imaging and Gel-Free Protein Quantification. Biochemistry. 2017;56(11):1585-95.

21. Kang MG, Lee H, Kim BH, Dunbayev Y, Seo JK, Lee C, et al. Structure-guided synthesis of a protein-based fluorescent sensor for alkyl halides. Chem Commun (Camb). 2017;53(66):9226-9.
22. Newman J, Peat TS, Richard R, Kan L, Swanson PE, Affholter JA, et al. Haloalkane dehalogenases: structure of a Rhodococcus enzyme. Biochemistry. 1999;38(49):16105-14.
23. Deo C, Abdelfattah AS, Bhargava HK, Berro AJ, Falco N, Farrants H, et al. The HaloTag as a general scaffold for far-red tunable chemigenetic indicators. Nature chemical biology. 2021.
24. Jencks WP. On the attribution and additivity of binding energies. Proceedings of the National Academy of Sciences. 1981;78(7):4046-50.
25. Wade RC, Gabdoulline RR, Ludemann SK, Lounnas V. Electrostatic steering and ionic tethering in enzyme-ligand binding: insights from simulations. Proc Natl Acad Sci U S A. 1998;95(11):5942-9.
26. Sun X, Zhang A, Baker B, Sun L, Howard A, Buswell J, et al. Development of SNAP-Tag Fluorogenic Probes for Wash-Free Fluorescence Imaging. ChemBioChem. 2011;12(14):2217-26.
27. Wibley JEA. Crystal structure of the human O6-alkylguanine-DNA alkyltransferase. Nucleic Acids Research. 2000;28(2):393-401.
28. Mollwitz B, Brunk E, Schmitt S, Pojer F, Bannwarth M, Schiltz M, et al. Directed evolution of the suicide protein O(6)-alkylguanine-DNA alkyltransferase for increased reactivity results in an alkylated protein with exceptional stability. Biochemistry. 2012;51(5):986-94.
29. Perugino G, Vettone A, Illiano G, Valenti A, Ferrara MC, Rossi M, et al. Activity and Regulation of Archaeal DNA Alkyltransferase. Journal of Biological Chemistry. 2012;287(6):4222-31.
30. Rossi F, Morrone C, Massarotti A, Ferraris DM, Valenti A, Perugino G, et al. Crystal structure of a thermophilic O6-alkylguanine-DNA alkyltransferase-derived self-labeling protein-tag in covalent complex with a fluorescent probe. Biochemical and Biophysical Research Communications. 2018;500(3):698-703.
31. Lavis LD. Teaching Old Dyes New Tricks: Biological Probes Built from Fluoresceins and Rhodamines. Annual Review of Biochemistry. 2017;86(1):825-43.
32. Lukinavicius G, Umezawa K, Olivier N, Honigmann A, Yang G, Plass T, et al. A near-infrared fluorophore for live-cell super-resolution microscopy of cellular proteins. Nat Chem. 2013;5(2):132-9.
33. Wang L, Tran M, D'Este E, Roberti J, Koch B, Xue L, et al. A general strategy to develop cell permeable and fluorogenic probes for multicolour nanoscopy. Nat Chem. 2020;12(2):165-72.
34. Grimm JB, English BP, Chen J, Slaughter JP, Zhang Z, Revyakin A, et al. A general method to improve fluorophores for live-cell and single-molecule microscopy. Nat Methods. 2015;12(3):244-50, 3 p following 50.
35. Grimm JB, Muthusamy AK, Liang Y, Brown TA, Lemon WC, Patel R, et al. A general method to fine-tune fluorophores for live-cell and in vivo imaging. Nat Methods. 2017;14(10):987-94.
36. Wang L, Hiblot J, Popp C, Xue L, Johnsson K. Environmentally Sensitive Color-Shifting Fluorophores for Bioimaging. Angewandte Chemie. 2020;132(49):22064-8.
37. Juillerat A, Gronemeyer T, Keppler A, Gendreizig S, Pick H, Vogel H, et al. Directed Evolution of O6-Alkylguanine-DNA Alkyltransferase for Efficient Labeling of Fusion Proteins with Small Molecules In Vivo. Chemistry & Biology. 2003;10(4):313-7.
38. Gronemeyer T, Chidley C, Juillerat A, Heinis C, Johnsson K. Directed evolution of O6-alkylguanine-DNA alkyltransferase for applications in protein labeling. Protein Eng Des Sel. 2006;19(7):309-16.
39. Hiblot J, Yu Q, Sabbadini MDB, Reymond L, Xue L, Schena A, et al. Luciferases with Tunable Emission Wavelengths. Angew Chem Int Ed Engl. 2017;56(46):14556-60.
40. Zhang Y, So M-k, Loening AM, Yao H, Gambhir SS, Rao J. HaloTag Protein-Mediated Site-Specific Conjugation of Bioluminescent Proteins to Quantum Dots. Angewandte Chemie International Edition. 2006;45(30):4936-40.
41. Masharina A, Reymond L, Maurel D, Umezawa K, Johnsson K. A fluorescent sensor for GABA and synthetic GABA(B) receptor ligands. Journal of the American Chemical Society. 2012;134(46):19026-34.

42. Ueno Y, Jose J, Loudet A, Pérez-Bolívar Cs, Anzenbacher P, Burgess K. Encapsulated Energy-Transfer Cassettes with Extremely Well Resolved Fluorescent Outputs. Journal of the American Chemical Society. 2011;133(1):51-5.
43. Mudd G, Pi IP, Fethers N, Dodd PG, Barbeau OR, Auer M. A general synthetic route to isomerically pure functionalized rhodamine dyes. Methods and Applications in Fluorescence. 2015;3(4).
44. Bottanelli F, Kromann EB, Allgeyer ES, Erdmann RS, Wood Baguley S, Sirinakis G, et al. Two-colour live-cell nanoscale imaging of intracellular targets. Nature communications. 2016;7(1).
45. Keppler A, Pick H, Arrivoli C, Vogel H, Johnsson K. Labeling of fusion proteins with synthetic fluorophores in live cells. Proceedings of the National Academy of Sciences. 2004;101(27):9955-9.
46. Gibson DG, Young L, Chuang RY, Venter JC, Hutchison CA, 3rd, Smith HO. Enzymatic assembly of DNA molecules up to several hundred kilobases. Nat Methods. 2009;6(5):343-5.
47. Bertani G. Lysogeny at mid-twentieth century: P1, P2, and other experimental systems. J Bacteriol. 2004;186(3):595-600.
48. Rossi AM, Taylor CW. Analysis of protein-ligand interactions by fluorescence polarization. Nature Protocols. 2011;6(3):365-87.
49. Team RDC. R: A language and environment for statistical computing

Vienna, Austria: R Foundation for Statistical Computing; 2010.
50. Wickham H, Averick M, Bryan J, Chang W, McGowan L, François R, et al. Welcome to the Tidyverse. Journal of Open Source Software. 2019;4(43).
51. Kuzmič P. Program DYNAFIT for the Analysis of Enzyme Kinetic Data: Application to HIV Proteinase. Analytical Biochemistry. 1996;237(2):260-73.
52. Straume M, Johnson ML. Monte Carlo method for determining complete confidence probability distributions of estimated model parameters. Methods Enzymol. 1992;210:117-29.
53. Cabrita LD, Gilis D, Robertson AL, Dehouck Y, Rooman M, Bottomley SP. Enhancing the stability and solubility of TEV protease using in silico design. Protein Sci. 2007;16(11):2360-7.
54. Kabsch W. Xds. Acta Crystallogr D Biol Crystallogr. 2010;66(Pt 2):125-32.
55. McCoy AJ, Grosse-Kunstleve RW, Adams PD, Winn MD, Storoni LC, Read RJ. Phaser crystallographic software. Journal of applied crystallography. 2007;40(Pt 4):658-74.
56. Smart OS, Womack TO, Sharff A, Flensburg C, Keller P, Paciorek W, et al. Grade Web Server. 2011.
57. Emsley P, Lohkamp B, Scott WG, Cowtan K. Features and development of Coot. Acta crystallographica Section D, Biological crystallography. 2010;66(Pt 4):486-501.
58. Murshudov GN, Skubak P, Lebedev AA, Pannu NS, Steiner RA, Nicholls RA, et al. REFMAC5 for the refinement of macromolecular crystal structures. Acta crystallographica Section D, Biological crystallography. 2011;67(Pt 4):355-67.
59. Adams PD, Afonine PV, Bunkoczi G, Chen VB, Davis IW, Echols N, et al. PHENIX: a comprehensive Python-based system for macromolecular structure solution. Acta crystallographica Section D, Biological crystallography. 2010;66(Pt 2):213-21.
60. Chen VB, Arendall WB, 3rd, Headd JJ, Keedy DA, Immormino RM, Kapral GJ, et al. MolProbity: all-atom structure validation for macromolecular crystallography. Acta crystallographica Section D, Biological crystallography. 2010;66(Pt 1):12-21.
61. DeLano WL. Pymol: An open-source molecular graphics tool. CCP4 Newsletter On Protein. Crystallography. 2002;40:82-92.
62. Adams PD, Afonine PV, Bunkóczi G, Chen VB, Davis IW, Echols N, et al. PHENIX: a comprehensive Python-based system for macromolecular structure solution. Acta Crystallogr D Biol Crystallogr. 2010;66(Pt 2):213-21.
63. Jurrus E, Engel D, Star K, Monson K, Brandi J, Felberg LE, et al. Improvements to the APBS biomolecular solvation software suite. Protein Sci. 2018;27(1):112-28.

64. Dolinsky TJ, Czodrowski P, Li H, Nielsen JE, Jensen JH, Klebe G, et al. PDB2PQR: expanding and upgrading automated preparation of biomolecular structures for molecular simulations. Nucleic Acids Res. 2007;35(Web Server issue):W522-5.

Supplementary information

for

Kinetic and structural characterization of the self-labeling protein tags HaloTag7, SNAP-tag and CLIP-tag

Jonas Wilhelm[1,9], Stefanie Kühn[1,9], Miroslaw Tarnawski[2], Guillaume Gotthard[3,7], Jana Tünnermann[1], Timo Tänzer[4], Julie Karpenko[4,8], Nicole Mertes[1], Lin Xue[1], Ulrike Uhrig[5], Jochen Reinstein[6], Julien Hiblot[1,4,10]* and Kai Johnsson[1,4,10]*.

[1]Department of Chemical Biology, Max Planck Institute for Medical Research, Heidelberg, Germany.

[2]Protein Expression and Characterization Facility, Max Planck Institute for Medical Research, Heidelberg, Germany.

[3] Structural Biology Group, European Synchrotron Radiation Facility (ESRF), Grenoble, France.

[4]Institute of Chemical Sciences and Engineering, École Polytechnique Fédérale de Lausanne (EPFL), Lausanne, Switzerland.

[5]Chemical Biology Core Facility, European Molecular Biology Laboratory, Heidelberg, Germany.

[6]Department of Biomolecular Mechanisms, Max Planck Institute for Medical Research, Heidelberg, Germany.

[7]Present addresses: Division of Biology and Chemistry–Laboratory for Biomolecular Research, Paul Scherrer Institute, Villigen, Switzerland. Department of Biology, Institute of Molecular Biology and Biophysics, ETH Zürich, Zürich, Switzerland.

[8]Present address: Laboratoire d'Innovation Thérapeutique, UMR7200 CNRS/Université de Strasbourg, Strasbourg Drug Discovery and Development Institute (IMS), 74 route du Rhin, 67401 Illkirch-Graffenstaden, France.

[9]These authors contributed equally: Jonas Wilhelm, Stefanie Kühn.

[10]These authors contributed equally: Julien Hiblot, Kai Johnsson.

* e-mail: julien.hiblot@mr.mpg.de; johnsson@mr.mpg.de

Supplementary information table of content

Chemical Synthesis

General information

All chemical reagents and (anhydrous) solvents for synthesis were purchased from commercial suppliers (Merck KGaA, Darmstadt, Germany; Honeywell, Charlotte, NC, USA; TCI, Tokyo, Japan; Thermo Fisher Scientific, Waltham, MA, USA; SiChem, Bremen, Germany) and were used without further purification or distillation. Anhydrous solvents were handled under argon atmosphere. SLP substrates were purchased from commercial sources, synthesized according to published procedures or gifts from colleagues. Details are given in **Material Table**.

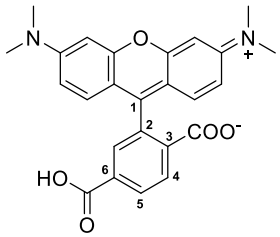

^{1}H- and ^{13}C-NMR spectra were recorded in deuterated solvents on a Bruker (Bruker Corp., Billerica, MA, USA) DPX400 (400 MHz for ^{1}H, 101 MHz for ^{13}C, respectively) or on a Bruker AVANCE III HD 400 (400 MHz for ^{1}H, 101 MHz for ^{13}C, respectively) equipped with a CryoProbe. Chemical shifts (δ) are reported in ppm referenced to the residual solvent peaks of DMSO-d_6 (δ_H = 2.50 ppm, δ_C = 39.52 ppm), acetone-d_6 (δ_H = 2.05 ppm, $\delta_C(CH_3)$ = 29.84 ppm, $\delta_C(CO)$ = 206.26 ppm) or $CDCl_3$ (δ_H = 7.26 ppm, δ_C = 77.16 ppm). Coupling constants J are reported in Hz and corresponding multiplicities are abbreviates as follows: s = singlet, d = doublet, t = triplet, q = quartet, p = pentet, m = multiplet and br = broad.

Reaction progress was monitored by thin layer chromatography (TLC) (Silica gel 60G F_{254} on TLC glass plates) in appropriate solvents. Reaction spots were visualized under UV lamp (254 nm or 366 nm) and/or by staining solutions. LC-MS was performed on a Shimadzu MS2020 (Shimadzu Corp., Kyoto, Japan) connected to a Nexera UHPLC system equipped with a Waters (Waters Crop., Milford, MA, USA) ACQUITY UPLC BEH C18 (1.7 µm, 2.1x50 mm) column. Buffer A: 0.1% formic acid in H_2O, Buffer B: acetonitrile. Measurements were done with an analytical gradient from 10% to 90% B over 6 min or from 1% to 90% B over 10 min.

Normal phase flash chromatography was performed on self-packed silica gel (60 M, 0.04 - 0.063 mm, Macherey-Nagel GmbH & Co. KG, Düren, Germany) columns or by using an Isolera One system (Biotage Sweden AB, Uppsala, Sweden) using pre-packed silica gel columns (ultra pure silica gel 12 g or 25 g). Solvent compositions are reported individually in parentheses.

Preparative reversed phase high-performance liquid chromatography (RP-HPLC) was conducted using a Waters SunFire™ Prep C18 OBDTM column (10 × 150 mm, 5 µm pore size, 4 mL/min. flow rate) or an Ascentis (Merck KGaA, Darmstadt, Germany) C18 column (10 × 250 mm, 5 µm pore size, 8 mL/min. flow rate) on either a Waters Alliance e2695 separation module connected to a 2998 PDA detector or a Dionex system equipped with an UVD (170 U, UV-Vis detector). Solvent A: 0.1%TFA in H_2O, Solvent B: acetonitrile.

High resolution mass spectra (HRMS) were measured by the MS-service of the EPF Lausanne (SSMI) on a Waters Xevo® G2-S Q-Tof spectrometer (Waters, Milford, MA, USA) with electron spray ionization (ESI) or by the MS-facility of the Max Planck Institute for Medical Research on a Bruker maXis IITM ETD.

Material Table: Substrate and chemical source used in the study

	Substrate	Source / reference
General	CPY-6-COOH	Butkevich *et al.,* (2016) (1)
	CPY-5-COOH	Butkevich *et al.,* (2016) (1)
	TMR-5-COOH	Mudd *et al.,* (2015) (2)
	TMR-6-COOH	Mudd *et al.,* (2015) (2)
	Cy3-COOH	Ueno *et al.,* (2011) (3)
	Cy5-COOH	Ueno *et al.,* (2011) (3)
	SiR-COOH	Lukinavicius *et al.,* (2013) (4)
	meAm-6-TMR	this study
	meAm-5-TMR	this study
	meAm-6-CPY	this study
	meAm-5-CPY	this study
HaloTag substrates	CA-TMR	Purchased from Promega, Madison, WI, USA
	CA-Alexa488	Purchased from Promega, Madison, WI, USA
	CA-Fluorescein	Purchased from Promega, Madison, WI, USA
	CA-Oregon green	Purchased from Promega, Madison, WI, USA
	CA-JF549	Gift from Dr. Luke Lavis, HHMI, Ashburn, VA, USA
	CA-JF503	Gift from Dr. Luke Lavis, HHMI, Ashburn, VA, USA
	CA-JF525	Gift from Dr. Luke Lavis, HHMI, Ashburn, VA, USA
	CA-JF608	Gift from Dr. Luke Lavis, HHMI, Ashburn, VA, USA
	CA-JF669	Gift from Dr. Luke Lavis, HHMI, Ashburn, VA, USA
	CA-TMR-az-F_4	Gift from Dr. Luke Lavis, HHMI, Ashburn, VA, USA
	CA-TMR-CN	Wang *et al.,* (2020) (5)
	CA-TMR-SCH_3	Wang *et al.,* (2020) (5)
	CA-TMR-SNH_2	Wang *et al.,* (2020) (5)
	CA-MaP555	Wang *et al.,* (2020) (5)
	CA-CPY	Butkevich *et al.,* (2016) (1)
	CA-500R	Butkevich *et al.,* (2016) (1)
	CA-510R	Purchased from Abberior GmbH, Göttingen, Germany
	CA-515R	Purchased from Abberior GmbH, Göttingen, Germany
	CA-580CP	Gift from Dr. Alexey N. Butkevich, MPI-MF, Heidelberg, Germany
	CA-LIVE580	Purchased from Abberior GmbH, Göttingen, Germany
	CA-Cy3	this study
	CA-Cy5	this study
	CA-TMR-biotin	this study
	CA-PEG-biotin	Purchased from Promega, Madison, WI, USA
	CA-Ac	this study
	CA-N_3	this study
	CA-Nor1	this study
	CA-Nor2	this study
	CA-Tz	this study

	CA-PhN_3	this study
	CA-Vbn	this study
	CA-BCN	this study
	CA-SCO	this study
SNAP substrates	BG	Purchased from Santa Cruz Biotechnology, Dallas, TX, USA
	CP	this study
	BG-NH_2	Keppler *et al.,* (2003) (6)
	CP-NH_2	Srikun *et al.*, (2010) (7)
	BG-TMR	Keppler *et al.,* (2004) (8)
	CP-TMR	Correa *et al.*, (2013) (9)
	BG-Alexa488	Purchased from NEB as SNAP-Surface® Alexa Fluor® 488, Ipswitch, MA, USA
	CP-Alexa488	this study
	BG-Fluorescein	Keppler *et al.,* (2003) (6)
	CP-Fluorescein	this study
	BG-CPY	Hiblot *et al.,* (2017) (10)
	CP-CPY	this study
	BG-5-TMR	this study
	BG-5-CPY	this study
	BG-MaP555	Wang *et al.,* (2020) (5)
	BG-SiR	Lukinavicius *et al.,* (2013) (4)
	CP-SiR	this study
	BG-JF549	Grimm *et al.,* (2015) (11)
	BG-JF646	Grimm *et al.,* (2015) (11)
	BG-Cy3	this study
	BG-sulfo-Cy3	Gautier *et al.,* (2008) (12)
	BG-Cy5	this study
	BG-sulfo-Cy5	Gautier *et al.,* (2008) (12)
	BG-Atto565	Correa *et al.,* (2013) (9)
	BG-Atto590	Bottanelli *et al.,* (2016) (13)
	BG-N_3	this study
	CP-N_3	this study
	BG-Nor2	this study
	CP-Nor2	this study
	BG-Tz	this study
	CP-Tz	this study
	BG-PhN_3	this study
	CP-PhN_3	this study
	BG-Vbn	this study
	CP-Vbn	this study
	BG-BCN	this study
	CP-BCN	this study
	BG-Ac	this study
	CP-Ac	this study

	BG-SCO	this study
	CP-SCO	this study
CLIP substrates	BC-NH_2	Gautier *et al.,* (2008) (12)
	BC-TMR	Gautier *et al.,* (2008) (12)
	BC-Alexa488	Purchased from NEB as CLIP-Surface® Alexa Fluor® 488, Ipswitch, MA, USA
	BC-Fluorescein	Gautier *et al.,* (2008) (12)
	BC-CPY	this study

Chemical Synthesis

1.1 Synthesis of substrate amines

1.1.1 2-(2-((6-chlorohexyl)oxy)ethoxy)ethan-1-amine (CA-NH_2)

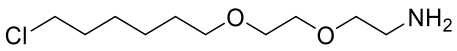

CA-NH_2 was synthesized according to the procedure from Zhang *et al*. 2006 (14).

1.1.2 6-((4-(aminomethyl)benzyl)oxy)-9*H*-purin-2-amine (BG-NH_2)

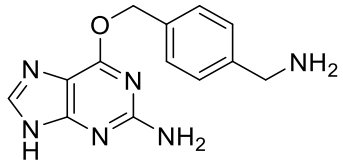

BG-NH_2 was synthesized according to the procedure from Keppler *et al*. 2003 (6).

1.1.3 4-((4-(aminomethyl)benzyl)oxy)-6-chloropyrimidin-2-amine (CP-NH_2)

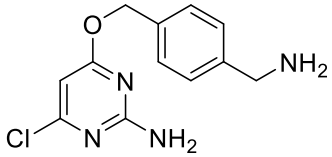

CP-NH_2 was synthesized according to the procedure from Srikun *et al*. 2010 (7).

1.1.4 2-((4-(aminomethyl)benzyl)oxy)pyrimidin-4-amine (BC-NH_2)

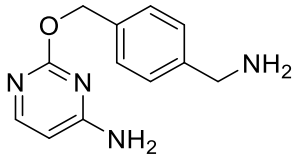

BC-NH_2 was synthesized according to the procedure from Gautier *et al*. 2008 (12).

1.2 General procedure A for peptide coupling reactions

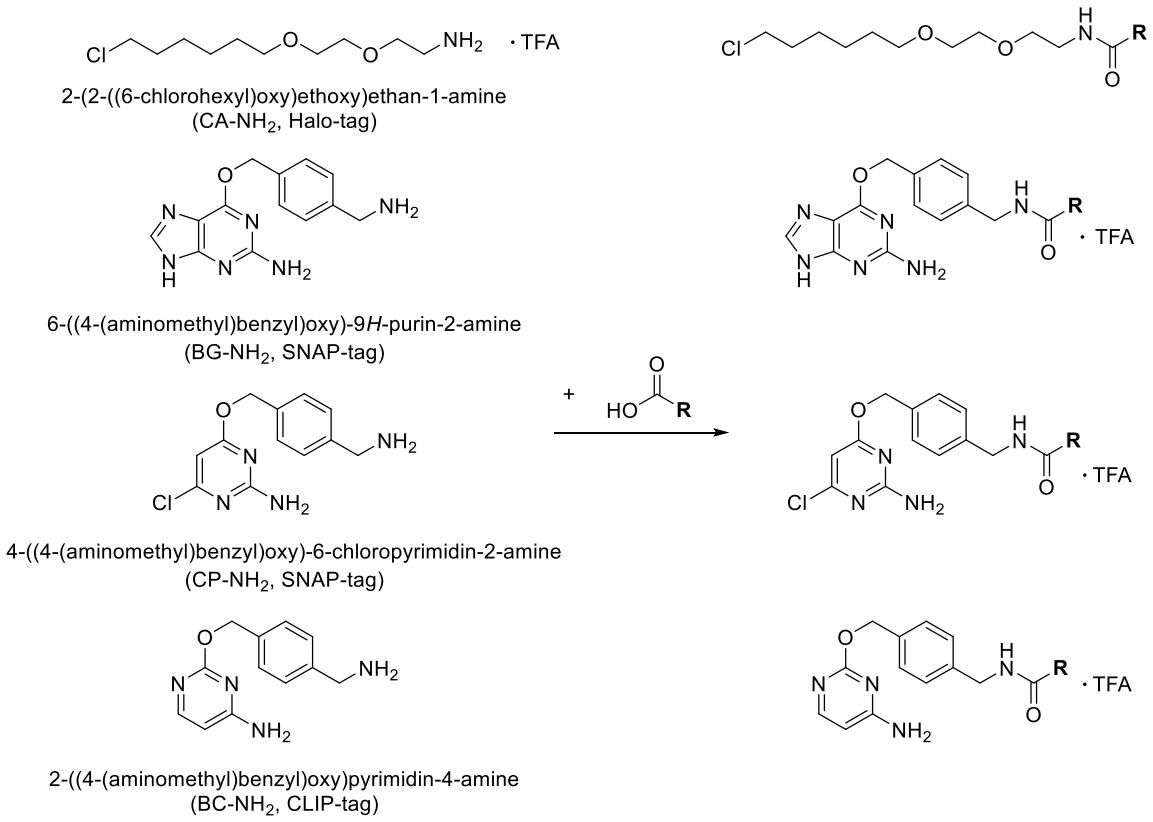

To a solution of TSTU (1.2 equiv.) in dry DMSO (0.3 mL), DIPEA (10.2 equiv. for Halo-tag-, 5.0 equiv. for SNAP-substrates) and different carboxylic acids (1.1 equiv.) were added. After 5 min., a solution of 10 mg of corresponding amine (1.0 equiv.) in dry DMSO (0.1 mL) was added and the reaction mixture was stirred at r.t. for 2 hours. The reaction mixture was quenched by addition of water (100 µL) and acidified with acetic acid (50 µL), then purified by semi-preparative HPLC, eluted with a gradient of MeCN/H_2O + 0.1% TFA (equilibration at 15% MeCN for 5 min, then gradient of 15 - 100% MeCN over 25 min, followed by 100% MeCN for 10 min.). Fractions containing the desired product were combined and lyophilized. Final compounds were stored as DMSO stocks for biochemical testing.

1.3 HT7 substrates

1.3.1 2-azido-N-(2-(2-((6-chlorohexyl)oxy)ethoxy)ethyl)acetamide (CA-N_3)

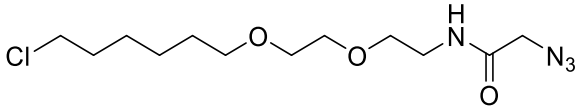

Reaction was conducted according to general procedure A using CA-NH_2 and 2-azidoacetic acid (4.6 µL, 32.6 µmol). The desired product (4.6 mg, 15.0 µmol) was obtained as a yellowish oil in 51% yield.

^{1}H NMR (400 MHz, DMSO-d_6) δ [ppm] = 8.15 (t, J = 5.8 Hz, 1H), 3.81 (s, 2H), 3.62 (t, J = 6.6 Hz, 2H), 3.53 – 3.40 (m, 6H), 3.37 (t, J = 6.6 Hz, 2H), 3.24 (dd, J = 5.7 Hz, J = 5.8 Hz, 2H), 1.75 – 1.65 (m, 2H), 1.54 – 1.43 (m, 2H), 1.43 – 1.25 (m, 4H).

^{13}C NMR (101 MHz, DMSO-d_6) δ [ppm] = 167.31, 70.17, 69.56, 69.40, 68.83, 50.69, 45.36, 38.67, 32.00, 29.04, 26.10, 24.91.

HRMS (ESI): calc. for $C_{12}H_{23}ClN_4NaO_3^+$ [M+Na]$^+$: 329.1351; found 329.1354.

1.3.2 (1R,4R)-N-(2-(2-((6-chlorohexyl)oxy)ethoxy)ethyl)bicyclo[2.2.1]hept-5-ene-2-carboxamide (CA-Nor1)

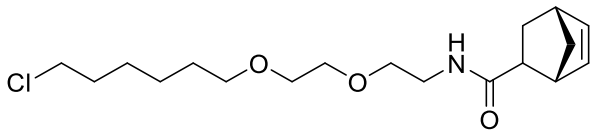

Reaction was conducted according to general procedure A using CA-NH_2 and (1R,4R)-bicyclo[2.2.1]hept-5-ene-2-carboxylic acid (6.2 µL, 32.6 µmol). The desired endo-isomer (5.6 mg, 16.3 µmol) of was obtained in 55% yield.

^{1}H NMR (400 MHz, DMSO-d_6) δ [ppm] = 7.59 (t, J = 5.7 Hz, 1H), 6.08 (dd, J = 5.8, 3.1 Hz, 1H), 5.80 (dd, J = 5.8, 3.0 Hz, 1H), 3.62 (t, J = 6.6 Hz, 2H), 3.54 – 3.30 (m, 8H), 3.23 – 3.02 (m, 3H), 2.84 – 2.71 (m, 2H), 1.77 – 1.63 (m, 3H), 1.55 – 1.43 (m, 2H), 1.42 – 1.18 (m, 7H).

^{13}C NMR (101 MHz, DMSO-d_6) δ [ppm] = 172.86, 136.76, 132.18, 70.18, 69.58, 69.45, 69.09, 49.35, 45.59, 45.37, 43.25, 42.08, 38.55, 32.02, 29.09, 28.35, 26.13, 24.94.

HRMS (ESI) calc. for $C_{18}H_{31}ClNO_3^+$ $[M+H]^+$: 344.1987; found 344.1989.

1.3.3 2-((1S,4S)-bicyclo[2.2.1]hept-5-en-2-yl)-N-(2-(2-((6-chlorohexyl)oxy)ethoxy)ethyl)acetamide (CA-Nor2)

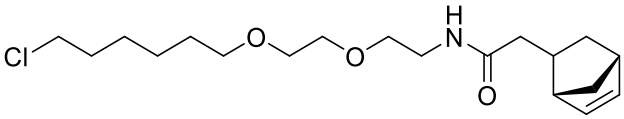

Reaction was conducted according to general procedure A using CA-NH_2 and 2-((1S,4S)-bicyclo[2.2.1]hept-5-en-2-yl)acetic acid (5.6 µL, 32.6 µmol) yielding 6.4 mg (17.9 µmol) of the desired product as a colorless oil in 60% yield.

^{1}H NMR (400 MHz, DMSO-d_6) δ [ppm] = 7.73 (t, J = 5.7 Hz, 1H), 6.15 (dd, J = 5.8, 3.0 Hz, 1H), 5.95 (dd, J = 5.8, 2.9 Hz, 1H), 3.62 (t, J = 6.6 Hz, 2H), 3.47 – 3.36 (m, 8H), 3.23 – 3.09 (m, 2H), 2.76 – 2.68 (m, 2H), 2.40 – 2.29 (m, 1H), 1.89 – 1.74 (m, 3H), 1.74 – 1.65 (m, 2H), 1.53 – 1.43 (m, 2H), 1.39 – 1.17 (m, 6H), 0.47 (m, J = 11.5, 4.4, 2.6 Hz, 1H).

^{13}C NMR (101 MHz, DMSO-d_6) δ [ppm] = 171.61, 136.88, 132.47, 70.15, 69.52, 69.42, 69.08, 49.03, 45.32, 45.13, 42.02, 40.58, 40.14, 39.93, 39.73, 39.51, 39.31, 39.10, 38.89, 38.35, 35.06, 31.99, 31.37, 29.04, 26.08, 24.89.

HRMS (ESI) calc. for $C_{19}H_{32}ClNNaO_3^+$ $[M+Na]^+$: 380.1963; found 380.1963.

1.3.4 N-(2-(2-((6-chlorohexyl)oxy)ethoxy)ethyl)-2-(4-(6-methyl-1,2,4,5-tetrazin-3-yl)phenyl)acetamide (CA-Tz)

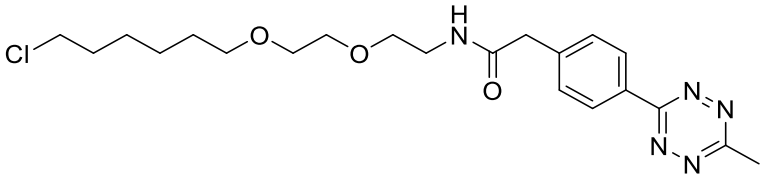

Reaction was conducted according to general procedure A using CA-NH_2 and 2-(4-(6-methyl-1,2,4,5-tetrazin-3-yl)phenyl)acetic acid (7.5 mg, 32.6 µmol) yielding 7.4 mg (17.0 µmol) of the desired product as a rose solid in 57% yield.

^{1}H NMR (400 MHz, DMSO-d_6) δ [ppm] = 8.44 – 8.36 (m, 2H), 8.23 (t, J = 5.6 Hz, 1H), 7.58 – 7.50 (m, 2H), 3.61 (t, J = 6.6 Hz, 2H), 3.56 (s, 2H), 3.53 – 3.40 (m, 6H), 3.36 (t, J = 6.6 Hz, 2H), 3.23 (q, J = 5.7 Hz, 2H), 2.99 (s, 3H), 1.75 – 1.62 (m, 2H), 1.53 – 1.42 (m, 2H), 1.42 – 1.25 (m, 4H).

^{13}C NMR (101 MHz, DMSO-d_6) δ [ppm] = 169.58, 167.05, 163.22, 141.29, 130.05, 130.00, 127.28, 70.20, 69.60, 69.45, 69.05, 45.37, 42.19, 38.79, 32.02, 29.07, 26.12, 24.93, 20.83.

HRMS (ESI) calc. for $C_{21}H_{31}ClN_5O_3^+$ $[M+H]^+$: 436.2110; found 436.2113.

1.3.5 4-azido-N-(2-(2-((6-chlorohexyl)oxy)ethoxy)ethyl)benzamide (CA-PhN$_3$)

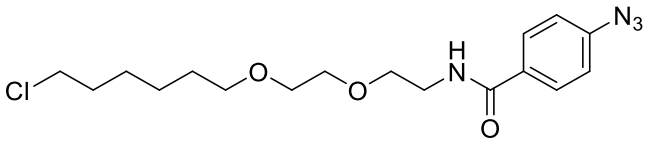

Reaction was conducted according to general procedure A using CA-NH$_2$ and 4-azidobenzoic acid (5.3 mg, 32.6 µmol) to obtain 6.1 mg (15.5 µmol) of the desired product as a colorless oil in 56% yield.

^{1}H NMR (400 MHz, DMSO-d_6) δ [ppm] = 8.52 (t, J = 5.6 Hz, 1H), 7.90 (d, J = 8.6 Hz, 2H), 7.20 (d, J = 8.6 Hz, 2H), 3.60 (t, J = 6.6 Hz, 2H), 3.56 – 3.49 (m, 4H), 3.50 – 3.44 (m, 2H), 3.44 – 3.30 (m, 4H), 1.74 – 1.61 (m, 2H), 1.51 – 1.39 (m, 2H), 1.40 – 1.20 (m, 4H).

^{13}C NMR (101 MHz, DMSO-d_6) δ [ppm] = 165.23, 142.19, 130.95, 129.06, 118.85, 70.17, 69.62, 69.40, 68.84, 45.35, 39.21, 32.00, 29.07, 26.12, 24.91.

HRMS (ESI) calc. for $C_{17}H_{25}ClN_4NaO_3^+$ [M+Na]$^+$: 391.1507; found 391.1511.

1.3.5.1 N-(2-(2-((6-chlorohexyl)oxy)ethoxy)ethyl)-4-vinylbenzamide (CA-Vbn)

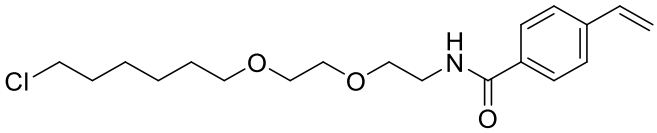

Reaction was conducted according to general procedure A using CA-NH$_2$ and 4-vinylbenzoic acid (4.8 mg, 32.6 µmol) to obtain 7.5 mg (21.2 µmol) of the desired product as a colorless oil in 72% yield.

^{1}H NMR (400 MHz, DMSO-d_6) δ [ppm] = 8.49 (t, J = 5.6 Hz, 1H), 7.83 (d, J = 8.2 Hz, 2H), 7.55 (d, J = 8.2 Hz, 2H), 6.78 (dd, J = 17.7, 10.9 Hz, 1H), 5.94 (d, J = 17.7 Hz, 1H), 5.36 (d, J = 10.9 Hz, 1H), 3.62 – 3.57 (m, 2H), 3.55 – 3.51 (m, 4H), 3.49 – 3.45 (m, 2H), 3.44 – 3.37 (m, 4H), 1.73 – 1.59 (m, 2H), 1.50 – 1.40 (m, 2H), 1.40 – 1.24 (m, 4H).

^{13}C NMR (101 MHz, DMSO-d_6) δ [ppm] = 166.28, 140.15, 136.39, 134.03, 127.99, 126.41, 116.59, 70.66, 70.11, 69.88, 69.33, 45.84, 39.67, 32.48, 29.55, 26.59, 25.39.

HRMS (ESI) calc. for $C_{19}H_{28}ClNNaO_3^+$ [M+Na]$^+$: 376.1650; found 376.1640.

1.3.6 ((1*R*,8*S*,9*s*)-bicyclo[6.1.0]non-4-yn-9-yl)methyl (2-(2-((6-chlorohexyl)oxy)ethoxy)ethyl)carbamate (CA-BCN)

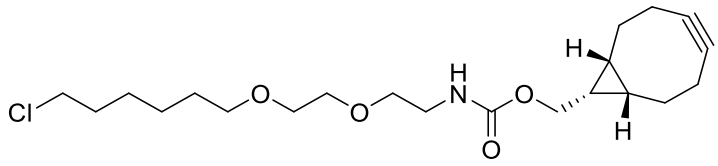

BCN-NHS (14.0 mg, 47.6 µmol, 1.1 eq) was dissolved in 500 µL DMSO. DIPEA (71.4 µL, 432 µmol, 10 equiv.) was added followed by CA-NH$_2$ (14.0 mg, 43.2 µmol, 1.0 equiv.) solubilized in DMSO. The solution was stirred for 30 min. The crude product was purified by preparative HPLC eluted with MeCN / H$_2$O (0.1% TFA) (50% - 90% MeCN over 60 min) to obtain 11.9 mg (29.8 µmol) of the product as a clear oil in 69% yield after lyophilization.

^{1}H NMR (400 MHz, DMSO-d6): δ = 7.07 (t, J=5.7, 1H), 4.03 (d, J=8.0, 2H), 3.62 (t, J=6.6, 2H), 3.52 – 3.44 (m, 4H), 3.38 (dt, J=11.3, 6.3, 4H), 3.11 (q, J=6.0, 2H), 2.30 – 2.06 (m, 6H), 1.78 – 1.64 (m, 2H), 1.59 – 1.42 (m, 4H), 1.41 – 1.19 (m, 4H), 0.95 – 0.78 (m, 2H).

^{13}C NMR (100 MHz, DMSO-d_6): δ = 156.4, 99.0, 70.2, 69.5, 69.4, 69.1, 61.3, 45.4, 40.1, 32.0, 29.1, 28.6, 26.1, 24.9, 20.8, 19.5, 17.6.

HRMS (ESI) calc. for [M+H]$^+$: 400.2249, found 400.2250.

1.3.6.1 Cyclooct-2-yn-1-yl (2-(2-((6-chlorohexyl)oxy)ethoxy)ethyl)carbamate (CA-SCO)

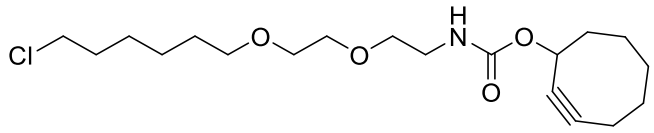

CA-NH_2 (15 mg, 44.4 µmol, 1.3 equiv.) was dissolved in dry DMSO (0.15 mL) and a solution of cyclooct-2-yn-1-yl (4-nitrophenyl) carbonate (10 mg, 34.2 µmol, 1.0 equiv.) in dry DMF (0.4 mL) was added followed by DIPEA (58 µL, 348 µmol: 10.2 equiv.). The reaction mixture was stirred at r.t. for 1h. The resulted mixture was acidified with 50 µL of acetic acid and afterwards purified by semi-preparative HPLC eluted with MeCN / H_2O (0.1% TFA) (15% MeCN for 2 min., then 15 - 100% MeCN over 25 min., followed by 100% MeCN for 15 min.) to give 8.7 mg (23.3 µmol) of the desired product as a colorless oil in 68% yield after lyophilization.

^{1}H NMR (400 MHz, DMSO-d_6) δ [ppm] = 7.18 (t, J = 5.9 Hz, 1H), 5.18 – 5.09 (m, 1H), 3.62 (t, J = 6.6 Hz, 2H), 3.50 – 3.43 (m, 4H), 3.40 – 3.34 (m, 4H), 3.09 (q, J = 5.9 Hz, 2H), 2.30 – 2.00 (m, 3H), 1.93 – 1.78 (m, 3H), 1.76 – 1.65 (m, 3H), 1.64 – 1.54 (m, 2H), 1.53 – 1.43 (m, 3H), 1.42 – 1.25 (m, 4H).

^{13}C NMR (101 MHz, DMSO-d_6) δ [ppm] = 155.29, 100.82, 91.79, 70.19, 69.53, 69.42, 68.99, 65.70, 45.38, 41.59, 40.07, 33.85, 32.03, 29.21, 29.06, 26.13, 25.78, 24.94, 19.95.

HRMS (ESI) calc. for $C_{19}H_{32}ClNNaO_4^+$ $[M+Na]^+$; 396.1912; found 396.1923.

1.3.7 *N*-(2-(2-((6-chlorohexyl)oxy)ethoxy)ethyl)acetamide (CA-Ac)

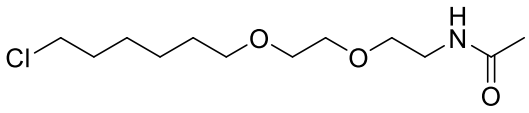

Tert-butyl (2-(2-((6-chlorohexyl)oxy)ethoxy)ethyl)carbamate (301 mg, 0.93 µmol, 1.0 equiv.) was deprotected by addition of TFA (2 mL) and afterwards dried under a stream of pressured air for 15 min. DIPEA (307 µL, 1.86 mmol, 2.0 equiv.) and DMSO (333 µL) were added followed by dropwise addition of acetic anhydride (131 µL, 1.39 mmol, 1.5 equiv.) while stirring. The reaction was stirred at r.t for 1 h. The mixture was quenched with saturated solution of $NaHCO_3$ (20 mL) and extracted with DCM (3 × 20 mL). The combined organic layers were washed with brine and dried over MgSO4. All volatiles were evaporated and the crude product was purified over normal phase flash chromatography (MeOH: DCM = 2% : 98% to 3% : 97%). The fractions containing the product were combined to give 238 mg (896 µmol) of the desired product as a colorless oil in 97% yield after evaporation.

^{1}H NMR (400 MHz, $CDCl_3$) δ [ppm] = 6.05 (s, 1H), 3.67 – 3.38 (m, 12H), 1.98 (s, 3H), 1.83 – 1.71 (m, 2H), 1.61 (p, J = 6.8 Hz, 2H), 1.52 – 1.31 (m, 4H).

^{13}C NMR (101 MHz, $CDCl_3$) δ [ppm] = 169.92, 71.09, 70.07, 69.83, 69.60, 44.84, 39.10, 32.32, 29.28, 26.49, 25.24, 23.10.

HRMS (ESI) calc. for $C_{12}H_{25}ClNO_3^+$ $[M+H]^+$: 266.1517; found 266.1518.

1.3.1 5-((2-(2-((6-chlorohexyl)oxy)ethoxy)ethyl)carbamoyl)-2-(6-(dimethylamino)-3-(dimethyliminio)-3H-xanthen-9-yl)benzoate (CA-5-TMR)

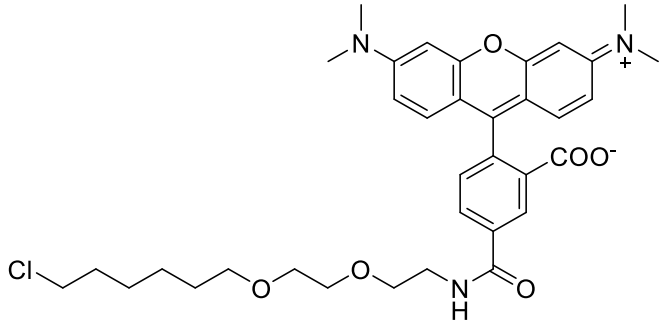

To a solution of TMR-5-COOH (2.5 mg, 5.81 µmol, 1.0 equiv.) in dry DMSO (500 µL), benzotriazolyloxytris(dimethylamino)-phosphonium hexafluorophosphat (BOP) (0.5 M in DMSO, 16.4 µL, 8.21 µmol, 1.5 equiv.) was added and the reaction was shaken at 500 rpm and r.t. for 5 min. DIPEA (3.84 µL, 23.2 µmol, 4.0 equiv.) and CA-NH_2 (1 M in DMSO, 8.71 µL, 8.71 µmol, 1.5 equiv.) were added and the reaction was shaken at 500 rpm and r.t. for 4 h. The crude product was acidified with acetic acid and purified over preparative HPLC eluted with MeCN / H_2O (0.1% FA) (10% - 90% MeCN over 50 min) to give 1.2 mg (1.89 µmol) of the desired product in 33% yield after lyophilization.

HRMS (ESI): calc. for $C_{36}H_{44}N_2O_6Cl^+$ $[M+H]^+$: 635.2887; found 635.2882.

1.3.2 5-((2-(2-((6-chlorohexyl)oxy)ethoxy)ethyl)carbamoyl)-2-(6-(dimethylamino)-3-(dimethyliminio)-10,10-dimethyl-3,10-dihydroanthracen-9-yl)benzoate (CA-5-CPY)

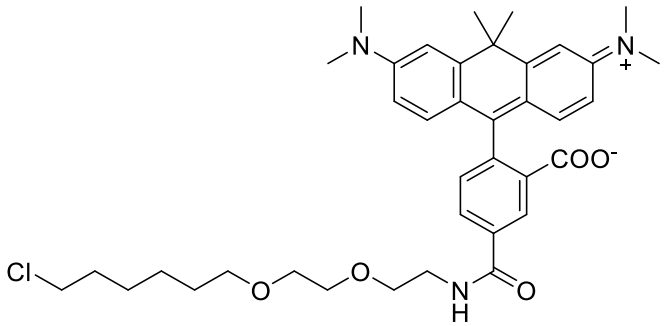

To a solution of CPY-5-COOH (2.5 mg, 5.48 µmol, 1.0 equiv.) in dry DMSO (1 mL), BOP (0.5 M in DMSO, 16.4 µL, 8.21 µmol, 1.5 equiv.) was added and the reaction was shaken at 500 rpm and r.t. for 5 min. DIPEA (3.62 µL, 21.9 µmol, 4.0 equiv.) and CA-NH_2 (1 M in DMSO, 8.21 µL, 8.21 µmol, 1.5 equiv.) were added and the reaction was shaken at 500 rpm and r.t. for 4 h. The crude product was acidified with acetic acid and purified over preparative HPLC eluted with MeCN / H_2O (0.1% FA) (10% - 90% MeCN over 50 min) to give 0.38 mg (0.57 µmol) of the desired product in 10% yield after lyophilization.

HRMS (ESI): calc. for $C_{38}H_{49}N_3O_5Cl^+$ $[M+H]^+$: 662.3360; found 662.3349.

1.3.3 1-(6-((2-(2-((6-chlorohexyl)oxy)ethoxy)ethyl)amino)-6-oxohexyl)-3,3-dimethyl-2-((E)-3-((Z)-1,3,3-trimethylindolin-2-ylidene)prop-1-en-1-yl)-3H-indol-1-ium (CA-Cy3)

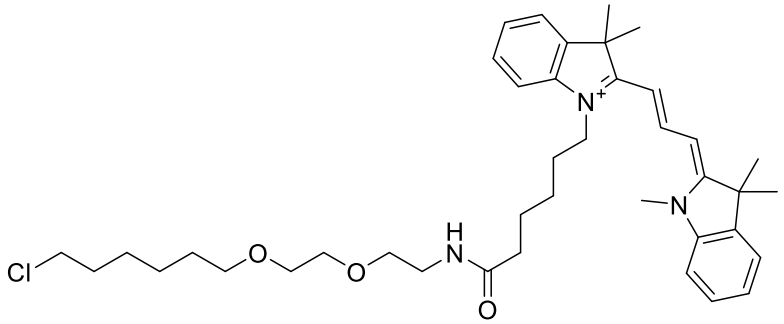

Cy3-COOH was synthesized according to Ueno et al. 2010 (3). To a solution of Cy3-COOH (100 mg, 219 µmol, 1.0 equiv.) in dry DMSO (2 mL), DIPEA (217 µL, 1.3 mmol, 6.0 equiv.) and TSTU (92.1 mg, 306 µmol, 1.4 equiv.) were added and the reaction mixture was stirred for 10 min. at r.t. CA-NH_2 (58 mg, 262 µmol, 1.2 equiv.) in 0.5 mL DMSO was added and the reaction was stirred for 30 min, at r.t. The reaction was quenched by addition of acetic acid (230 µL) and 10% H_2O, followed by purification over preparative HPLC eluted with MeCN / H_2O (0.1% FA) (10% - 90% MeCN over 60 min) to give 102 mg (154 µmol) of the desired product in 70% yield after lyophilization.

HRMS (ESI): calc. for $C_{40}H_{57}N_3O_3Cl^+$ $[M]^+$: 662.4083; found 662.4084.

1.3.4 1-(6-((2-(2-((6-chlorohexyl)oxy)ethoxy)ethyl)amino)-6-oxohexyl)-3,3-dimethyl-2-((1E,3E)-5-((Z)-1,3,3-trimethylindolin-2-ylidene)penta-1,3-dien-1-yl)-3H-indol-1-ium (CA-Cy5)

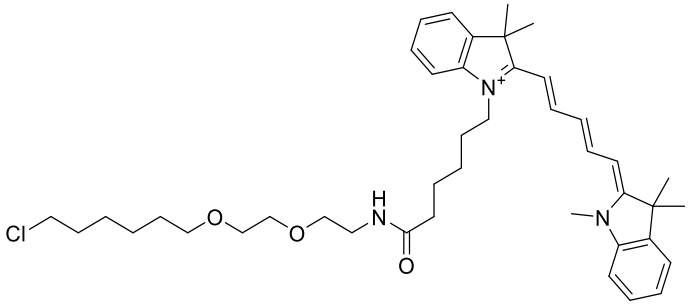

Cy5-COOH was synthesized according to Ueno et al. 2010 (3). To a solution of Cy5-COOH (100 mg, 207 µmol, 1.0 equiv.) in dry DMSO (2 mL), DIPEA (205 µL, 1.24 mmol, 6.0 equiv.) and TSTU (87.1 mg, 289 µmol, 1.4 equiv.) were added and the reaction mixture was stirred for 10 min. at r.t. CA-NH_2 (55.5 mg, 248 µmol, 1.2 equiv.) in 0.5 mL DMSO was added and the reaction was stirred for 30 min, at r.t. The reaction was quenched by addition of acetic acid (291 µL) and 10% H_2O, followed by purification over preparative HPLC eluted with MeCN / H_2O (0.1% FA) (10% - 90% MeCN over 60 min) to give 98 mg (142 µmol) of the desired product in 69% yield after lyophilization.

HRMS (ESI): calc. for $C_{42}H_{59}N_3O_3Cl^+$ $[M]^+$: 688.4239; found 688.4239.

1.3.5 4-carboxy-2-(3-(dimethyliminio)-6-((4-methoxy-4-oxobutyl)(methyl)amino)-3H-xanthen-9-yl)benzoate (CA-TMR-biotin-1)

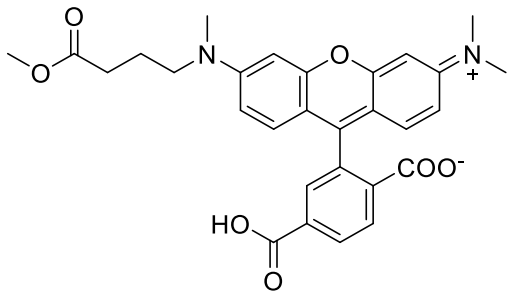

The compound was synthesized according to the procedure from Masharina et al. 2012 (15).

1.3.6 4-((2-(2-((6-chlorohexyl)oxy)ethoxy)ethyl)carbamoyl)-2-(3-(dimethyliminio)-6-((4-methoxy-4-oxobutyl)(methyl)amino)-3H-xanthen-9-yl)benzoate (CA-TMR-biotin-2)

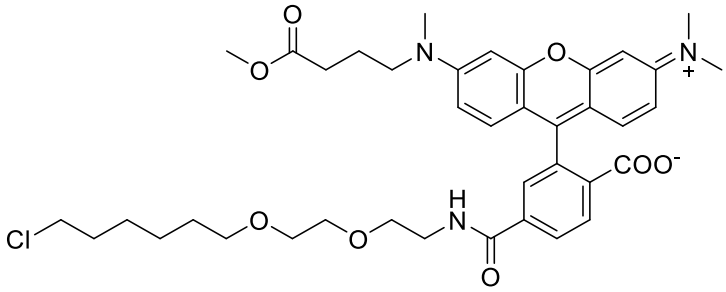

To a solution of CA-TMR-biotin-1 (17.0 mg, 32.9 µmol, 1.0 equiv.) in dry DMF, TSTU (11.9 mg, 39.5 µmol, 1.2 equiv.) and DIPEA (32.6 µL, 197 µmol, 6.0 equiv.) were added and the reaction was stirred at r.t. for 5 min. CA-NH_2 (14.7 mg, 65.8 µmol, 2.0 equiv.) was added and the reaction was stirred at r.t. for 2 h. The crude product was acidified with acetic acid and purified via preparative eluted with MeCN / H_2O (0.1% TFA) (10% - 90% MeCN over 50 min) to give 10 mg (13.8 µmol) of the desired product in 42% yield after lyophilization.

HRMS (ESI): calc. for $C_{39}H_{49}N_3O_8Cl^+$ $[M+H]^+$: 722.3208; found 722.3202.

1.3.7 2-(6-((3-carboxypropyl)(methyl)amino)-3-(dimethyliminio)-3H-xanthen-9-yl)-4-((2-(2-((6-chlorohexyl)oxy)ethoxy)ethyl)carbamoyl)benzoate (CA-TMR-biotin-3)

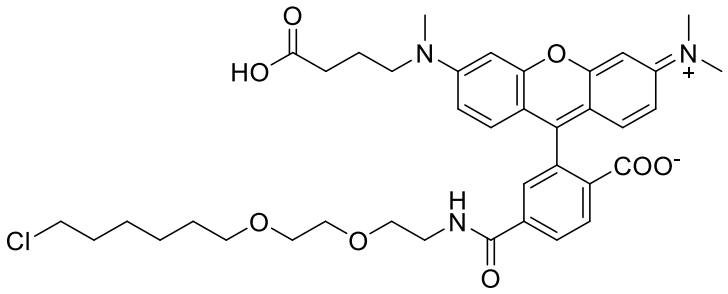

To a solution of CA-TMR-biotin-2 (8.0 mg, 11.1 µmol, 1.0 equiv.) in THF:H_2O (4:1), lithium hydroxide (1M in H_2O, 22.2 µL, 22.2 µmol, 2.0 equiv.) was added and the reaction was stirred at r.t. for 6 h. The crude product was acidified with acetic acid and purified via preparative HPLC eluted with MeCN / H_2O (0.1% TFA) (10% - 90% MeCN over 50 min) to give 6.3 mg (8.9 µmol) of the desired product in 80% yield after lyophilization.

HRMS (ESI): calc. for $C_{39}H_{49}N_3O_8Cl^+$ $[M+H]^+$: 708.3051; found 708.3049.

1.3.8 4-((2-(2-((6-chlorohexyl)oxy)ethoxy)ethyl)carbamoyl)-2-(3-(dimethyliminio)-6-((4,18-dioxo-22-((3aR,4R,6aS)-2-oxohexahydro-1H-thieno[3,4-d]imidazol-4-yl)-8,11,14-trioxa-5,17-diazadocosyl)(methyl)amino)-3H-xanthen-9-yl)benzoate (CA-TMR-biotin)

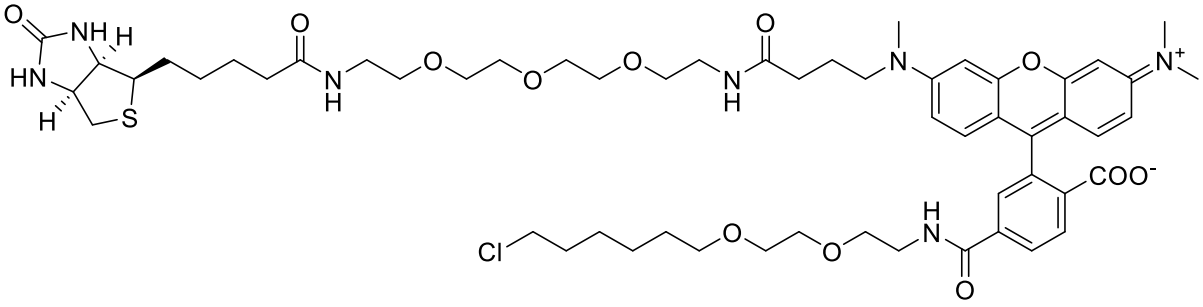

To a solution of CA-TMR-biotin-3 (6.0 mg, 8.47 µmol, 1.0 equiv.) in dry DMF, TSTU (3.06 mg, 10.2 µmol, 1.2 equiv.) and DIPEA (8.4 µL, 50.8 µmol, 6.0 equiv.) were added and the reaction was stirred at r.t. for 5 min. Biotin-PEG3-NH_2 (7.09 mg, 16.9 µmol, 2.0 equiv.) was added and the reaction was stirred at r.t. for another 2 h. The crude product was acidified with acetic acid and purified via preparative HPLC eluted with MeCN / H_2O (0.1% TFA) (10% - 90% MeCN over 50 min) to give 6.2 mg (5.6 µmol) of the desired product in 66% yield after lyophilization.

HRMS (ESI): calc. for $C_{56}H_{80}N_7O_{12}ClS^{2+}$ $[M+2H]^{2+}$: 554.7628; found 554.7632.

1.4 SNAP substrates based on benzylguanine (BG)

1.4.1 *N*-(4-(((2-amino-9*H*-purin-6-yl)oxy)methyl)benzyl)-2-azidoacetamide (BG-N_3)

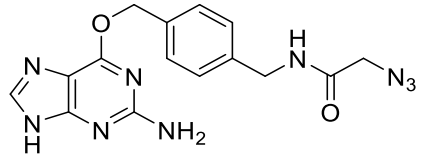

Reaction was conducted according to general procedure A using BG-NH_2 and 2-azidoacetic acid (40.7 µmol; 5.7 µL) and 11.1 mg (23.8 µmol) of the desired product were obtained as a colorless TFA-salt in 64% yield.

^{1}H NMR (400 MHz, DMSO-d_6) δ [ppm] = 8.65 (t, J = 5.9 Hz, 1H), 8.34 (s, 1H), 7.55 – 7.44 (m, 2H), 7.36 – 7.28 (m, 2H), 5.52 (s, 2H), 4.31 (d, J = 5.9 Hz, 2H), 3.89 (s, 2H).

HRMS (ESI) calc. for $C_{15}H_{16}N_9O_2^+$ [M+H]$^+$: 354.1421; found 354.1423.

1.4.2 *N*-(4-(((2-amino-9*H*-purin-6-yl)oxy)methyl)benzyl)-2-((1*S*,4*S*)-bicyclo[2.2.1]hept-5-en-2-yl)acetamide (BG-Nor2)

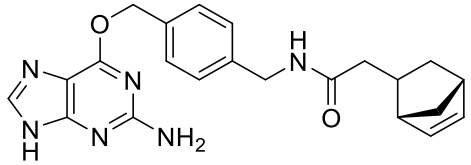

Reaction was conducted according to general procedure A with a reduced reaction time of 15 min. using BG-NH_2 and 2-((1*S*,4*S*)-bicyclo[2.2.1]hept-5-en-2-yl)acetic acid (40.7 µmol; 7.0 µL) resulting in 15.9 mg (30.7 µmol) of the desired product as a colorless TFA-salt in 83% yield.

^{1}H NMR (400 MHz, DMSO-d_6) δ [ppm] = 8.47 (s, 1H), 8.29 (t, J = 6.0 Hz, 1H), 7.49 (d, J = 8.1 Hz, 2H), 7.27 (d, J = 8.1 Hz, 2H), 6.16 (dd, J = 5.7, 3.0 Hz, 1H), 5.96 (dd, J = 5.7, 2.9 Hz, 1H), 5.53 (s, 2H), 4.25 (d, J = 6.0 Hz, 2H), 2.77 – 2.69 (m, 2H), 2.45 – 2.34 (m, 1H), 1.95 (dd, J = 13.8, 7.6 Hz, 1H), 1.90 – 1.77 (m, 2H), 1.33 – 1.26 (m, 1H), 1.25 – 1.19 (m, 1H), 0.50 (m, J = 11.4, 4.5, 2.5 Hz, 1H).

^{13}C NMR (101 MHz, DMSO-d_6) δ [ppm] = 171.71, 158.83, 158.03, 153.44, 140.89, 140.30, 137.07, 133.90, 132.45, 128.84, 127.13, 68.12, 49.10, 45.26, 42.09, 41.71, 40.67, 35.15, 31.47.

HRMS (ESI) calc. for $C_{22}H_{25}N_6O_2^+$ [M+H]$^+$: 405.2034; found 405.2034.

1.4.3 *N*-(4-(((2-amino-9*H*-purin-6-yl)oxy)methyl)benzyl)-2-(4-(6-methyl-1,2,4,5-tetrazin-3-yl)phenyl)acetamide (BG-Tz)

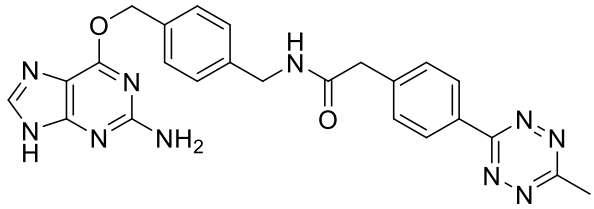

Reaction was conducted according to general procedure A using BG-NH_2 and 2-(4-(6-methyl-1,2,4,5-tetrazin-3-yl)phenyl)acetic acid (40.7 µmol, 9.4 mg) to give 12.4 mg (17.0 µmol) of the desired product as a rose TFA-salt in 56% yield.

^{1}H NMR (400 MHz, DMSO-d_6) δ [ppm] = 8.70 (t, J = 5.9 Hz, 1H), 8.45 – 8.39 (m, 2H), 8.37 (s, 1H), 7.60 – 7.53 (m, 2H), 7.52 – 7.44 (m, 2H), 7.33 – 7.26 (m, 2H), 5.51 (s, 2H), 4.31 (d, J = 5.9 Hz, 2H), 3.64 (s, 2H), 2.99 (s, 3H), 2.54 (s, 3H).

^{13}C NMR (101 MHz, DMSO-d_6) δ [ppm] = 170.04, 167.53, 163.69, 159.37, 158.85, 158.53, 154.36, 141.59, 140.96, 140.84, 140.19, 134.78, 130.62, 130.61, 129.34, 127.81, 68.28, 42.69, 40.90, 21.31.

HRMS (ESI) calc. for $C_{24}H_{23}N_{10}O_2^+$ [M+H]$^+$: 483.2000; found 483.2006.

1.4.4 *N*-(4-(((2-amino-9*H*-purin-6-yl)oxy)methyl)benzyl)-4-azidobenzamide (BG-PhN_3)

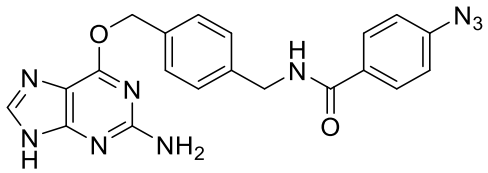

Reaction was conducted according to general procedure A with a reduced reaction time of 15 min. using BG-NH_2 and 4-azidobenzoic acid (6.6 mg, 40.7 µmol) to obtain 15.5 mg (29.3 µmol) of the desired product as a colorless TFA-salt in 79% yield.

^{1}H NMR (400 MHz, DMSO-d_6) δ [ppm] = 9.10 (t, J = 5.9 Hz, 1H), 8.38 (s, 1H), 7.99 – 7.89 (m, 2H), 7.55 – 7.46 (m, 2H), 7.38 – 7.33 (m, 2H), 7.25 – 7.16 (m, 2H), 5.52 (s, 2H), 4.48 (d, J = 5.9 Hz, 2H).

^{13}C NMR (101 MHz, DMSO-d_6) δ [ppm] = 165.27, 158.91, 158.61, 158.26, 153.77, 142.36, 140.57, 140.02, 134.19, 130.81, 129.15, 128.89, 127.36, 118.96, 67.94, 42.48.

HRMS (ESI) calc. for $C_{20}H_{18}N_9O_2^+$ $[M+H]^+$: 416.1578; found 416.1577.

1.4.5 *N*-(4-(((2-amino-9*H*-purin-6-yl)oxy)methyl)benzyl)-4-vinylbenzamide (BG-VBn)

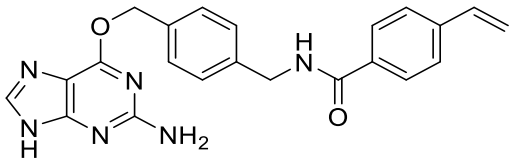

Reaction was conducted according to general procedure A with a reduced reaction time of 15 min. using BG-NH_2 and 4-vinylbenzoic acid (40.7 µmol; 6.5 mg) to obtain 14.7 mg (28.6 µmol) of the desired product as a colorless TFA-salt in 77% yield.

^{1}H NMR (400 MHz, DMSO-d_6) δ [ppm] = 9.09 (t, J = 6.0 Hz, 1H), 8.44 (s, 1H), 7.87 (d, J = 8.3 Hz, 2H), 7.57 (d, J = 8.3 Hz, 2H), 7.51 (d, J = 7.9 Hz, 2H), 7.36 (d, J = 7.9 Hz, 2H), 6.79 (dd, J = 17.7, 11.0 Hz, 1H), 5.95 (d, J = 17.7 Hz, 1H), 5.53 (s, 2H), 5.37 (d, J = 11.0 Hz, 1H), 4.49 (d, J = 6.0 Hz, 2H).

^{13}C NMR (101 MHz, DMSO-d_6) δ [ppm] = 165.81, 158.85, 158.62, 158.28, 153.55, 140.79, 140.13, 139.84, 135.91, 134.06, 133.43, 128.92, 127.61, 127.35, 126.03, 116.24, 68.09, 42.46.

HRMS (ESI) calc. for $C_{22}H_{21}N_6O_2^+$ $[M+H]^+$: 401.1721; found 401.1707.

1.4.6 ((1R,8S,9s)-bicyclo[6.1.0]non-4-yn-9-yl)methyl (4-(((2-amino-9*H*-purin-6-yl)oxy)methyl)benzyl)carbamate (BG-BCN)

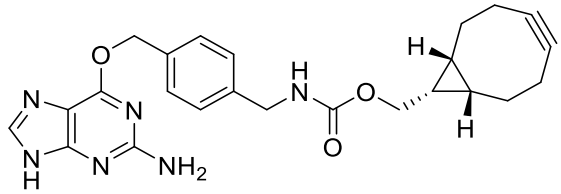

A solution of ((1*R*,8*S*,9*s*)-bicyclo[6.1.0]non-4-yn-9-yl)methyl (2,5-dioxopyrrolidin-1-yl) carbonate (10 mg, 34.3 µmol, 1.0 equiv.) in dry DMSO (0.4 mL) was added to a solution of 10.2 mg BG-NH_2 (37.8 µmol, 1.1 equiv.) in dry DMSO (0.1 mL) followed by 28.4 µL of DIPEA (172 µmol, 5 equiv.). The reaction was stirred at r.t. for 30 min. The resulted mixture was acidified with acetic acid (3 µL) and H_2O (53 µL), then purified by semi-preparative HPLC eluted with MeCN / H_2O (0.1% TFA) (10% MeCN for 10 min., then 10 - 90% MeCN over 55 min. followed by 99% MeCN for 5 min.) to give 14.0 mg (31.4 µmol) of the desired product as a colorless solid in 91% yield after lyophilization.

^{1}H NMR (400 MHz, DMSO-d_6) δ [ppm] = 8.36 (s, 1H), 7.70 (t, J = 6.2 Hz, 1H), 7.52 – 7.46 (m, 2H), 7.28 (d, J = 8.0 Hz, 2H), 5.51 (s, 2H), 4.18 (d, J = 6.0 Hz, 2H), 4.06 (d, J = 8.0 Hz, 2H), 2.28 – 2.07 (m, 6H), 1.52 (d, J = 12.4 Hz, 2H), 1.28 (dt, J = 18.3, 9.1 Hz, 1H), 0.86 (t, J = 9.8 Hz, 2H).

HRMS (ESI) calc. for $C_{24}H_{27}N_6O_3^+$ $[M+H]^+$: 447.2139; found 447.2135.

1.4.6.1 *N*-(4-(((2-amino-9*H*-purin-6-yl)oxy)methyl)benzyl)acetamide (BG-Ac)

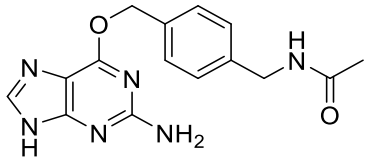

BG-NH_2 (300 mg, 1.11 mmol, 1.0 equiv.) was dissolved in dry DMSO (2.5 mL) and 367 µL of DIPEA (2.22 mmol, 2.0 equiv.) was added followed by dropwise addition of acetic anhydride (156 µL, 1.66 mmol, 1.5 equiv.) while stirring. The reaction mixture was stirred at r.t.

for 1 h. Afterwards, the reaction was quenched with acetic acid (387 µL) and H_2O (341 µL) followed by centrifugation at 3'000 rpm for 3 min. The pellet was washed twice with H_2O and afterwards lyophilized to obtain 190 mg (608 µmol) of the desired product as a colorless solid in 55% yield.

^{1}H NMR (400 MHz, DMSO-d_6) δ [ppm] = 8.30 (s, 1H), 7.45 (d, J = 8.1 Hz, 2H), 7.27 (d, J = 7.9 Hz, 2H), 6.82 (s, 2H), 5.48 (s, 2H), 4.24 (d, J = 5.9 Hz, 2H), 1.86 (s, 3H).

HRMS (ESI) calc. for $C_{15}H_{17}N_6O_2^+$ [M+H]$^+$: 313.1408; found 313.1406.

1.4.7 Cyclooct-2-yn-1-yl (4-(((2-amino-9*H*-purin-6-yl)oxy)methyl)benzyl)carbamate (BG-SCO)

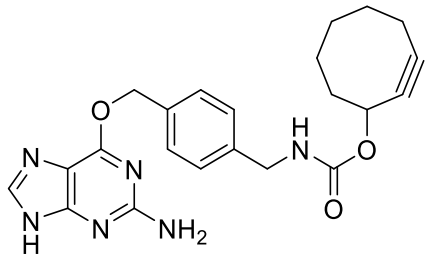

BG-NH_2 (10 mg, 37.0 µmol, 1.0 equiv.) was dissolved in dry DMSO (0.5 mL) and a solution of cyclooct-2-yn-1-yl (4-nitrophenyl) carbonate (10.7 mg, 37 µmol, 1.0 equiv.) in dry DMF (0.4 mL) was added followed by DIPEA (30.6 µL, 142 µmol: 5.0 equiv.). The reaction mixture was stirred at r.t. for 1 h. The resulted mixture was acidified with acetic acid (25 µL) and afterwards purified by semi-preparative HPLC eluted with MeCN / H_2O (0.1% TFA) (15% MeCN for 5 min., then 15 - 100% MeCN over 25 min., followed by 100% MeCN for 15 min.) to give 16 mg (23.3 µmol) of the desired product as a colorless TFA-salt in 81% yield after lyophilization.

^{1}H NMR (400 MHz, DMSO-d_6) δ [ppm] = 8.44 (s, 1H), 7.81 (t, J = 6.1 Hz, 1H), 7.50 (d, J = 8.0 Hz, 2H), 7.28 (d, J = 8.0 Hz, 2H), 5.52 (s, 2H), 5.20 – 5.11 (m, 1H), 4.17 (d, J = 6.1 Hz, 2H), 2.30 – 2.02 (m, 3H), 1.96 – 1.85 (m, 1H), 1.89 – 1.76 (m, 2H), 1.76 – 1.64 (m, 1H), 1.64 – 1.53 (m, 2H), 1.55 – 1.41 (m, 1H).

^{13}C NMR (101 MHz, DMSO-d_6) δ [ppm] = 158.86, 158.10, 155.53, 153.58, 140.80, 140.06, 134.15, 128.90, 127.16, 107.66, 100.97, 91.76, 68.06, 65.95, 43.50, 41.58, 33.85, 29.21, 25.79, 19.95.

HRMS (ESI) calc. for $C_{22}H_{24}N_6NaO_3^+$ [M+Na]$^+$: 443.1802; found 443.1797.

1.4.8 5-((4-(((2-amino-9H-purin-6-yl)oxy)methyl)benzyl)carbamoyl)-2-(6-(dimethylamino)-3-(dimethyliminio)-2,3,4,4a-tetrahydro-1H-xanthen-9-yl)benzoate (BG-5-TMR)

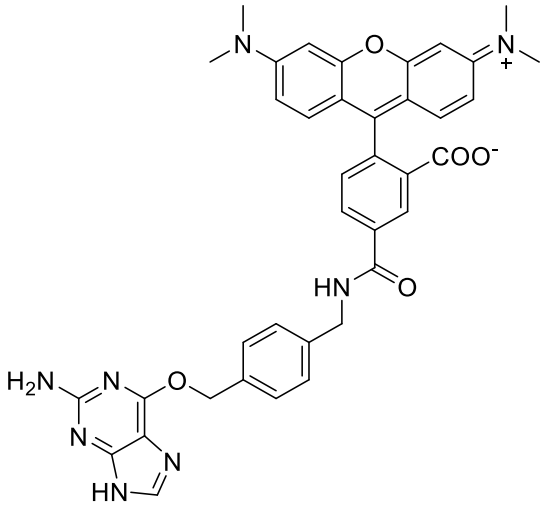

TSTU (1.45 mg, 4.82 µmol, 1.2 equiv.) was dissolved in dry DMSO-d_6 (500 µL). TMR-5-COOH (1.15 mg, 2.68 µmol, 1.0 equiv.) was dissolved in the TSTU solution and DIPEA (1.77 µL, 10.7 µmol, 4.0 equiv.) was added. The mixture was stirred at r.t. for 10 min. BG-NH_2 (1.08 mg, 4.01 µmol, 1.5 equiv.) was dissolved in dry DMSO-d_6 (200 µL) and added to the reaction. The reaction mixture was

stirred at r.t. for 1 h. The compound was purified over preparative HPLC eluted with MeCN / H_2O (0.1% TFA) (10% MeCN for 10 min., then 10 - 90% MeCN over 40 min., followed by 90% MeCN for 5 min.) to give after lyophilization 378 µg (554 nmol) of the desired product in 21% yield.

HRMS (ESI): calc. for $C_{38}H_{37}N_8O_5$ $[M+2H]^{2+}$: 342.1399; found 342.1394.

^{1}H NMR (TMR-5-COOH) (400 MHz, DMSO-d_6) δ [ppm] = 8.39 (s, J = 1.5 Hz, 1H), 8.28 (dd, J = 8.1, 1.5 Hz, 1H), 7.33 (d, J = 8.0 Hz, 1H), 6.58 – 6.45 (m, 6H), 2.95 (s, 12H).

^{13}C NMR (TMR-5-COOH) (101 MHz, DMSO-d_6) δ [ppm] = 168.31, 166.09, 152.03, 135.96, 132.76, 128.50, 109.05, 97.95, 40.15, 39.99, 39.79.

1.4.9 5-((4-(((2-amino-9H-purin-6-yl)oxy)methyl)benzyl)carbamoyl)-2-(6-(dimethylamino)-3-(dimethyliminio)-10,10-dimethyl-1,2,3,4,4a,10-hexahydroanthracen-9-yl)benzoate (BG-5-CPY)

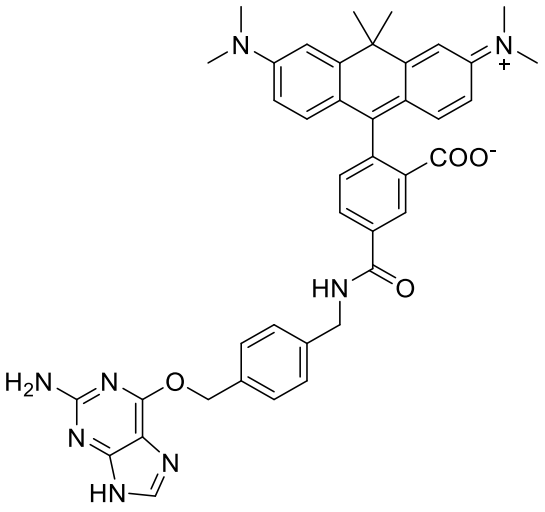

TSTU (1.44 mg, 4.78 µmol, 1.2 equiv.) was dissolved in dry DMSO-d_6 (500 µL). CPY-5-COOH (2.0 mg, 4.38 µmol, 1.1 equiv.) was dissolved in the TSTU solution and DIPEA (2.63 µL, 15.9 µmol, 4 equiv.) was added. The mixture was stirred at r.t. for 10 min. BG-NH_2 (1.08 mg, 3.98 µmol, 1.5 equiv.) was dissolved in dry DMSO-d_6 (200 µL) and added to the reaction. The reaction mixture was stirred at r.t. for 1 h. The compound was purified over preparative HPLC eluted with MeCN / H_2O (0.1% TFA) (10% MeCN for 10 min., then 10 - 90% MeCN over 40 min., followed by 90% MeCN for 5 min.) to give 346 µg (488 nmol) of the desired product in 18% yield after lyophilization.

HRMS (ESI): calc. for $C_{41}H_{42}N_8O_4$ $[M+2H]^{2+}$: 355.1659; found 355.1659.

1.4.9.1 1-(6-((4-(((2-amino-9H-purin-6-yl)oxy)methyl)benzyl)amino)-6-oxohexyl)-3,3-dimethyl-2-((E)-3-((Z)-1,3,3-trimethylindolin-2-ylidene)prop-1-en-1-yl)-3H-indol-1-ium (BG-Cy3)

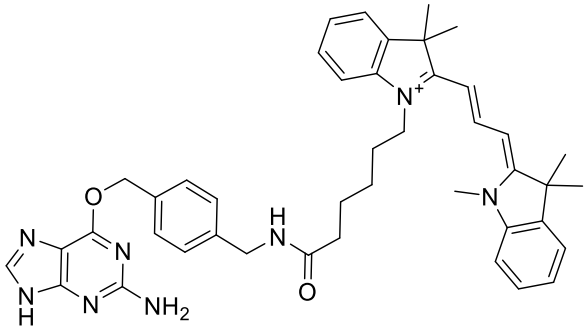

Cy3-COOH was synthesized according to Ueno et al. 2010 (3). To a solution of Cy3-COOH (100 mg, 219 µmol, 1.0 equiv.) in dry DMSO (1.5 mL), DIPEA (217 µL, 1.3 mmol, 6.0 equiv.) and TSTU (92.1 mg, 306 µmol, 1.4 equiv.) were added and the reaction mixture was stirred for 10 min. at r.t. BG-NH_2 (70.9 mg, 262 µmol, 1.2 equiv.) was added and the reaction was stirred for 30 min. at r.t. The

reaction was quenched by addition of acetic acid (230 µL) and 10% H_2O, followed by purification over preparative HPLC eluted with MeCN / H_2O (0.1% FA) (10% - 90% MeCN over 60 min.) to give. 28.5 mg (40.1 µmol) of the desired product in 18% yield after lyophilization.

HRMS (ESI): calc. for $C_{43}H_{50}N_8O_2^{2+}$ $[M+H]^{2+}$: 355.2023; found 355.2022.

1.4.10 1-(6-((4-(((2-amino-9H-purin-6-yl)oxy)methyl)benzyl)amino)-6-oxohexyl)-3,3-dimethyl-2-((1E,3E)-5-((Z)-1,3,3-trimethylindolin-2-ylidene)penta-1,3-dien-1-yl)-3H-indol-1-ium (BG-Cy5)

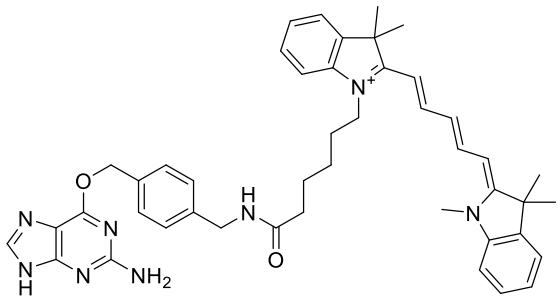

Cy5-COOH was synthesized according to Ueno et al. 2010(3). To a solution of Cy5-COOH (50.0 mg, 103 µmol, 1.0 equiv.) in dry DMSO (1.5 mL), DIPEA (103 µL, 620 µmol, 6.0 equiv.) and TSTU (43.6 mg, 145 µmol, 1.4 equiv.) were added and the reaction mixture was stirred for 10 min. at r.t. BG-NH_2 (33.5 mg, 124 µmol, 1.2 equiv.) was added and the reaction was stirred for 30 min. at r.t. The reaction was quenched by addition of acetic acid (109 µL) and 10% H_2O, followed by purification over preparative HPLC eluted with MeCN / H_2O (0.1% FA) (10% - 90% MeCN over 60 min.) to give 45 mg (61.1 µmol) of the desired product in 59% yield after lyophilization.

HRMS (ESI): calc. for $C_{45}H_{52}N_8O_2^{2+}$ $[M+H]^{2+}$: 368.2101; found 368.2102.

1.5 SNAP substrates based on chloropyrimidine (CP)

1.5.1 *N*-(4-(((2-amino-6-chloropyrimidin-4-yl)oxy)methyl)benzyl)-2-azidoacetamide (CP-N_3)

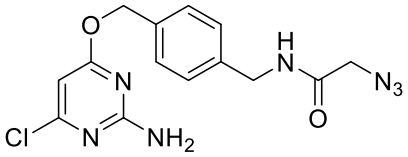

Reaction was conducted according to general procedure A using CP-NH_2 and 2-azidoacetic acid (5.8 µL, 41.6 µmol) to obtain 10.1 mg (21.9 µmol) of the desired product as a colorless TFA-salt in 58% yield.

^{1}H NMR (400 MHz, DMSO-d_6) δ [ppm] = 8.62 (t, J = 5.8 Hz, 1H), 7.40 (d, J = 7.7 Hz, 2H), 7.28 (d, J = 7.7 Hz, 2H), 6.13 (s, 1H), 5.29 (s, 2H), 4.30 (d, J = 5.8 Hz, 2H), 3.88 (s, 2H).

^{13}C NMR (101 MHz, DMSO-d_6) δ [ppm] = 170.28, 167.32, 162.77, 160.01, 138.90, 134.90, 128.44, 127.46, 94.42, 67.21, 50.78, 42.01.

HRMS (ESI) calc. for $C_{14}H_{15}ClN_7O_2^+$ $[M+H]^+$: 348.0970; found 348.0971.

1.5.2 *N*-(4-(((2-amino-6-chloropyrimidin-4-yl)oxy)methyl)benzyl)-2-((1*S*,4*S*)-bicyclo[2.2.1]hept-5-en-2-yl)acetamide (CP-Nor2)

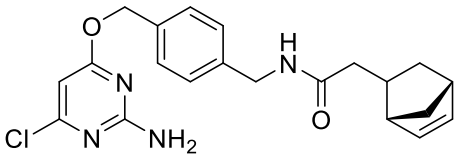

Reaction was conducted according to general procedure A with a reduced reaction time of 15 min. using CP-NH_2 and 2-((1*S*,4*S*)-bicyclo[2.2.1]hept-5-en-2-yl)acetic acid (7.1 µL, 41.6 µmol) resulting in 14.5 mg (28.3 µmol) of the desired product as a colorless TFA-salt in 75% yield.

^{1}H NMR (400 MHz, DMSO-d_6) δ [ppm] = 8.25 (t, J = 5.9 Hz, 1H), 7.38 (d, J = 8.1 Hz, 2H), 7.23 (d, J = 8.1 Hz, 2H), 7.10 (brs, 2H), 6.16 (dd, J = 5.7, 3.0 Hz, 1H), 6.13 (s, 1H), 5.96 (dd, J = 5.7, 2.9 Hz, 1H), 5.28 (s, 2H), 4.24 (d, J = 5.9 Hz, 2H), 2.77 – 2.69 (m, 2H), 2.46 – 2.35 (m, 1H), 1.94 (dd, J = 13.8, 7.6 Hz, 1H), 1.90 – 1.76 (m, 2H), 1.35 – 1.26 (m, 1H), 1.26 – 1.18 (m, 1H), 0.50 (m, J = 11.4, 4.3, 2.5 Hz, 1H).

^{13}C NMR (101 MHz, DMSO-d_6) δ [ppm] = 171.61, 170.28, 162.75, 159.97, 139.81, 137.01, 134.53, 132.42, 128.31, 127.11, 94.39, 67.23, 49.07, 45.24, 42.06, 41.69, 40.64, 35.11, 31.45.

HRMS (ESI) calc. for $C_{21}H_{23}ClN_4NaO_2^+$ [M+Na]$^+$; 421.1402; found 421.1403.

1.5.3 *N*-(4-(((2-amino-6-chloropyrimidin-4-yl)oxy)methyl)benzyl)-2-(4-(6-methyl-1,2,4,5-tetrazin-3-yl)phenyl)acetamide (CP-Tz)

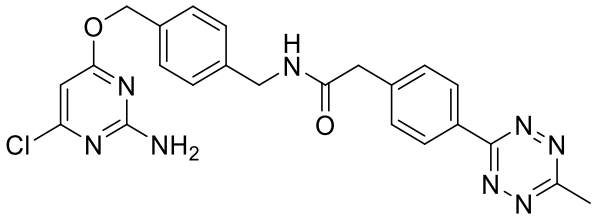

Reaction was conducted according to general procedure A using CP-NH_2 and 2-(4-(6-methyl-1,2,4,5-tetrazin-3-yl)phenyl)acetic acid (9.6 mg, 41.6 µmol). The product was purified by preparative HPLC eluted with MeCN / H_2O (0.1% TFA) (10% MeCN for 10 min., then 10 - 90% MeCN over 40 min., followed by 90% MeCN for 10 min.) to give 2.6 mg (4.4 µmol) of the desired product as a rose TFA-salt in 12% yield after lyophilization.

^{1}H NMR (400 MHz, DMSO-d_6) δ [ppm] = 8.66 (t, J = 5.9 Hz, 1H), 8.41 (d, J = 8.3 Hz, 2H), 7.56 (d, J = 8.3 Hz, 2H), 7.38 (d, J = 7.9 Hz, 2H), 7.26 (d, J = 7.9 Hz, 2H), 7.10 (s, 2H), 6.13 (s, 1H), 5.28 (s, 2H), 4.29 (d, J = 5.9 Hz, 2H), 3.63 (s, 2H), 2.99 (s, 3H).

^{13}C NMR (101 MHz, DMSO-d_6) δ [ppm] = 170.28, 169.51, 167.04, 163.21, 162.76, 159.99, 141.13, 139.32, 134.75, 130.14, 130.07, 128.42, 127.34, 94.40, 67.22, 42.21, 42.09, 20.83.

HRMS (ESI) calc. for $C_{23}H_{22}ClN_8O_2^+$ [M+H]$^+$: 477.1549; found 477.1553.

1.5.4 *N*-(4-(((2-amino-6-chloropyrimidin-4-yl)oxy)methyl)benzyl)-4-azidobenzamide (CP-PhN_3)

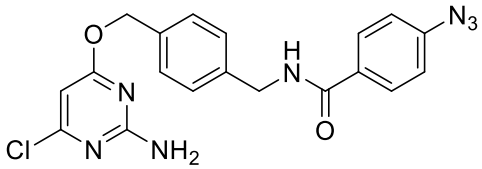

Reaction was conducted according to general procedure A with a reduced reaction time of 15 min. using BG-NH_2 and 4-azidobenzoic acid (6.8 mg, 41.6 µmol) to obtain 12.0 mg (22.9 µmol) of the desired product as a colorless TFA-salt in 61% yield.

^{1}H NMR (400 MHz, DMSO-d_6) δ [ppm] = 9.06 (t, J = 5.9 Hz, 1H), 7.94 (d, J = 8.4 Hz, 2H), 7.39 (d, J = 7.9 Hz, 2H), 7.32 (d, J = 7.9 Hz, 2H), 7.21 (d, J = 8.4 Hz, 2H), 7.10 (s, 2H), 5.29 (s, 2H), 4.47 (d, J = 5.9 Hz, 2H).

^{13}C NMR (101 MHz, DMSO-d_6) δ [ppm] = 170.27, 165.20, 162.75, 159.97, 142.30, 139.59, 134.66, 130.83, 129.12, 128.36, 127.29, 118.90, 94.38, 67.23, 42.44.

HRMS (ESI) calc. for $C_{19}H_{16}ClN_7NaO_2^+$ [M+Na]$^+$: 432.0946; found 432.0942.

1.5.5 *N*-(4-(((2-amino-6-chloropyrimidin-4-yl)oxy)methyl)benzyl)-4-vinylbenzamide (CP-Vbn)

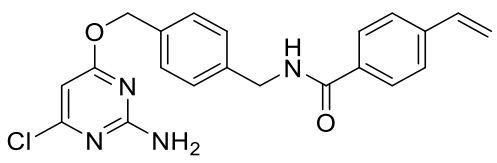

Reaction was conducted according to general procedure A with a reduced reaction time of 15 min. using CP-NH_2 and 4-vinylbenzoic acid (41.6 µmol; 6.2 mg) to obtain 11.6 mg (22.8 µmol) of the desired product as a colorless TFA-salt in 60% yield.

^{1}H NMR (400 MHz, DMSO-d_6) δ [ppm] = 9.04 (t, J = 6.0 Hz, 1H), 7.87 (d, J = 8.3 Hz, 2H), 7.57 (d, J = 8.3 Hz, 2H), 7.40 (d, J = 8.1 Hz, 2H), 7.34 (d, J = 8.1 Hz, 2H), 6.79 (dd, J = 17.7, 10.9 Hz, 1H), 7.10 (brs, 2H), 6.12 (s, 1H), 5.95 (d, J = 17.7 Hz, 1H), 5.37 (d, J = 10.9 Hz, 1H), 5.29 (s, 2H), 4.47 (d, J = 6.0 Hz, 2H).

^{13}C NMR (101 MHz, DMSO-d_6) δ [ppm] = 170.29, 165.77, 162.77, 159.99, 139.80, 139.68, 135.91, 134.66, 133.45, 128.41, 127.61, 127.31, 126.00, 116.20, 94.40, 67.27, 42.43.

HRMS (ESI) calc. for $C_{21}H_{20}ClN_4O_2^+$ [M+H]$^+$: 395.1269; found 395.1258.

1.5.6 4-(Benzyloxy)-6-chloropyrimidin-2-amine (CP)

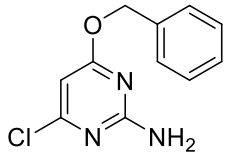

2-Amino-4,6-dichloropyrimidine (200 mg, 1.22 mmol, 1.0 equiv.) was dissolved in dry DMF (2 mL). Benzyl alcohol (63 µL, 1.22 mmol, 1.0 equiv.), KO^{t}Bu (342.2 mg, 3.04 mmol, 2.5 equiv.) and KI (20.2 mg, 0.122 mmol, 0.1 equiv.) were added and the reaction mixture was stirred at room temperature for 4 h. Afterwards, the reaction was quenched with water and extracted with EtOAc (3 ×). The combined organic layers were washed with brine and dried over $MgSO_4$. The volatiles were evaporated and the crude product was purified over normal phase flash chromatography (hexane:DCM = 50% : 50% to 100% DCM). The fractions containing the product were combined, volatiles were evaporated and 134 mg (0.569 mmol) of the desired product was obtained as a yellowish solid in 47% yield.

^{1}H NMR (400 MHz, $CDCl_3$): δ = 7.43–7.30 (m, 5H), 6.01 (d, J = 0.7 Hz, 1H), 5.31 (s, 2H), 2.26 (s, 3H) ppm.

^{13}C NMR (101 MHz, $CDCl_3$): δ = 170.6, 168.4, 162.6, 136.7, 128.7, 128.5, 128.0, 127.4, 97.2, 93.0, 77.4, 77.1, 76.7, 67.5, 123.7 ppm.

HRMS (ESI) calc. for $C_{11}H_{11}ClN_3O^+$ [M+H]$^+$: 236.0585; found 236.0583.

1.5.7 ((1*R*,8*S*,9*s*)-bicyclo[6.1.0]non-4-yn-9-yl)methyl(4-(((2-amino-6-chloropyrimidin-4-yl)oxy)methyl)benzyl)carbamate (CP-BCN)

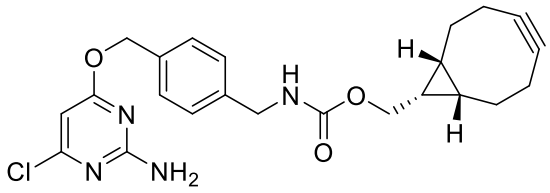

((1*R*,8*S*,9*s*)-bicyclo[6.1.0]non-4-yn-9-yl)methyl (2,5-dioxopyrrolidin-1-yl) carbonate (10.0 mg, 34.3 µmol; 1.0 equiv.) was dissolved in dry DMSO (0.5 mL) and DIPEA (28.4 µL, 172 µmol, 5 equiv.) followed by CP-NH_2 (10.0 mg, 37.8 µmol, 1.1 equiv.) were added. The reaction was stirred at r.t. for 30 min. The resulted mixture was acidified with acetic acid (3 µL) and H_2O (53 µL), then purified by preparative HPLC eluted with MeCN / H_2O (0.1% TFA) (10% MeCN for 10 min., then 10 - 90% MeCN over 55 min., followed by 99% MeCN for 5 min.) to give 1.4 mg (3.11 µmol) of the desired product as a colorless solid in 9% yield after lyophilization.

^{1}H NMR (400 MHz, DMSO-d_6) δ [ppm] = 7.68 (q, J = 6.4 Hz, 1H), 7.38 (d, J = 8.0 Hz, 2H), 7.25 (d, J = 7.8 Hz, 2H), 6.12 (s, 1H), 5.28 (s, 2H), 4.17 (d, J = 6.1 Hz, 2H), 4.06 (d, J = 8.0 Hz, 2H), 2.29 – 1.72 (m, 6H), 1.71 – 1.38 (m, 2H), 1.35 – 0.60 (m, 3H).

HRMS (ESI) calc. for $C_{23}H_{26}ClN_4O_3^+$ [M+H]$^+$: 441.1688; found 441.1688.

1.5.8 *N*-(4-(((2-amino-6-chloropyrimidin-4-yl)oxy)methyl)benzyl)acetamide (CP-Ac)

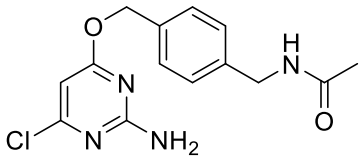

CP-NH_2 (300 mg, 1.13 mmol, 1.0 equiv.) was dissolved in dry DMSO (1.5 mL) and DIPEA (375 µL, 2.27 mmol, 2.0 equiv.) was added followed by dropwise addition of acetic anhydride (160 µL, 1.70 mmol, 1.5 equiv.) while stirring. The reaction mixture was stirred at r.t. for 1 h. Afterwards, the reaction was quenched with acetic acid (387 µL) and H_2O (341 µL) followed by purification over preparative HPLC eluted with MeCN / H_2O (0.1% TFA) (30% MeCN for 10 min., then 30 - 90% MeCN over 55 min., followed by 99% MeCN for 5 min.) to give 201 mg (655 µmol) of the desired product as a colorless solid in 58% yield after lyophilization.

^{1}H NMR (400 MHz, DMSO-d_6) δ [ppm] = 8.33 (t, J = 6.0 Hz, 1H), 7.41 – 7.35 (m, 2H), 7.28 – 7.22 (m, 2H), 7.09 (s, 2H), 6.13 (s, 1H), 5.29 (s, 2H), 4.24 (d, J = 5.9 Hz, 2H), 1.86 (s, 3H).

HRMS (ESI) calc. for $C_{14}H_{16}ClN_4O_2^+$ $[M+H]^+$: 307.0956; found 307.0957.

1.5.9 Cyclooct-2-yn-1-yl (4-(((2-amino-6-chloropyrimidin-4-yl)oxy)methyl)benzyl)carbamate (CP-SCO)

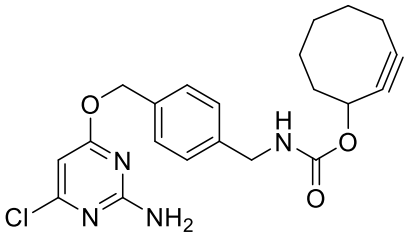

CP-NH_2 (10 mg; 37.8 µmol, 1.3 equiv.) was dissolved in dry DMF (0.3 mL) and a solution of 8.4 mg cyclooct-2-yn-1-yl (4-nitrophenyl) carbonate (29.1 µmol, 1.0 equiv.) in dry DMF (0.2 mL) was added followed by DIPEA (24.0 µL, 145 µmol: 5.0 equiv.). The reaction mixture was stirred at r.t. for 2 h. The resulted mixture was acidified with acetic acid (25 µL) and afterwards purified by semi-preparative HPLC eluted with MeCN / H_2O (0.1% TFA) (15% MeCN for 2 min., then 15 - 100% MeCN over 25 min., followed by 100% MeCN for 15 min.) to give 12.0 mg (22.7 µmol) of the desired product as a colorless TFA-salt in 78% yield after lyophilization.

^{1}H NMR (400 MHz, DMSO-d_6) δ [ppm] = 7.78 (t, J = 6.2 Hz, 1H), 7.38 (d, J = 8.1 Hz, 2H), 7.24 (d, J = 8.1 Hz, 2H), 6.13 (s, 1H), 5.28 (s, 2H), 5.21 – 5.11 (m, 1H), 4.15 (d, J = 6.2 Hz, 2H), 2.29 – 2.02 (m, 3H), 1.95 – 1.85 (m, 1H), 1.85 – 1.78 (m, 2H), 1.76 – 1.65 (m, 1H), 1.65 – 1.54 (m, 2H), 1.54 – 1.42 (m, 1H).

^{13}C NMR (101 MHz, DMSO-d_6) δ [ppm] = 170.30, 162.78, 159.99, 155.51, 139.64, 134.73, 128.40, 127.11, 100.94, 94.41, 91.76, 67.25, 65.93, 43.50, 41.58, 33.84, 29.21, 25.79, 19.96.

HRMS (ESI) calc. for $C_{21}H_{23}ClN_4NaO_3^+$ $[M+Na]^+$: 437.1351; found 437.1358.

1.5.10 2-(6-amino-3-iminio-4,5-disulfonato-3*H*-xanthen-9-yl)-4-((4-(((2-amino-6-chloropyrimidin-4-yl)oxy)methyl)benzyl)carbamoyl)benzoate (CP-Alexa488)

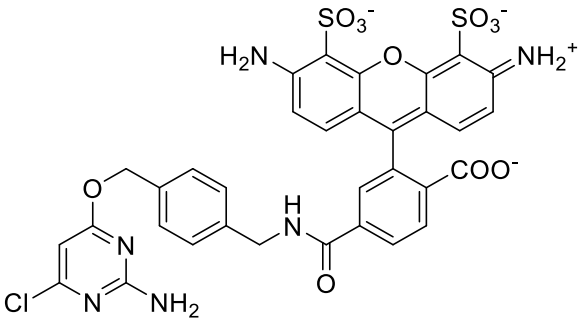

In an Eppendorf tube, CP-NH_2 (0.34 µg, 1.27 µmol, 2.0 equiv.) was dissolved in dry DMSO (100 µL) followed by addition of DIPEA (885 µL, 5.1 µmol, 8.0 equiv.) and a solution of 2-(6-amino-3-iminio-4,5-disulfonato-3H-xanthen-9-yl)-4-(((2,5-dioxopyrrolidin-1-yl)oxy)carbonyl)benzoate (0.4 mg, 0.64 µmol, 1.0 equiv.) in dry DMSO (100 µL). The reaction was kept at r.t. for 1 h. The compound was purified over preparative HPLC eluted with MeCN / H_2O (0.1% TFA) (10% MeCN for 10 min., then 10 - 90% MeCN over 40 min., followed by 90% MeCN for 5 min.) to give 195 µg (252 nmol) of the desired product as a yellow solid in 79% yield after lyophilization.
HRMS (ESI) calc. for $C_{33}H_{25}ClN_6O_{11}S_2$ $[M+3H]^+$: 781.0784; found 781.0772.

1.5.11 4-((4-(((2-amino-6-chloropyrimidin-4-yl)oxy)methyl)benzyl)carbamoyl)-2-(6-hydroxy-3-oxo-3H-xanthen-9-yl)benzoate (CP-Fluorescein)

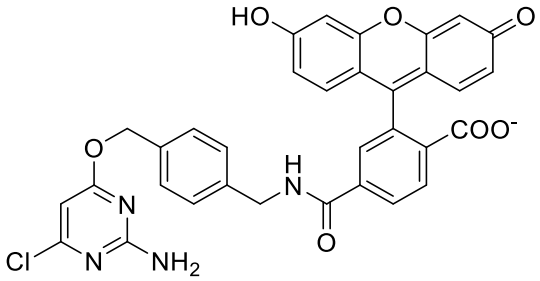

Fluorescein-6-COOH (25.0 mg, 66.4 µmol, 1.0 equiv.) was dissolved in dry DMSO (1.25 mL) and DIPEA (22.0 µL, 133 µmol, 2.0 equiv.) as well as TSTU (24.0 mg, 79.7 µmol, 1.2 equiv.) were added and the mixture was stirred at r.t. for 30 min. Afterwards, CP-NH_2 (26.4 mg, 99.7 µmol, 1.5 equiv.) was added and the reaction mixture was stirred at r.t. for 1 h. The resulted mixture was quenched with acetic acid (22.0 µL) and 10% H_2O, then the compound was purified over preparative HPLC eluted with MeCN / H_2O (0.1% TFA) (10% MeCN for 10 min., then 10 - 90% MeCN over 40 min., followed by 90% MeCN for 5 min.) to give 31 mg (49.8 µmol) of the desired product in 75% yield after lyophilization.
HRMS (ESI) calc. for $C_{33}H_{24}ClN_4O_7^+$ $[M+H]^+$: 623.1328; found 623.1327.

1.5.12 4-((4-(((2-amino-6-chloropyrimidin-4-yl)oxy)methyl)benzyl)carbamoyl)-2-(6-(dimethylamino)-3-(dimethyliminio)-10,10-dimethyl-3,10-dihydroanthracen-9-yl)benzoate (CP-CPY)

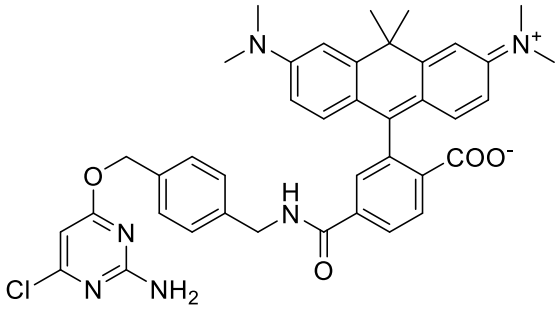

CPY-6-COOH(1) (250 mg, 530 µmol, 1.0 equiv.) was dissolved in dry DMSO (2 mL) and DIPEA (362 µL, 2.19 mmol, 4.0 equiv.) as well as TSTU (231 mg, 767 µmol, 1.4 equiv.) were added and the mixture was stirred at r.t. for 5 min. Afterwards, CP-NH_2 (217 mg, 821 µmol, 1.5 equiv.) was added and the reaction mixture was stirred at r.t. for 35 min. The resulted mixture was acidified with acetic acid (362 µL) and H_2O (500 µL), then the compound was purified over preparative HPLC eluted with MeCN / H_2O (0.1% TFA) (10% MeCN for 10 min., then 10 - 90% MeCN over 40 min., followed by 90% MeCN for 5 min.) to give 130 mg (184.9 µmol) of the desired product in 34% yield after lyophilization.
^{1}H NMR (400 MHz, acetone-d_6) δ [ppm] = 8.51 (t, J = 6.4 Hz, 1H), 8.23 (d, J = 8.1 Hz, 1H), 8.12 (d, J = 8.7 Hz, 1H), 7.67 (s, 1H), 7.39 – 7.30 (m, 4H), 7.11 (s, 2H), 6.67 (s, 4H), 6.36 (s, 1H), 6.07 (m, J = 10.7, 2.5 Hz, 1H), 5.30 (m, J = 11.2, 2.5 Hz, 2H), 4.55 (d, J = 5.9 Hz, 2H), 3.11 (s, 12H), 1.89 (d, J = 2.5 Hz, 3H), 1.76 (d, J = 2.4 Hz, 3H).
^{13}C NMR (101 MHz, acetone-d_6) δ [ppm] = 171.72, 165.87, 161.60, 140.12, 136.37, 134.01, 129.34, 129.25, 128.85, 120.23, 113.03, 110.69, 96.16, 68.31, 44.02, 40.62, 35.59, 33.04, 30.42, 30.22, 30.03, 29.84, 29.65, 29.45, 29.26, 26.13.

HRMS (ESI) calc. for $C_{40}H_{39}ClN_6O_4^+$ $[M+H]^+$: 703.2794; found 703.2792.

1.5.13 4-((4-(((2-amino-6-chloropyrimidin-4-yl)oxy)methyl)benzyl)carbamoyl)-2-(7-(dimethylamino)-3-(dimethyliminio)-5,5-dimethyl-3,5-dihydrodibenzo[b,e]silin-10-yl)benzoate (CP-SiR)

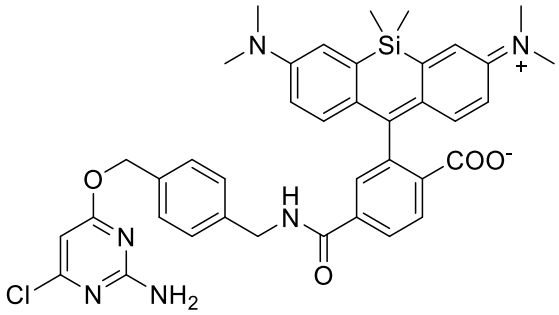

SiR-6-COOH(4) (481 mg, 1.02 mmol, 1.1 equiv.) was dissolved in dry DMSO (4 mL) and DIPEA (919 µL, 5.56 mmol, 6.0 equiv.) was added. The mixture was sonicated until complete solution and TSTU (391 mg, 1.30 mmol, 1.4 equiv.) were added and the mixture was stirred at r.t. for 5 min. Afterwards, CP-NH_2 (294 mg, 1.11 mmol, 1.2 equiv.) was added and the reaction mixture was stirred at r.t. for 2h. The resulted mixture was quenched by addition of acetic acid (973 µL) and 10% H_2O, followed by purification over preparative HPLC eluted with MeCN / H_2O (0.1% FA) (10% - 90% MeCN over 60 min) to give. 355 mg (494 µmol) of the desired product in 53% yield after lyophilization.

HRMS (ESI): calc. for $C_{39}H_{39}N_6O_4Si^+$ $[M+H]^+$: 719.2563; found 719.2561.

1.6 CLIP substrates

1.6.1 4-((4-(((4-aminopyrimidin-2-yl)oxy)methyl)benzyl)carbamoyl)-2-(6-(dimethylamino)-3-(dimethyliminio)-10,10-dimethyl-3,10-dihydroanthracen-9-yl)benzoate (BC-CPY)

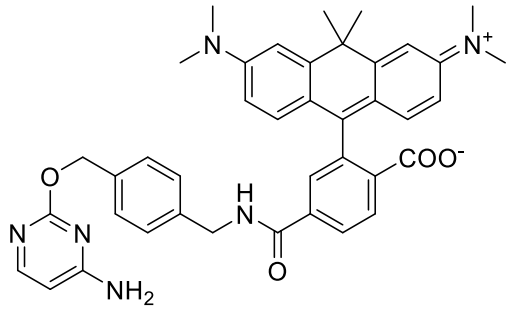

CPY-6-COOH(1) (250 mg, 530 µmol, 1.0 equiv.) was dissolved in dry DMSO (2 mL). DIPEA (362 µL, 2.19 mmol, 4.0 equiv.) and TSTU (231 mg, 767 µmol, 1.4 equiv.) were added and the mixture was stirred at r.t. for 5 min. Afterwards, BC-NH_2 (189 mg, 821 µmol, 1.5 equiv.) was added and the reaction mixture was stirred at r.t. for 35 min. The resulted mixture was acidified with acetic acid (362 µL) and H_2O (500 µL), then compound was purified over preparative HPLC eluted with MeCN / H_2O (0.1% TFA) (10% MeCN for 10 min., then 10 - 90% MeCN over 40 min., followed by 90% MeCN for 5 min.) to give 180 mg (269.1 µmol) of the desired product in 49% yield after lyophilization.

^{1}H NMR (400 MHz, acetone-d_6) δ [ppm] = 8.51 (t, J = 6.9 Hz, 1H), 8.21 (d, J = 8.1 Hz, 1H), 8.10 – 8.01 (m, 2H), 7.61 (s, 1H), 7.38 (d, J = 7.4 Hz, 2H), 7.32 (d, J = 7.8 Hz, 2H), 7.27 (s, 1H), 7.05 (s, 2H), 6.61 (s, 4H), 6.40 (d, J = 6.6, 2.4 Hz, 1H), 5.36 (s, 2H), 4.56 – 4.50 (m, 2H), 3.04 (s, 12H), 1.88 (d, J = 2.5 Hz, 3H), 1.76 (d, J = 2.6 Hz, 3H).

^{13}C NMR (101 MHz, acetone-d_6) δ [ppm] = 169.57, 165.97, 162.80, 152.54, 152.01, 148.78, 141.22, 140.20, 136.01, 130.47, 129.26, 128.83, 126.23, 124.12, 120.13, 112.83, 110.38, 100.42, 69.65, 44.02, 43.89, 40.54, 39.65, 35.58, 33.19, 30.42, 30.23, 30.03, 29.84, 29.65, 29.46, 29.26.

HRMS (ESI): calc. for $C_{40}H_{42}N_6O_4^{2+}$ $[M+2H]^{2+}$: 335.1628; found 335.1629.

1.7 Additional substrates

1.7.1 2-(6-(dimethylamino)-3-(dimethyliminio)-3H-xanthen-9-yl)-4-(methylcarbamoyl)benzoate (meAm-6-TMR)

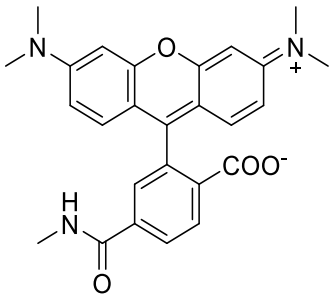

To a solution of TMR-6-COOH (1.0 mg, 2.32 µmol, 1.1 equiv.) in dry DMSO (500 µL), TSTU (763 µg, 2.53 µmol, 1.2 equiv.) was added and the mixture was stirred at r.t. for 5 min. Afterwards, DIPEA (1.4 µL, 8.45 µmol, 4 equiv.) and methylamine (2 M, 1.06 µL, 2.11 µmol, 1 equiv.) were added and the reaction mixture was stirred at r.t. overnight. The compound was purified over preparative HPLC eluted with MeCN / H_2O (0.1% TFA) (10% MeCN for 10 min., then 10 - 90% MeCN over 40 min., followed by 90% MeCN for 5 min.) to give 91.1 µg (205.4 nmol) of the desired product in 10% yield after lyophilization.

^{1}H NMR (TMR-6-COOH) (400 MHz, DMSO-d_6) δ [ppm] = 8.21 (dd, J = 8.0, 1.4 Hz, 1H), 8.17 – 7.99 (m, 1H), 7.61 – 7.56 (m, 1H), 6.58 – 6.45 (m, 6H), 2.95 (s, 12H).

^{13}C NMR (TMR-6-COOH) (101 MHz, DMSO-d_6) δ [ppm] = 168.56, 166.53, 152.67, 152.47, 131.16, 128.91, 109.56, 105.91, 98.43, 40.46, 40.26.

HRMS (ESI): calc. for $C_{26}H_{26}N_3O_4^+$ $[M+H]^+$: 444.1918; found 444.1914.

1.7.2 2-(6-(dimethylamino)-3-(dimethyliminio)-10,10-dimethyl-3,10-dihydroanthracen-9-yl)-4-(methylcarbamoyl)benzoate (meAm-6-CPY)

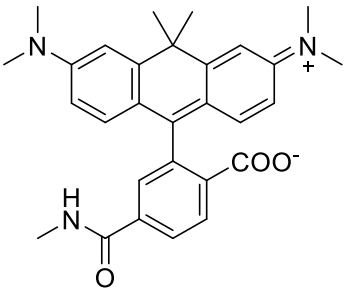

To a solution of CPY-6-COOH (1.0 mg, 2.19 µmol, 1.1 equiv.) in dry DMSO (500 µL), TSTU (719 µg, 2.39 µmol, 1.2 equiv.) was added and the mixture was stirred at r.t. for 5 min. Afterwards, DIPEA (1.32 µL, 7.97 µmol, 4.0 equiv.) and methylamine (2 M, 0.996 µL, 1.99 µmol, 1.0 equiv.) were added and the reaction mixture was stirred at r.t. overnight. The compound was purified over preparative HPLC eluted with MeCN / H_2O (0.1% TFA) (10% MeCN for 10 min., then 10 - 90% MeCN over 40 min., followed by 90% MeCN for 5 min.) to give 97.7 µg (208.1 nmol) of the desired product in 10% yield after lyophilization.

HRMS (ESI): calc. for $C_{29}H_{32}N_3O_3$ $[M+H]^+$: 470.2438; found 470.2434.

1.7.3 2-(6-(dimethylamino)-3-(dimethyliminio)-3H-xanthen-9-yl)-5-(methylcarbamoyl)benzoate (meAm-5-TMR)

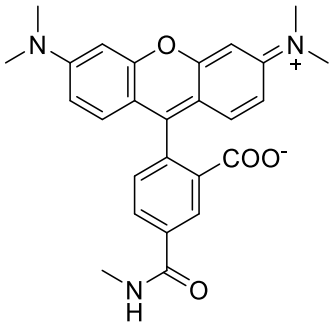

To a solution of TMR-5-COOH (2.5 mg, 5.81 µmol, 1.0 equiv.) in dry DMSO (500 µL), BOP (2.59 mg, 8.71 µmol, 1.5 equiv.) was added and the reaction was shaken at r.t. and 500 rpm for 5 min. DIPEA (3.84 µL, 23.2 µmol, 4.0 equiv.) and methylamine (2M in THF, 4.36 µL, 8.71 µmol, 1.5 equiv.) were added and the reaction was shaken at r.t. and 500 rpm for 4 h. The crude product was acidified with acetic acid and purified over preparative HPLC eluted with MeCN / H_2O (0.1% FA) (10% - 90% MeCN over 50 min) to give 0.97 mg (2.19 µmol) of the desired product in 38% yield after lyophilization.

^{1}H NMR (TMR-5-COOH) (400 MHz, DMSO-d_6) δ [ppm] = 8.39 (s, J = 1.5 Hz, 1H), 8.28 (dd, J = 8.1, 1.5 Hz, 1H), 7.33 (d, J = 8.0 Hz, 1H), 6.58 – 6.45 (m, 6H), 2.95 (s, 12H).

^{13}C NMR (TMR-5-COOH) (101 MHz, DMSO-d_6) δ [ppm] = 168.31, 166.09, 152.03, 135.96, 132.76, 128.50, 109.05, 97.95, 40.15, 39.99, 39.79.

HRMS (ESI): calc. for $C_{26}H_{26}N_3O_4^+$ $[M+H]^+$: 444.1923; found 444.1914.

1.7.4 2-(6-(dimethylamino)-3-(dimethyliminio)-10,10-dimethyl-3,10-dihydroanthracen-9-yl)-5-(methylcarbamoyl)benzoate (meAm-5-CPY)

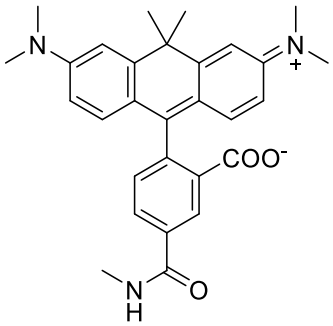

To a solution of CPY-5-COOH (2.5 mg, 5.48 µmol, 1.0 equiv.) in dry DMSO (1 mL), BOP (0.5 M in DMSO, 17.4 µL, 8.71 µmol, 1.5 equiv.) was added and the reaction was shaken at r.t and 500 rpm for 5 min. DIPEA (3.62 µL, 21.9 µmol, 4.0 equiv.) and methylamine (2 M in THF, 4.11 µL, 8.21 µmol, 1.5 equiv.) were added and the reaction was shaken at 500 rpm, r.t. for 4 h. The crude product was acidified with acetic acid and purified over preparative HPLC eluted with MeCN / H_2O (0.1% FA) (10% - 90% MeCN over 50 min) to give 0.77 mg (1.64 µmol) of the desired product in 30% yield after lyophilization.

HRMS (ESI): calc. for $C_{29}H_{32}N_3O_3^+$ $[M+H]^+$: 470.2443; found 470.2437.

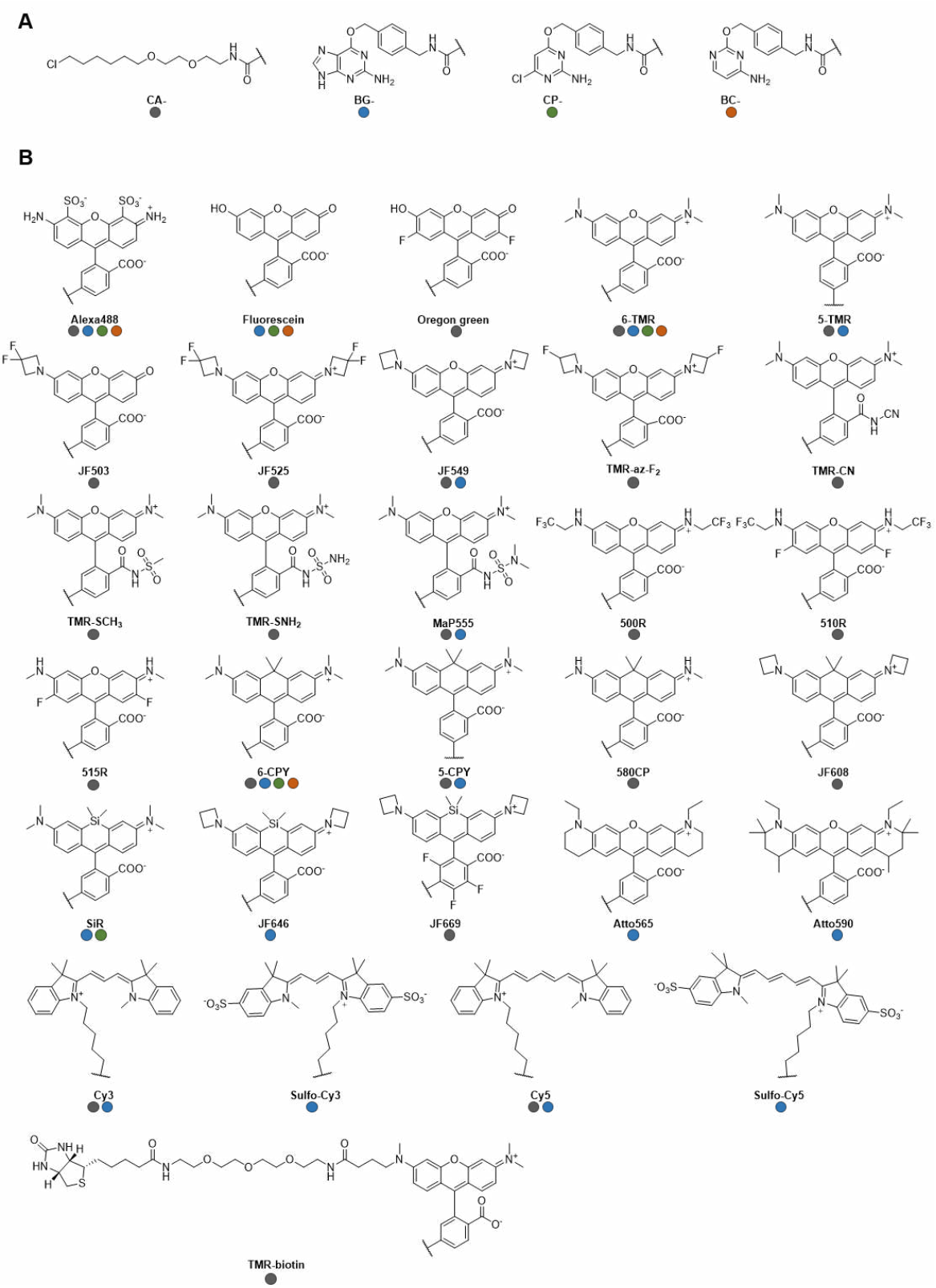

Figure S1: Chemical structures of SLP substrates. (continued on the next page)

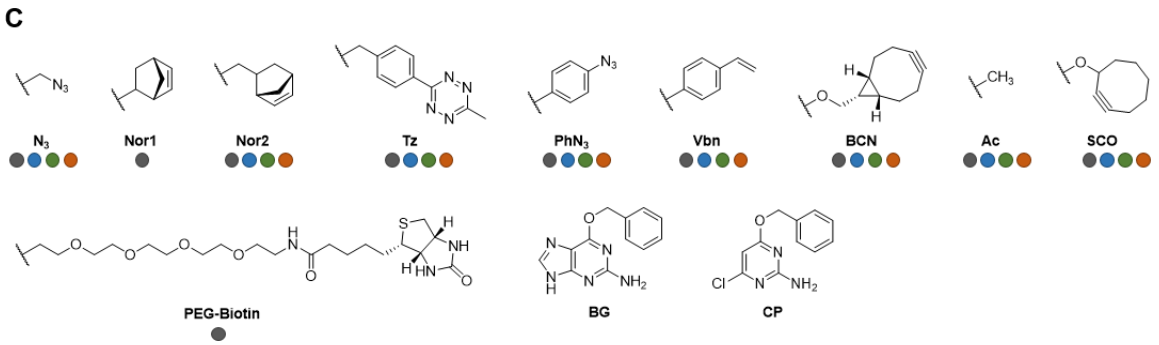

Figure S1 (continued): Chemical structures of SLP substrates.

A. Chemical structures of HT7 (CA), SNAP (BG and CP) and CLIP (BC) core substrates. **B**. Chemical structures of fluorescent substituents. **C**. Chemical structures of non-fluorescent substituents. Colored dots indicate the tested substrates for the corresponding SLPs (grey = CA, blue = BG, green = CP and orange = BC)**.**

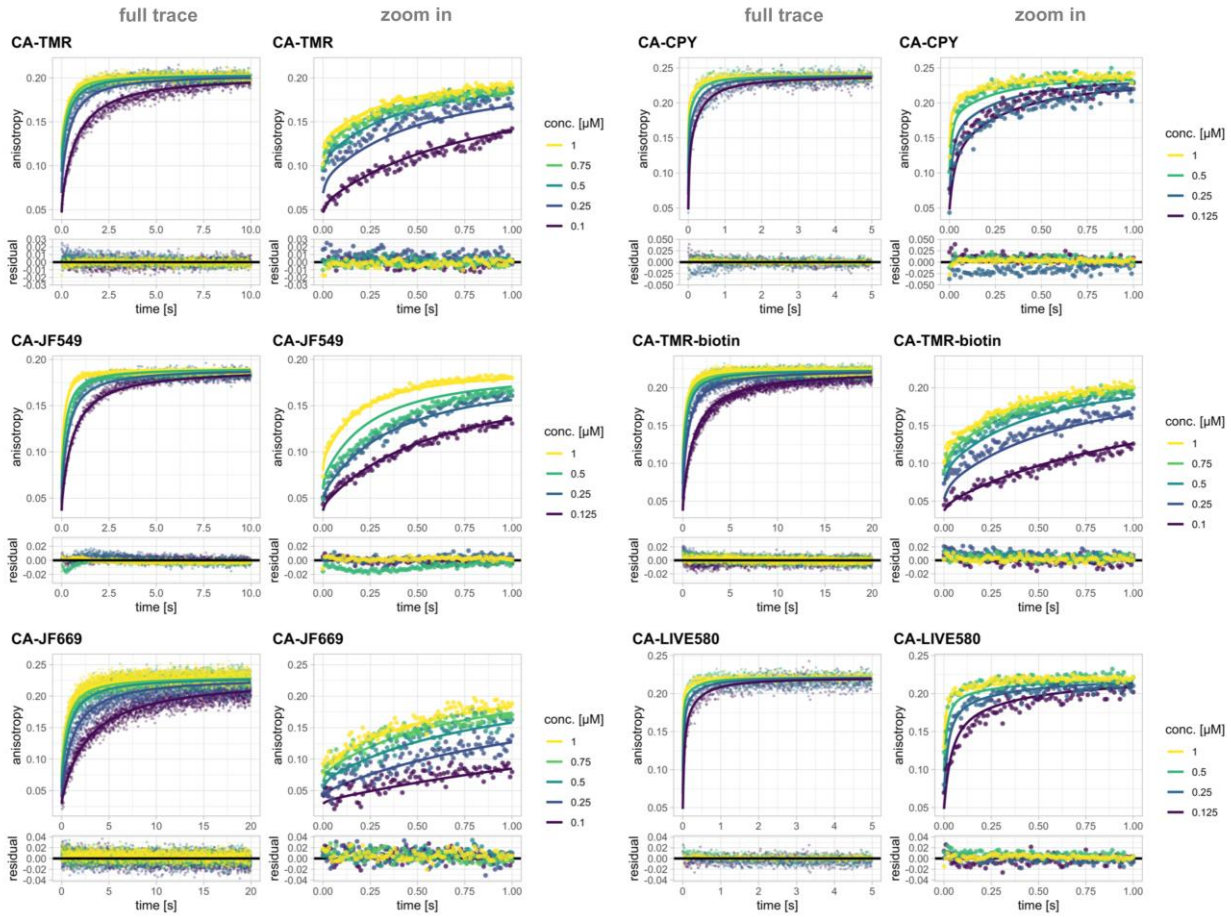

Figure S2: Labeling kinetics of HT7 with fluorescent CA substrates.

Full anisotropy traces (points) and predications of fits based on model 2 (lines) along with zoom on the first second are represented on the top panels. Residuals from the fits are depicted in the bottom panels. Kinetics were recorded by following fluorescence anisotropy changes over time using a stopped flow device. All conditions are 1:1 mixtures of protein and substrate at the given concentrations (conc.). For structures of CA substrates see **Fig. S1.**

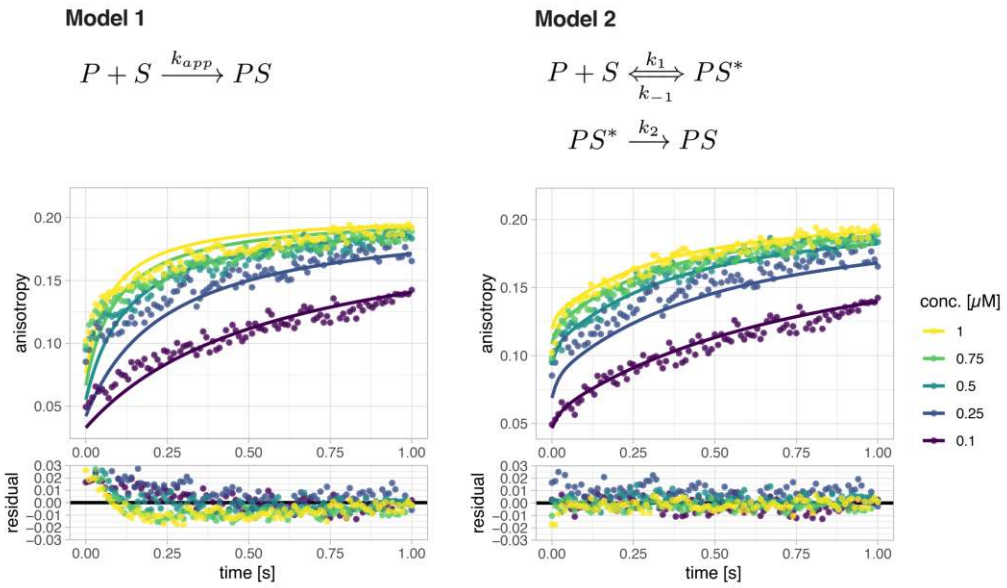

Figure S3: Comparison of model 1 and model 2 fitted to HT7 labeling kinetics.

Anisotropy traces (points) and predications of fits based on either model 1 or model 2 (lines) of the labeling reaction between HT7 and CA-TMR are represented in the top panels. Residuals from the fits are depicted in the bottom panels. Kinetics were recorded by following fluorescence anisotropy changes over time using a stopped flow device. All conditions are 1:1 mixtures of protein and substrate at the given concentrations (conc.). Model 2 describes the data better than the simplified model 1. For structures of CA substrates see **Fig. S1.**

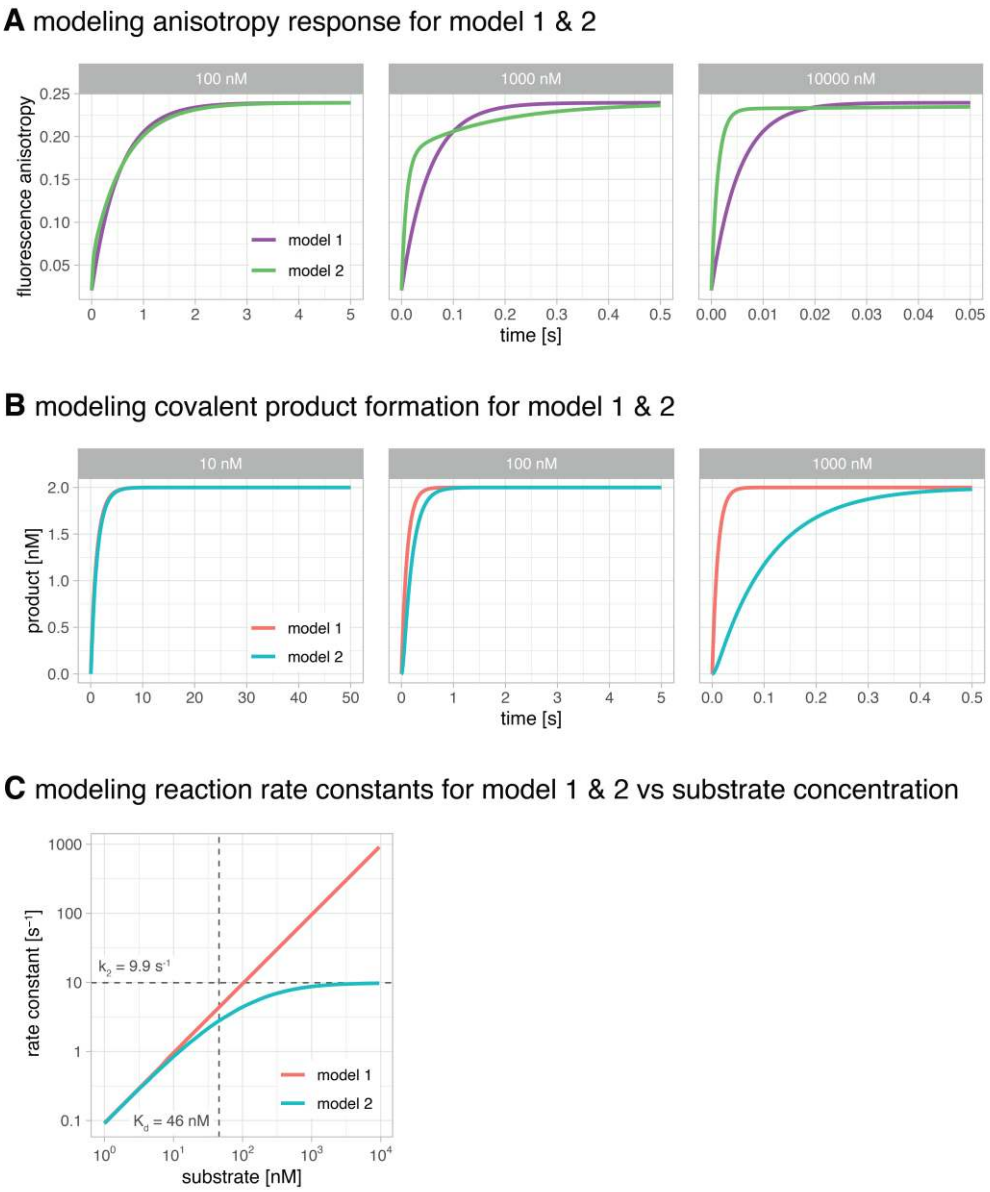

Figure S4: Modeling of HT7 labeling kinetics using measured parameters to compare the kinetic models 1 and 2.

A. Modeling of the fluorescence anisotropy response at different reactant concentrations using model 1 and 2 with parameters determined for HT7 labeling with CA-TMR. At concentrations below K_d (327 nM for CA-TMR) both models yield a rather similar response. At concentrations higher than K_d (1000 nM) the response for model 2 shows a strong biphasic character as observed in the measured data, which is not matching the monoexponential behavior of model 1. At very high concentrations (10000 nM) the response for model 2 is again close to a monoexponential curve but the kinetic is much faster than the model 1 curve. This happens since the rise in fluorescence anisotropy for model 2 in the first milliseconds is not due to covalent reaction but mostly binding (k_1). The binding rate constant k_1 is faster than k_{app} if k_{-1} is not zero ($k_{app} = k_1 * k_2 / (k_2 + k_{-1})$). Hence directly estimating k_{app} from fluorescence anisotropy traces by fitting model 1 to the data is only valid for concentrations below K_d or if $k_{-1} << k_2$. **B.** Modeling the formation of covalently labeled product at different reactant concentrations using model 1 and 2 with parameters determined for HT7 labeling with CA-CPY. At concentrations below K_d (46 nM for CA-CPY) both models yield a rather similar behavior. At higher concentrations model 1 predicts a much faster product formation than model 2 since it does not account for enzyme saturation. **C.** Plot of the apparent first order reaction rate constant for product formation against substrate concentration for model 1 and 2 with parameters for CA-CPY. In contrast to model 1, model 2 accounts for enzyme saturation leading to a maximum reaction rate of $k_{max} = k_2 = 9.9\ s^{-1}$. The models start do diverge significantly once the substrate concentration exceeds K_d (46 nM). As a consequence, model 2 should be used for predicting formation of labeled HT7 if labeling is performed at high concentrations.

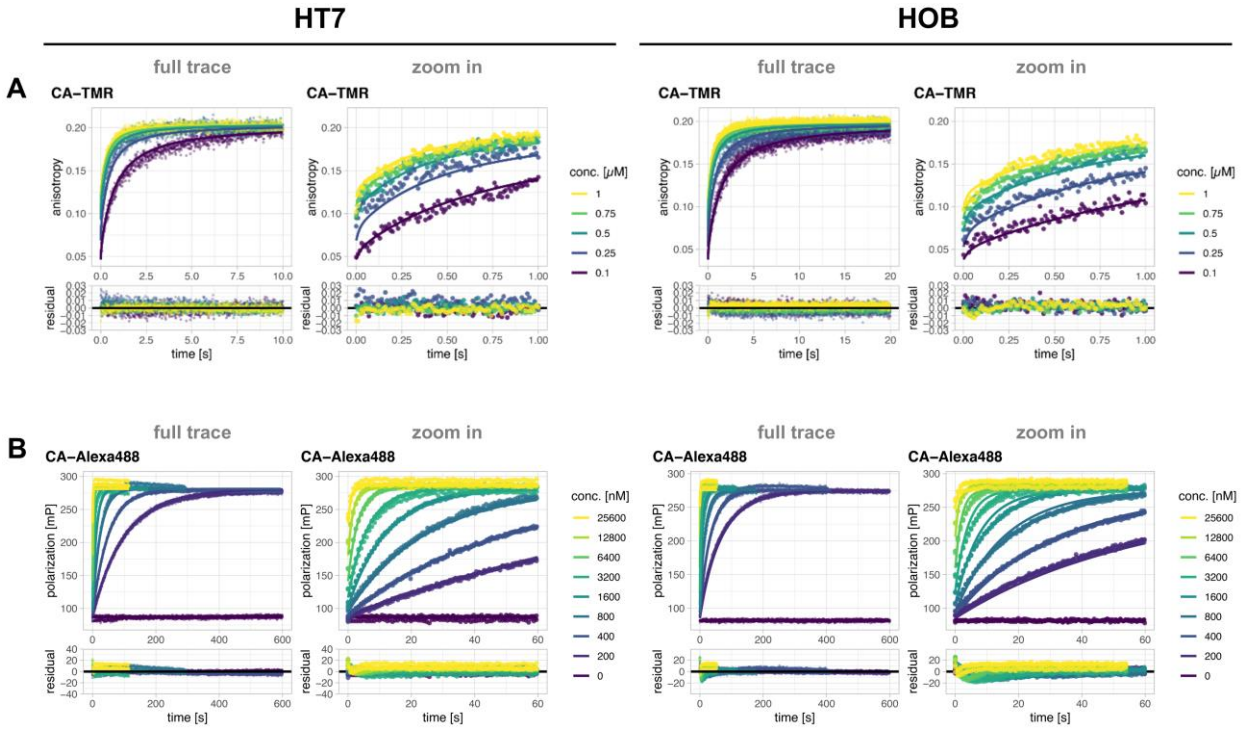

Figure S5: Labeling kinetics of HT7 and HOB with CA-TMR (**A**) and CA-Alexa488 (**B**).

A: Labeling kinetics of HT7 and HOB with CA-TMR. Full anisotropy traces (points) and predications of fits based on model 2 (lines) along with zoom on the initial part are represented on the top panels. Residuals from the fits are depicted in the bottom panels. Kinetics were recorded by following fluorescence anisotropy changes over time using a stopped flow device. All conditions are 1:1 mixtures of protein and substrate at the given concentrations (conc.). **B:** Labeling kinetics of HT7 and HOB with CA-Alexa488. Full fluorescence polarization traces (points) and predications of fits based on model 1 (lines) along with zoom on the initial part are represented on the top panels. Residuals from the fits are depicted in the bottom panels. Kinetics were recorded by following fluorescence polarization changes over time using a plate reader. All experiments were performed at a fixed substrate concentration of 50 nM with varying protein concentrations. For structures of CA substrates see **Fig. S1.**

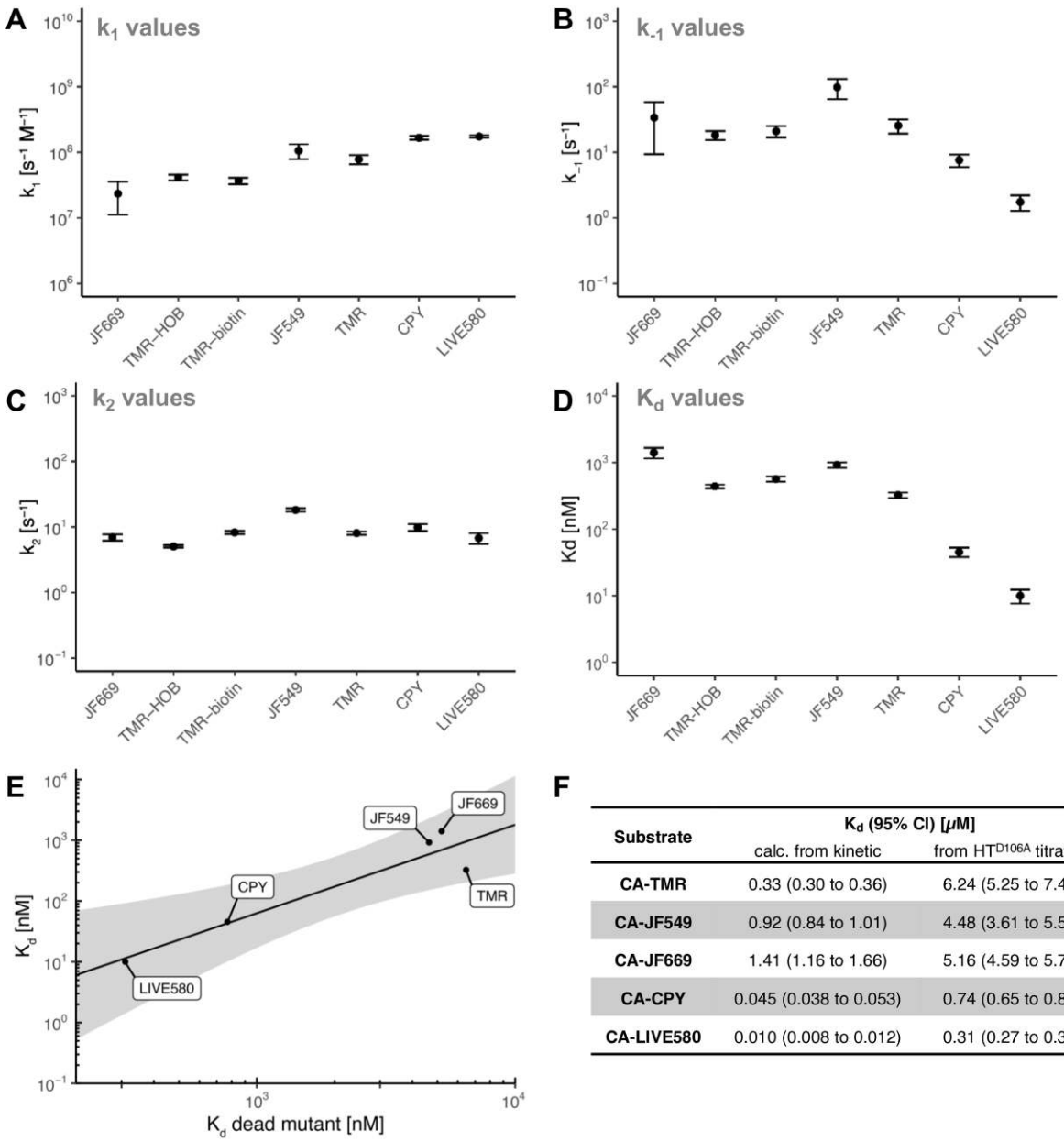

Substrate	K_d (95% CI) [μM]	
	calc. from kinetic	from HT^{D106A} titration
CA-TMR	0.33 (0.30 to 0.36)	6.24 (5.25 to 7.41)
CA-JF549	0.92 (0.84 to 1.01)	4.48 (3.61 to 5.55)
CA-JF669	1.41 (1.16 to 1.66)	5.16 (4.59 to 5.79)
CA-CPY	0.045 (0.038 to 0.053)	0.74 (0.65 to 0.85)
CA-LIVE580	0.010 (0.008 to 0.012)	0.31 (0.27 to 0.35)

Figure S6: Rate and equilibrium constants of HT7 labeling with various fluorescent CA substrates.

Rate constants k_1 (**A**), k_{-1} (**B**), k_2 (**C**) and the calculated dissociation constants ($K_d = k_{-1}/k_1$, **D.**) obtained from fitting model 2 to stopped flow labeling experiments of HT7 and HOB. The catalytic rate constant (k_2) is rather constant among these substrates, while there are significant differences in the dissociation constant (K_d). The K_d variations are due to large differences in k_{-1} and minor differences in k_1. As a result, differences in k_{app} can be mostly explained by affinity differences of HT7 towards its substrates. **E.** Correlation between the calculated K_d from the stopped flow kinetic experiments and the K_d obtained from titration experiments performed with the dead mutant $HT7^{D106A}$. Log transformed values were fitted to a linear model (log(y) = 1.455 * log(x) - 2.567; black line, 95% confidence bands in grey, depicting the area in which the true regression line lies with 95% confidence). The linear correlation in logarithmic space suggests that the K_d of CA rhodamine substrates with $HT7^{D106A}$ could represent a valid proxy to estimate their K_d with the native HT7. **F** K_d values of the tested substrates calculated from the kinetics (k_1/k_{-1}) and measured by fluorescence polarization titration against the dead mutant HT^{D106A}.

A

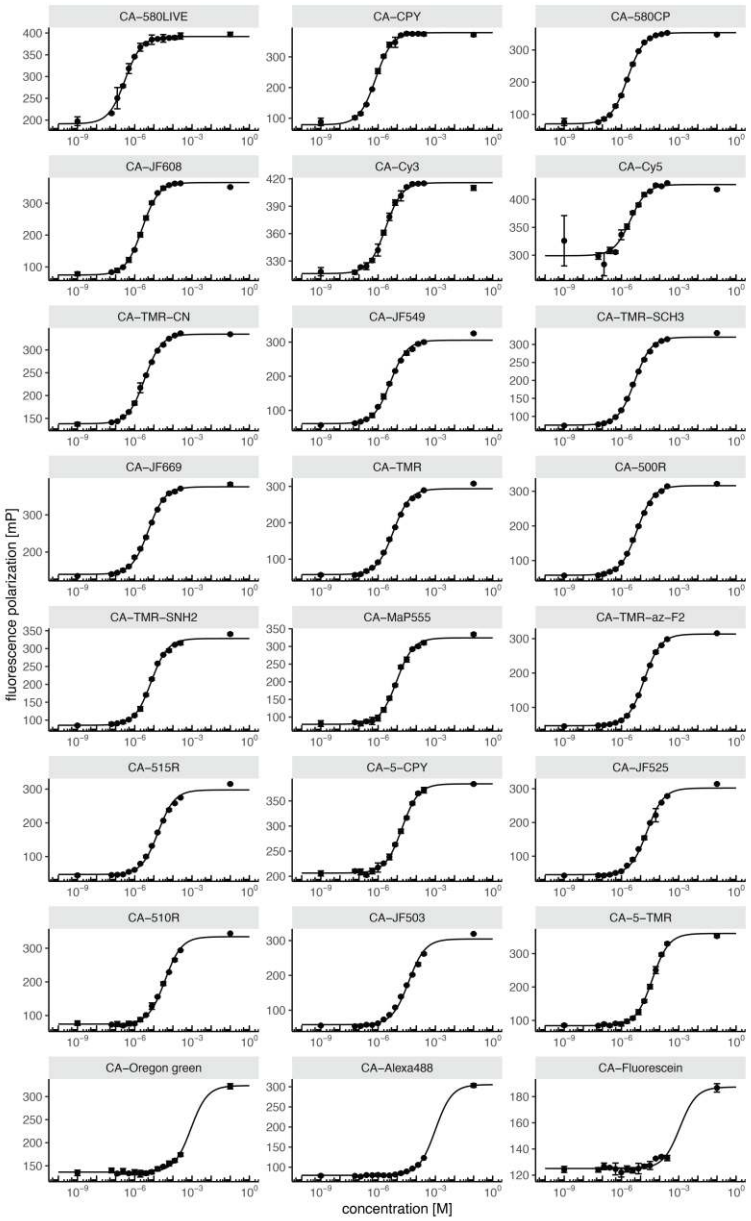

B

substrate	K_d [µM] (95%CI)
CA–580LIVE	0.31 (0.27 to 0.35)
CA–CPY	0.74 (0.65 to 0.85)
CA–580CP	2.08 (1.94 to 2.23)
CA–JF608	2.43 (2.16 to 2.73)
CA–Cy3	2.44 (2.08 to 2.87)
CA–Cy5	2.92 (1.70 to 5.08)
CA–TMR–CN	3.29 (2.98 to 3.62)
CA–JF549	4.48 (3.61 to 5.55)
CA–TMR–SCH3	4.94 (4.36 to 5.61)
CA–JF669	5.16 (4.59 to 5.79)
CA–TMR	6.24 (5.25 to 7.41)
CA–500R	6.51 (5.92 to 7.16)
CA–TMR–SNH2	7.23 (6.20 to 8.43)
CA–MaP555	9.36 (8.06 to 10.9)
CA–TMR–az–F2	15.5 (14.8 to 16.3)
CA–515R	16.7 (13.5 to 20.8)
CA–5–CPY	17.6 (15.9 to 19.6)
CA–JF525	21.8 (17.9 to 26.5)
CA–510R	38.4 (32.1 to 45.9)
CA–JF503	39.7 (30.1 to 52.0)
CA–5–TMR	40.9 (36.9 to 45.4)
CA–Oregon green	866 (697 to 1109)
CA–Alexa488	992 (894 to 1109)
CA–Fluorescein	1135 (736 to 2098)

Figure S7: Affinity of the dead mutant $HT7^{D106A}$ to fluorescent CA substrates**.**

A. Titration curves of fluorescent CA substrates against $HT7^{D106A}$ measured via fluorescence polarization. The FP value of each dye fully bound to native HT7 was added at c = 0.1 M to improve fitting of the upper plateau. (See corresponding methods section for more details). **B.** Table summarizing fitted K_d values with 95% confidence intervals. For structures of CA substrates see **Fig. S1.**

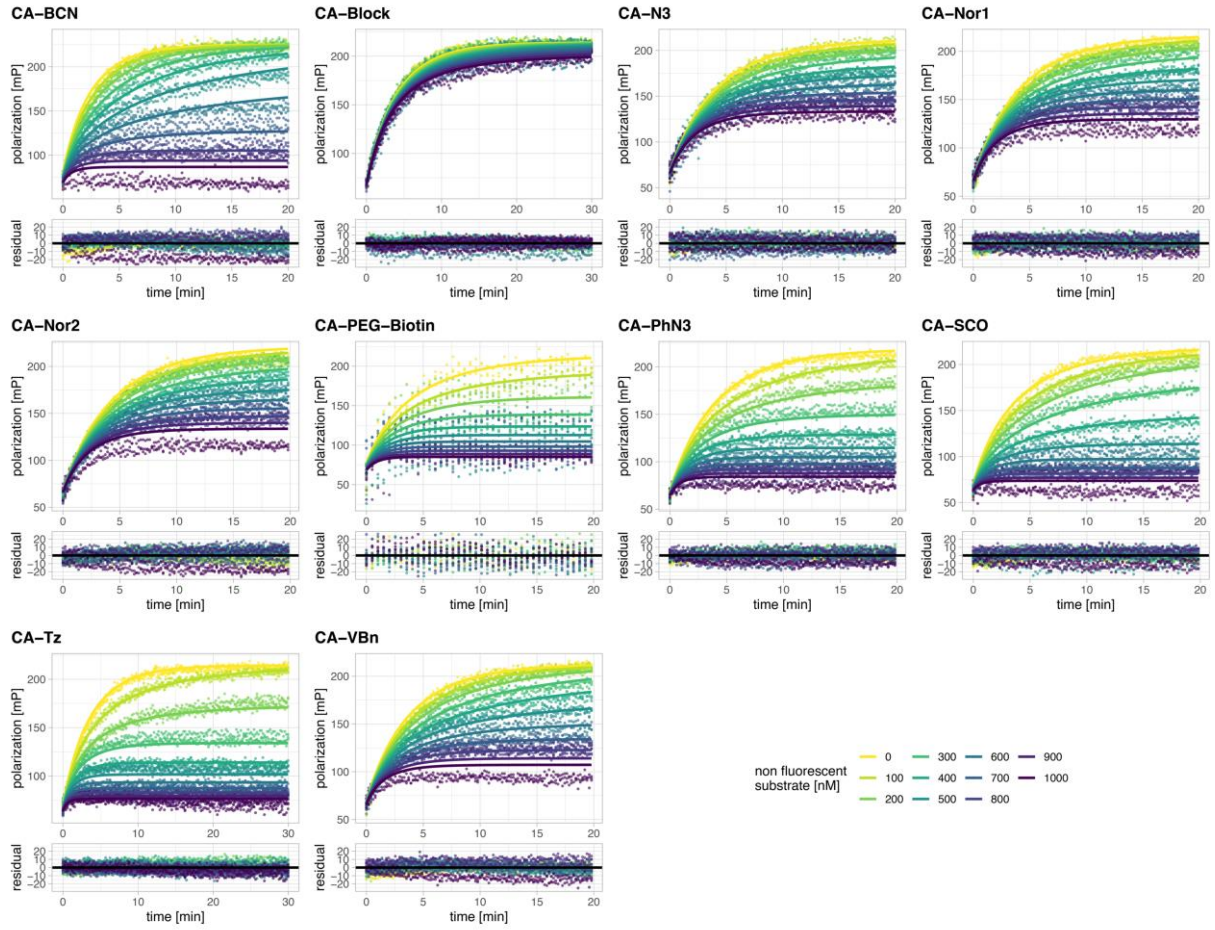

Figure S8: Labeling kinetics of HT7 with non-fluorescent CA substrates.

Fluorescence polarization traces (points) of kinetic competition assays and predications of fits (lines) based on a simple competitive model (see methods section for details) of HT7 labeling with CA-Alexa488 in the presence of different concentrations of non-fluorescent CA substrates are represented on the top panels. Residuals from the fits are depicted in the bottom panels. Kinetics were recorded by following fluorescence polarization changes over time using a plate reader. For structures of CA substrates see **Fig. S1.**

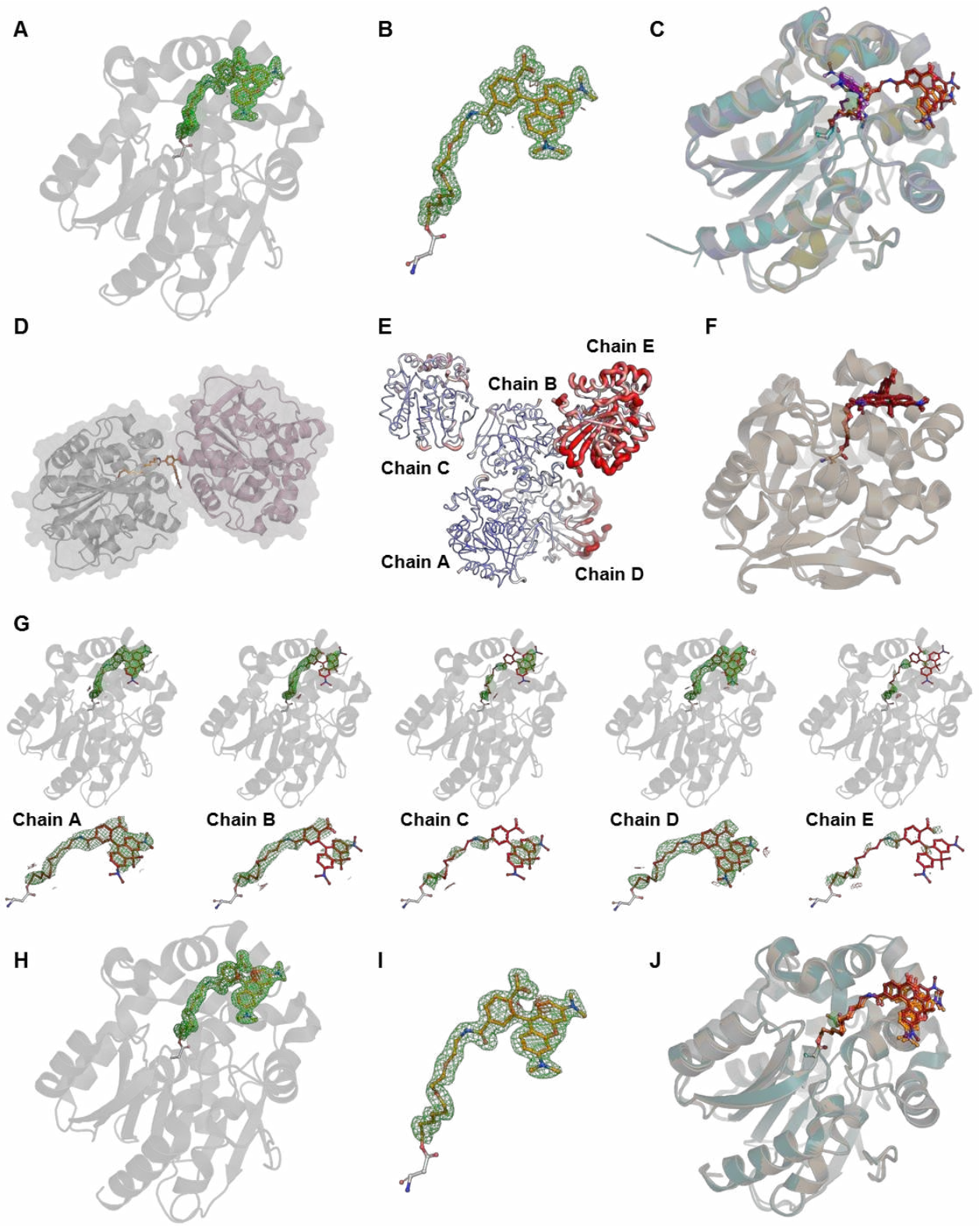

Figure S9: Validation of HT7-TMR and HT7-CPY X-ray structures.

A. Omit-map of the TMR ligand of the HT7-TMR X-ray structure. The protein is represented as grey cartoon with the catalytic aspartate (grey) and the TMR ligand (orange) represented as sticks. **B.** Zoom on the isolated labeled catalytic aspartate of HT7-TMR. The omit map of the alkane-TMR is contoured at 3 σ and represented as green and red mesh for missing and extra density, respectively. **C**.

Structure alignment of HT7-TMR and HT7-CPY (chain A) with different X-ray structures of HaloTag. All structures are represented as cartoons with their respective catalytic aspartate and ligands represented as sticks. When present the chloride is represented as green sphere. **D**. Alkane-TMR constraints by the crystal packing. Two monomers of HT7-TMR are represented as grey and light-pink cartoons and surfaces. The conformation of alkane-TMR (orange sticks) of the grey monomer is constrained by the light-pink monomer that was generated as symmetry mate. **E**. B-factor putty representation of the different chains of the asymmetric unit of the HT7-CPY crystal structure. Blue = 15; Red = 120. Chain E and to a lesser extent Chain D present an overall higher B-factor compared the other monomers. **F**. Structure alignment of the different monomers in the asymmetric unit of the HT7-CPY structure. The monomers are represented as wheat cartoon with the catalytic aspartate and alkane-CPY represented as sticks; all featuring similar conformations. **G**. Omit-maps of the alkane-CPY ligands of the different monomers in the HT7-CPY asymmetric unit. Proteins are represented as grey cartoons with the catalytic aspartates (grey) and alkane-CPYs (firebrick) represented as sticks. **H**. Omit-map of the TMR ligand of the HOB-TMR X-ray structure. The protein is represented as grey cartoon with the catalytic aspartate (grey) and the TMR ligand (orange) represented as sticks. **I.** Zoom on the isolated labeled catalytic aspartate of HOB-TMR. The omit map of the alkane-TMR is contoured at 3 σ and represented as green and red mesh for missing and extra density, respectively. **J**. Structure alignment of HT7-TMR, HT7-CPY (chain A) and HOB-TMR. Proteins are represented as grey, wheat and dark-green cartoons, respectively. The alkane-TMR and -CPY ligands are represented as orange and firebrick sticks, respectively. The catalytic aspartate is represented as sticks of the same color as the cartoons.

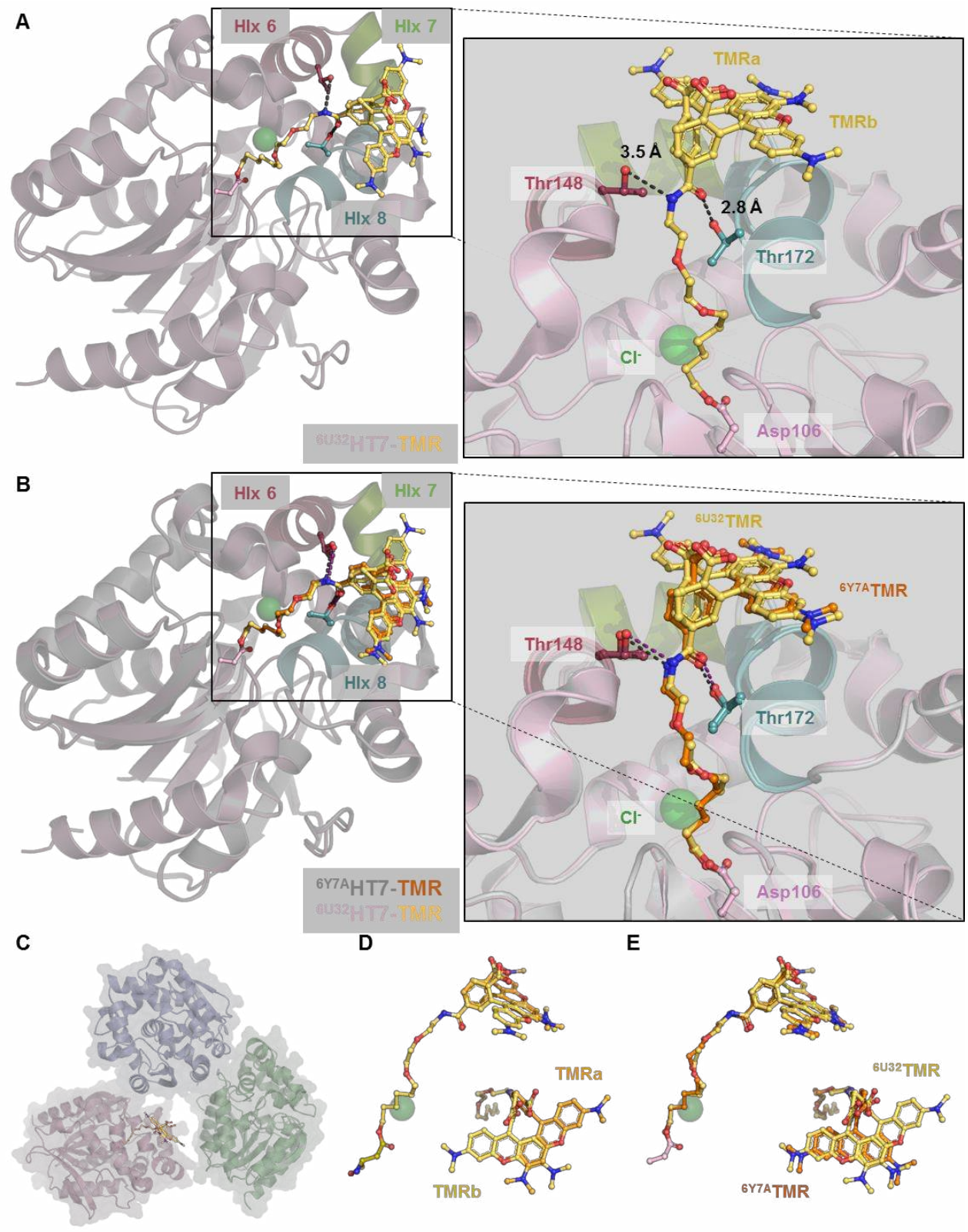

Figure S10: Structural comparison between HT7-TMR structures from PDB IDs 6U32 and 6Y7A.

A. Structure of HT7-TMR (PDB ID 6U32, previously published (16)) featuring two conformations of the alkane-TMR ligand **B**. Structural comparison between ^{6U32}HT7-TMR and ^{6Y7A}HT7-TMR (PDB ID 6Y7A, this study). Hydrogen bonds between ^{6Y7A}HT7-TMR and ^{6U32}HT7-

TMR and their respective reacted substrates are represented as black and dark-purple lines, respectively. **C**. ^{6U32}HT7-TMR crystal packing. Three monomers of HT7-TMR are represented as blue, green and pink cartoons. The conformation of the alkane-TMR (yellow/orange sticks) of the pink monomer is not constrained by the other symmetry mates. **D**. Zoom on the catalytic aspartate and alkane-TMR substrate highlighting the alternative conformations observed in the ^{6U32}HT7-TMR crystal structure. The two alternative TMR conformations (a and b) are represented as different tone of yellow/orange sticks. **E**. Structural comparison of the substrate positioning between ^{6U32}HT7-TMR and ^{6Y7A}HT7-TMR. Alkane-^{6U32}TMR and alkane-^{6Y7A}TMR are represented as yellow and orange sticks, respectively. The ^{6Y7A}TMR present a very similar conformation than one of the ^{6U32}TMR conformation which can't be observed due to the crystal packing in the ^{6Y7A}HT7-TMR crystal structure.

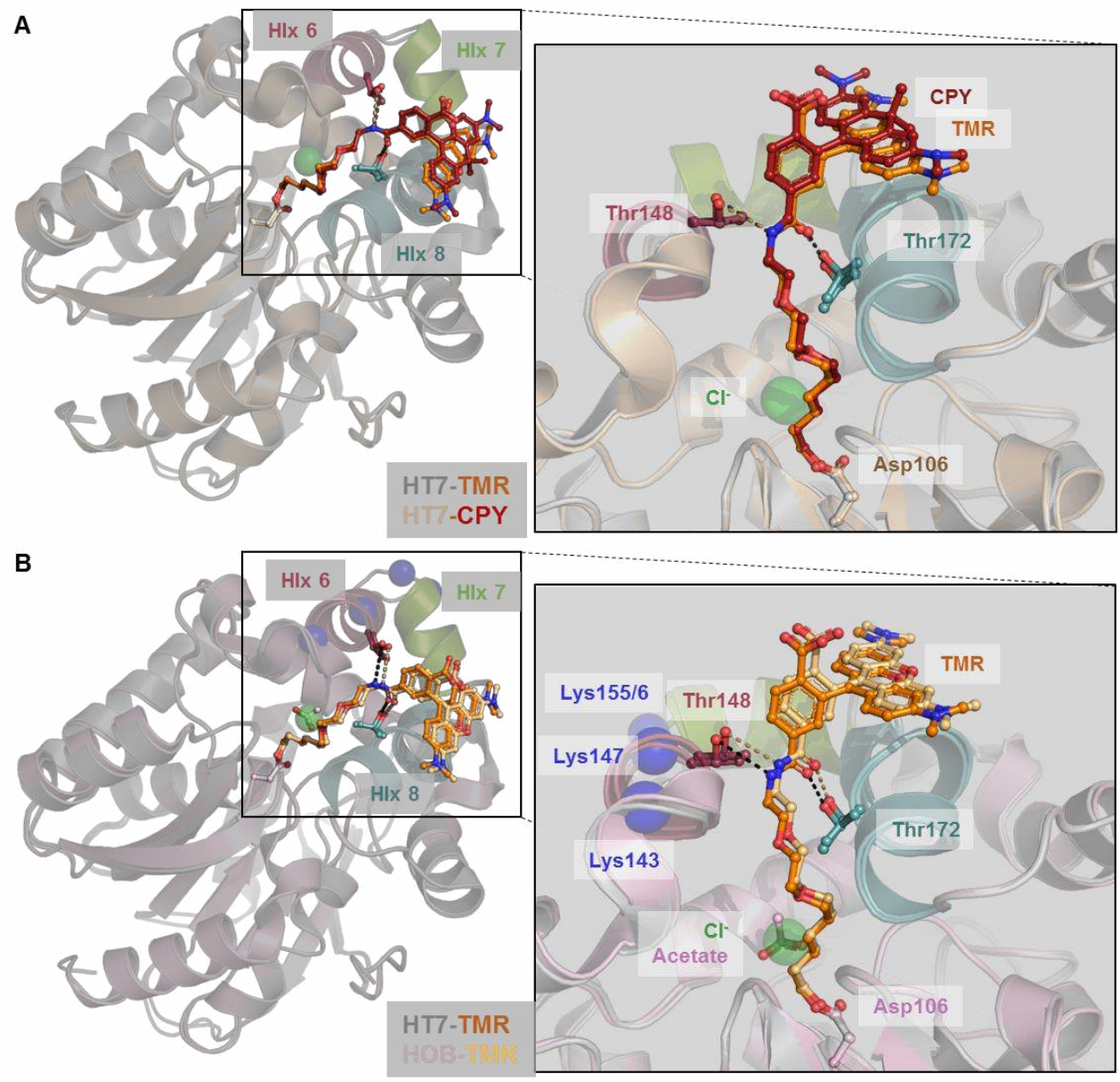

Figure S11: Structural comparison between HT7-TMR, HT7-CPY (**A**) and HOB-TMR (**B**).

A. Structural comparison between HT7-TMR and HT7-CPY. Hydrogen bonds between HT7-TMR and HT7-CPY and their respective reacted substrates are represented as black and sand dashed lines, respectively. **B**. Structural comparison between HT7-TMR and HOB-TMR. Hydrogen bonds between HT7 and HOB and their respective reacted substrates are represented as black and sand dashed lines, respectively.

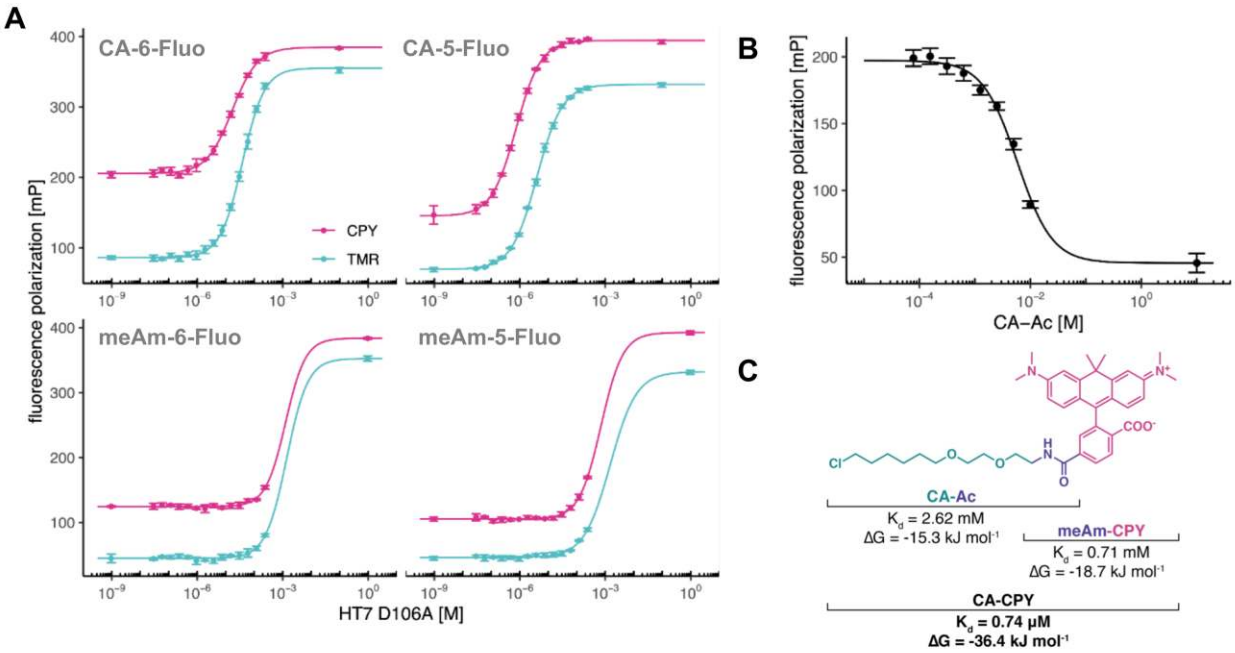

D

dye	position	ligand	K_d [µM]	95% CI [µM]
TMR	5 position	CA	39.4	(35.7 to 43.4)
		meAm	1930	(1660 to 2291)
	6 position	CA	6.24	(5.25 to 7.41)
		meAm	1512	(1402 to 1640)
CPY	5 position	CA	16.8	(15.2 to 18.6)
		meAm	1987	(1688 to 2398)
	6 position	CA	0.74	(0.65 to 0.85)
		meAm	707	(497 to 785)

Figure S12: Biochemical study of the interaction of HT7 with CA-fluorophores.

A. Affinity of the dead mutant $HT7^{D106A}$ towards different fluorophore derivatives measured via fluorescence polarization assay. The FP value of each dye as CA substrate fully bound to native HT7 was added at c = 0.1 M or c = 1 M in order to improve fitting of the upper plateau. **B.** Affinity of $HT7^{D106A}$ to CA-Ac measured via fluorescence polarization competition assay against CA-TMR. **C.** Summary of dissociation constants (K_d) and calculated free binding energies (ΔG) of $HT7^{D106A}$ with CA-Ac, mAm-5-CPY and CA-5-CPY. The representation highlights the additive nature of the binding energies from the chloroalkane and the CPY moieties for the binding energy of the full substrate. **D.** Table summarizing values and confidence intervals (95%) of the fits.

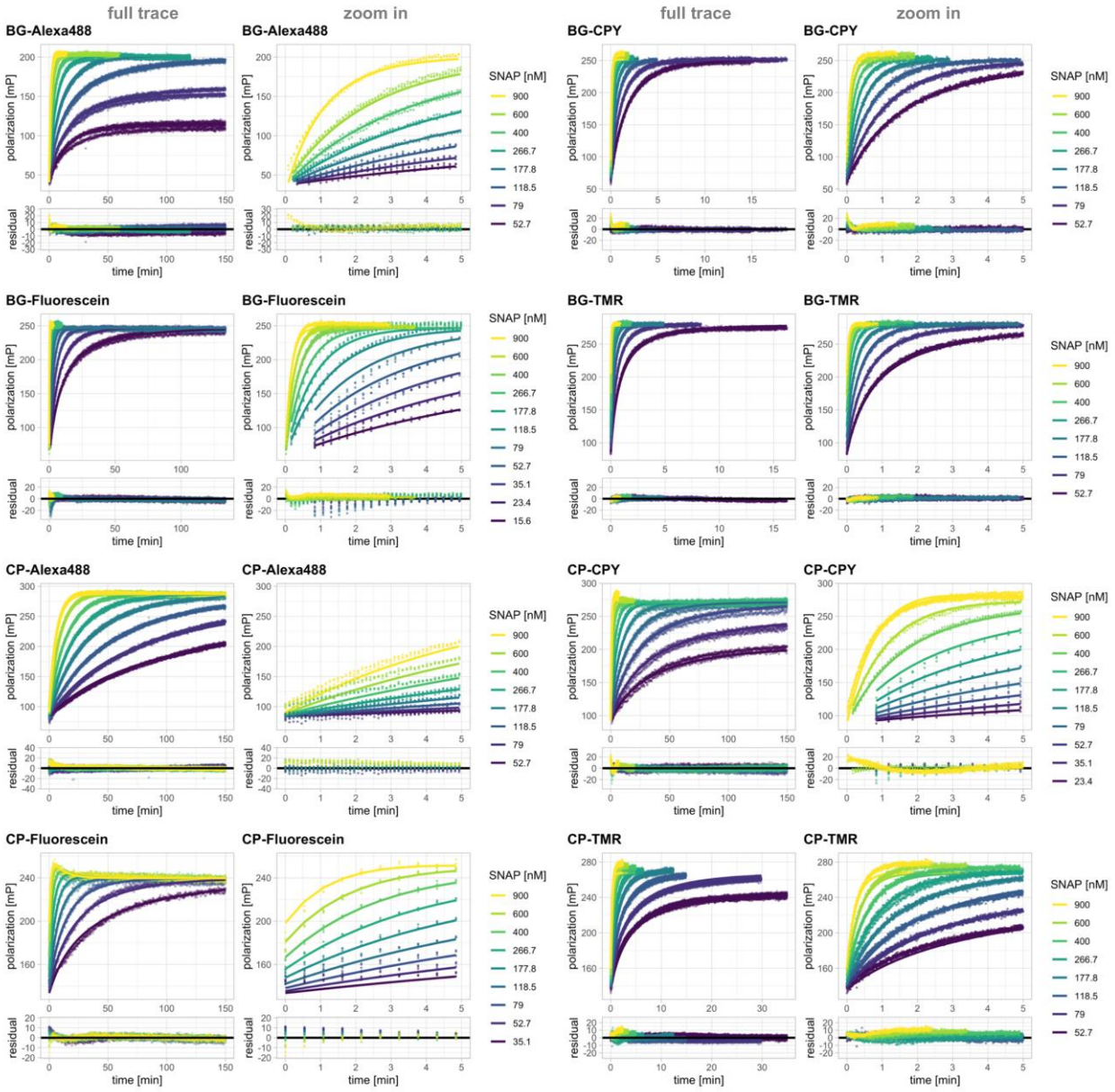

Figure S13: Labeling kinetics of SNAP with fluorescent BG and CP substrates.

Full fluorescence polarization traces (points) and predications of fits based on model 1 or 1.2 (lines) along with zoom on the initial 5 minutes are represented on the top panels. Most substrates were fitted to model 1 except CP-Fluorescein and CP-CPY, which showed an additional phase (model 1.2). Residuals from the fits are depicted in the bottom panels. Kinetics were recorded by following fluorescence polarization changes over time using a plate reader. Labeling was performed at different concentrations of SNAP protein. Substrate concentrations were aimed at 20 nM based on the dyes extinction coefficient but fitted in the model since significant deviations from the expected stoichiometry were observed. For structures of BG and CP substrates see **Fig. S1.**

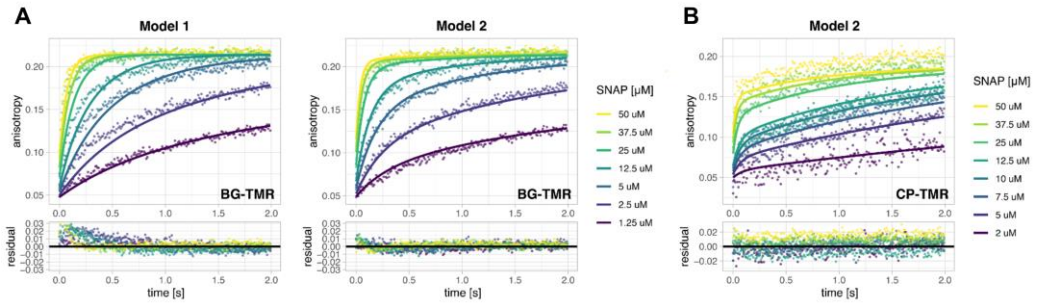

C

Substrate	K_d (95% CI) [µM]		k_{app} (± SD) [$M^{-1}s^{-1}$]	
	calc. from stopped flow kinetics	from $SNAP^{C456A}$ titrations	calc. from stopped flow kinetics	fitted from plate reader kinetics
BG-TMR	2.06 (1.98 to 2.14)	0.77 (0.66 to 0.90)	2.714 (± 0.008) × 10^5	4.292 (± 0.007) × 10^5
CP-TMR	16.69 (15.89 to 17.49)	5.64 (5.04 to 6.30)	0.805 (± 0.004) × 10^5	0.769 (± 0.001) × 10^5

Figure S14: Labeling kinetics of SNAP measured by stopped flow fluorescence anisotropy.

A. Comparative data analysis of SNAP labeling kinetics with BG-TMR. Anisotropy traces (points) and predications of fits based on either model 1 or model 2 (lines) of the labeling reaction between SNAP and BG-TMR are represented in the top panels. Residuals from the fits are depicted in the bottom panels. Labeling was performed at different concentrations of SNAP protein and a constant substrate concentration of 1 µM. Model 2 describes the data better than the simplified model 1. (for model description see **Fig. 1**). **B.** Kinetic traces of SNAP labeling with CP-TMR represented as previously explained and fit with model 2. For structures of BG and CP substrates see **Fig. S1. C.** K_d and k_{app} values calculated from parameters obtained by fitting model 2 to stopped flow anisotropy data ($K_d = k_{-1}/k_1$, $k_{app} = k_1*k_2/(k_{-1}+k_2)$) compared to values directly fitted to fluorescence polarization assay with $SNAP^{C145A}$ (K_d) and plate reader kinetics at lower SNAP concentrations fitted with model 1 (k_{app}).

A

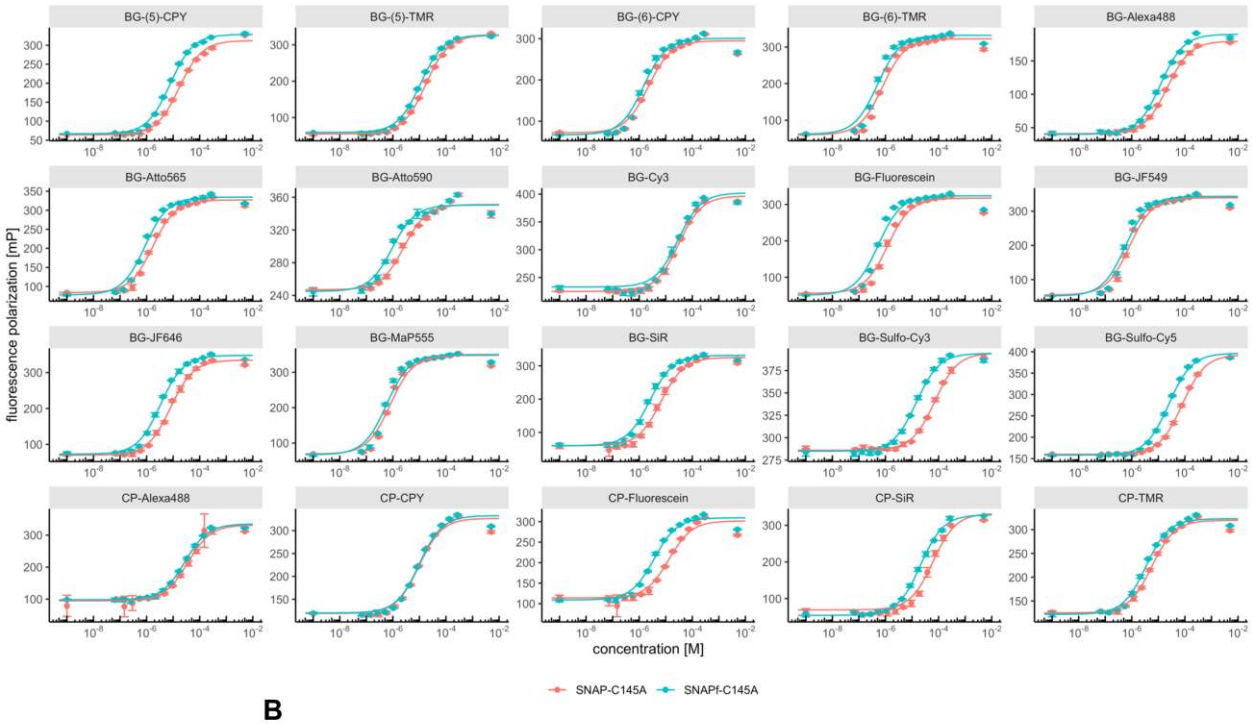

B

Substrate	K_d $SNAP^{C145A}$ (95% CI) [µM]	K_d $SNAPf^{C145A}$ (95% CI) [µM]	ΔK_d
BG-(5)-CPY	17.0 (15.7 - 18.3)	7.71 (7.24 - 8.21)	2.20
BG-(5)-TMR	17.2 (16.5 - 17.9)	10.9 (10.4 - 11.6)	1.58
BG-(6)-CPY	2.20 (1.90 - 2.54)	1.44 (1.23 - 1.69)	1.53
BG-(6)-TMR	0.77 (0.66 - 0.90)	0.50 (0.43 - 0.58)	1.54
BG-Alexa488	21.8 (20.8 - 22.8)	12.2 (11.4 - 13.1)	1.79
BG-Atto565	1.73 (1.55 - 1.94)	0.88 (0.78 - 0.99)	1.97
BG-Atto590	2.60 (2.22 - 3.05)	0.95 (0.80 - 1.12)	2.74
BG-Cy3	31.0 (28.3 - 34.0)	29.3 (24.6 - 34.8)	1.06
BG-Fluorescein	1.21 (1.04 - 1.41)	0.52 (0.44 - 0.62)	2.33
BG-JF549	0.82 (0.71 - 0.95)	0.58 (0.50 - 0.67)	1.41
BG-JF646	7.97 (7.38 - 8.59)	3.32 (3.06 - 3.61)	2.40
BG-MaP555	0.80 (0.69 - 0.92)	0.58 (0.50 - 0.67)	1.38
BG-SiR	6.64 (5.87 - 7.51)	2.52 (2.29 - 2.76)	2.63
BG-Sulfo-Cy3	71.3 (66.4 - 76.5)	14.6 (13.1 - 16.3)	4.88
BG-Sulfo-Cy5	79.5 (76.2 - 83.0)	24.8 (23.3 - 26.3)	3.21
CP-Alexa488	35.1 (26.3 - 46.4)	27.5 (25.4 - 29.8)	1.28
CP-CPY	9.61 (8.30 - 11.1)	9.77 (8.66 - 11.0)	0.98
CP-Fluorescein	13.2 (10.5 - 16.5)	3.65 (3.18 - 4.18)	3.62
CP-SiR	61.9 (52.5 - 72.7)	20.9 (19.5 - 22.4)	2.96
CP-TMR	5.64 (5.04 - 6.30)	3.37 (3.08 - 3.70)	1.67

Figure S15: Comparison of fluorophore substrate affinities between the dead mutants $SNAP^{C145A}$ and $SNAPf^{C145A}$.

A. Titration curves obtained for the dead mutants $SNAP^{C145A}$ and $SNAPf^{C145A}$ measured via fluorescence polarization. The FP value of each dye fully bound to native SNAP/SNAPf was added at c = 0.005 M to improve fitting of the upper plateau. (See corresponding methods section for more details). **B**. Table summarizing fitted K_d values with 95% confidence intervals. For structures of BG and CP substrates see **Fig. S1.**

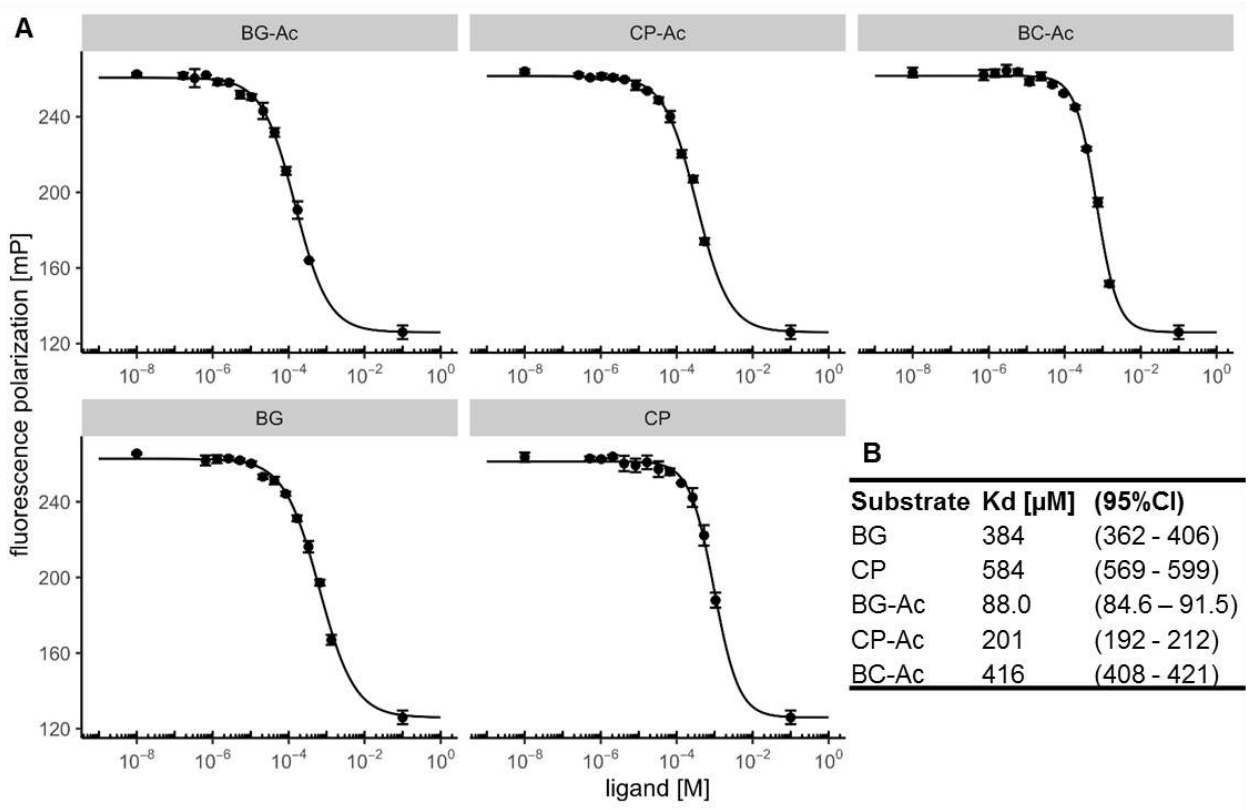

Figure S16: Comparison of non-derivatized core substrate affinities with the dead mutant SNAP^{C145}.

A. Titration curves obtained for the dead mutant SNAP^{C145A} measured via competitive fluorescence polarization. The FP value of free dye was added at c = 0.1 M to improve fitting of the lower plateau. (See corresponding methods section for more details) **B**. Table summarizing fitted K_d values with 95% confidence intervals. For structures of substrates see **Fig. S1.**

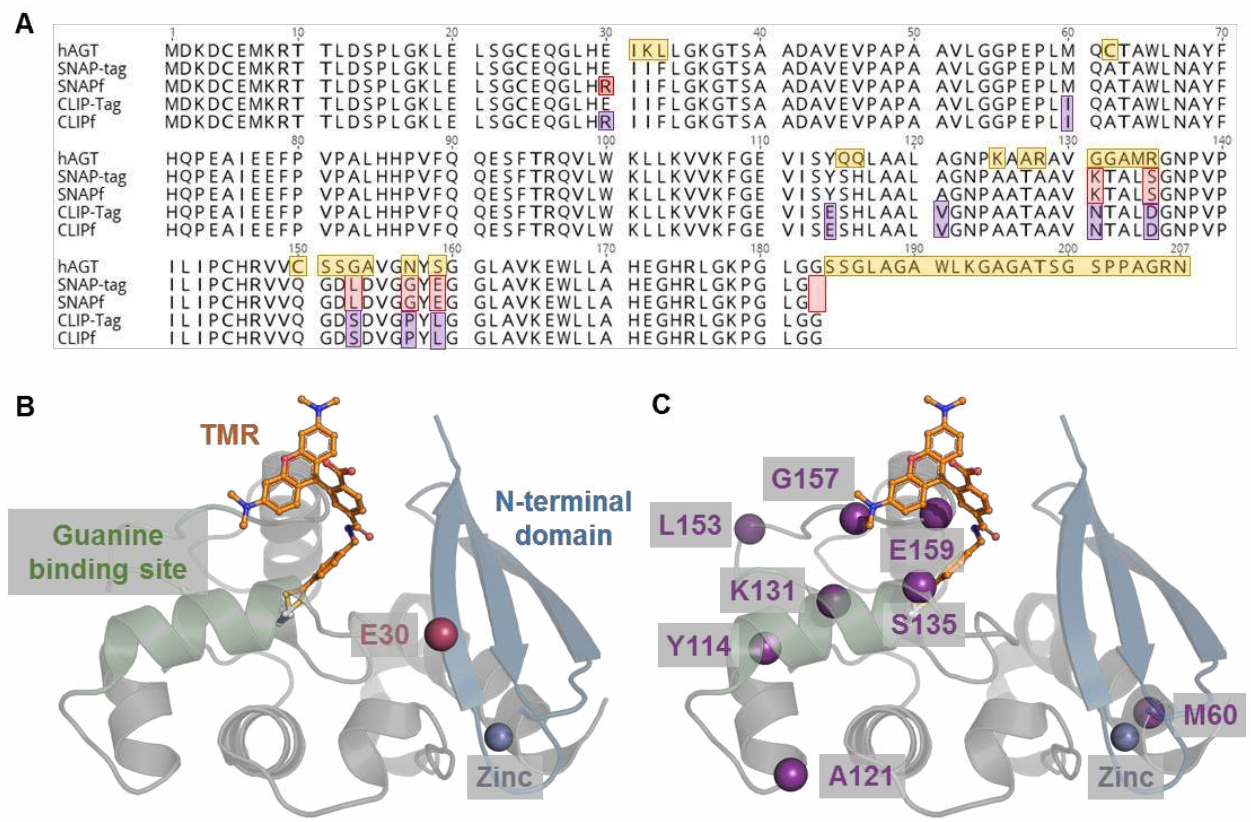

Figure S17: Sequence alignment and structural comparison between SNAP and CLIP variants.

A. Sequence alignment of hAGT, SNAP, SNAPf, CLIP and CLIPf. Differences are highlighted in yellow, red and violet in the hAGT, SNAP(f) and CLIP(f) sequences, respectively. **B.** Crystal structure of SNAP labeled with TMR. SNAP is represented as grey cartoon despite for the BG binding site and the N-terminal domain that are represented in green and blue, respectively. The catalytic cysteine is represented as grey sticks and the benzyl-TMR as orange sticks. The residue E30 which is mutated to an arginine (R) in SNAPf is highlighted as a red sphere. **C.** Crystal structure of SNAP labeled with TMR with α-carbons of the residues that differ between SNAP and CLIP represented as purple spheres.

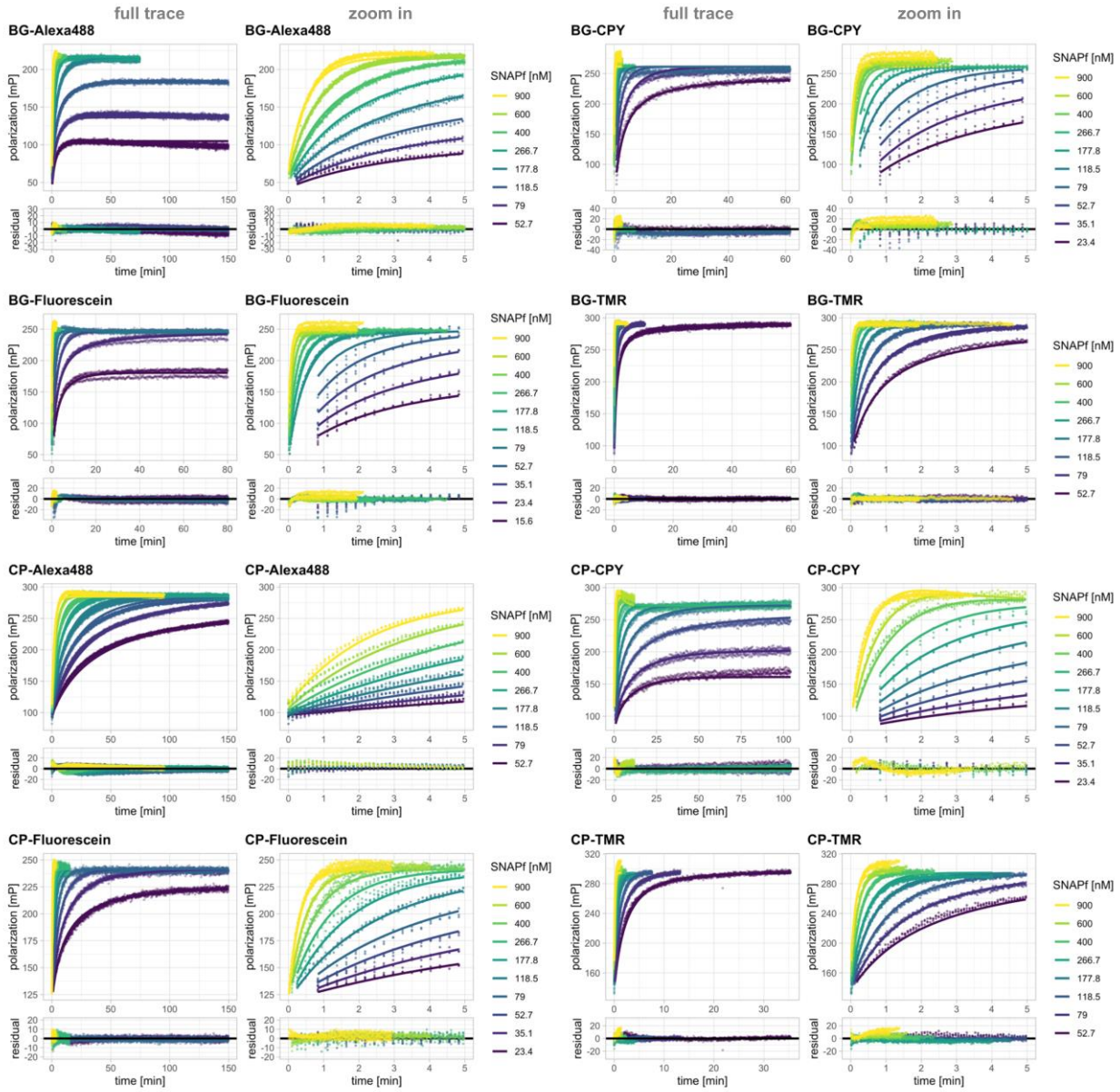

Figure S18: Labeling kinetics of SNAPf with fluorescent BG and CP substrates.

Full fluorescence polarization traces (points) and predications of fits based on model 1 or 1.2 (lines) along with zoom on the initial 5 minutes are represented on the top panels. All substrates were fitted to model 1 except CP-CPY, which showed an additional phase (model 1.2). Residuals from the fits are depicted in the bottom panels. Kinetics were recorded by following fluorescence polarization changes over time using a plate reader. Labeling was performed at different concentrations of SNAPf protein. Substrate concentrations were aimed at 20 nM based on the dyes extinction coefficient but fitted in the model since significant deviations from the expected stoichiometry were observed. For structures of BG and CP substrates see **Fig. S1.**

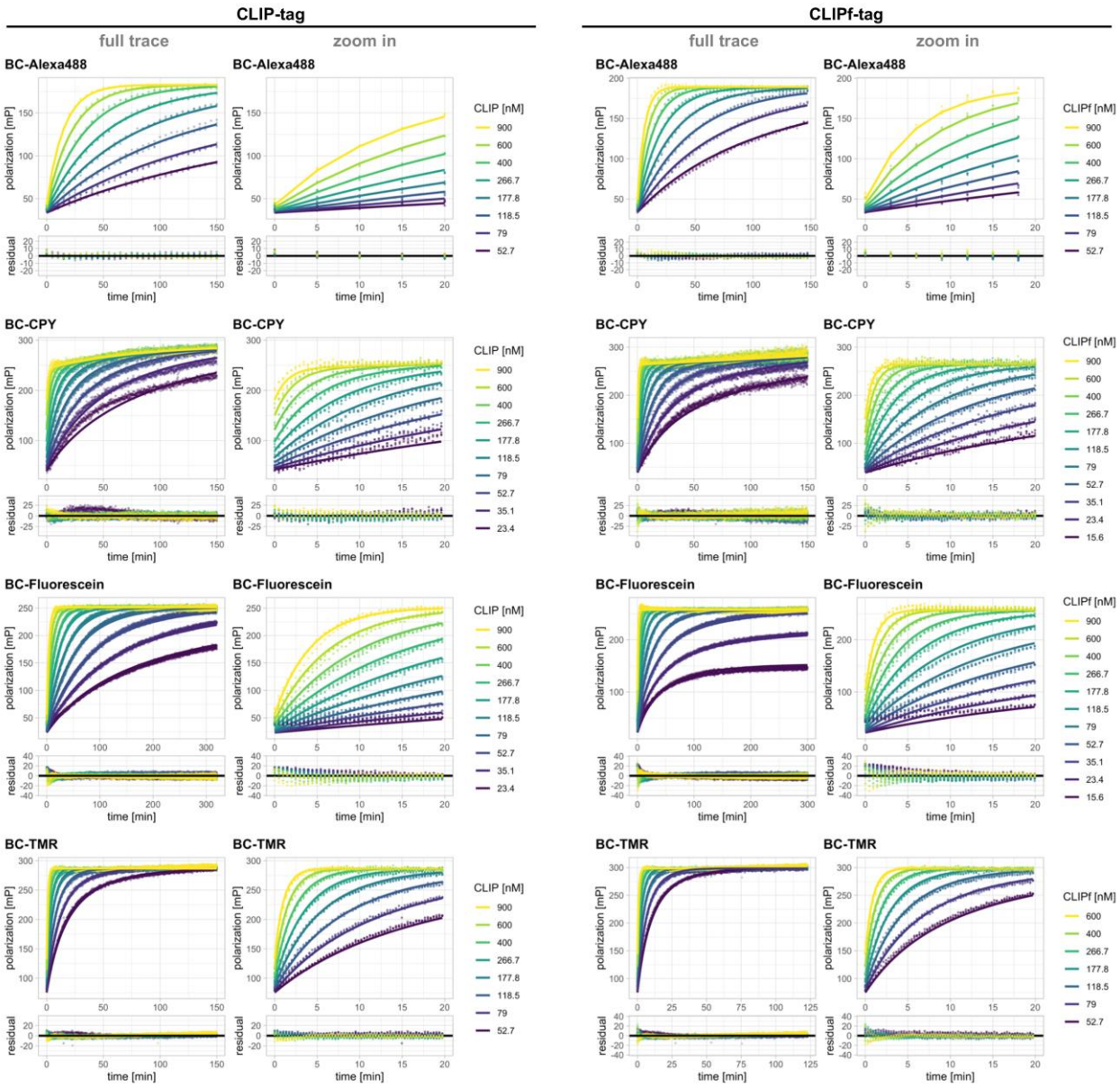

Figure S19: Labeling kinetics of CLIP and CLIPf with fluorescent BC substrates.

Full fluorescence polarization traces (points) and predications of fits based on model 1 or 1.2 (lines) along with zoom on the initial 20 minutes are represented on the top panels. All substrates were fitted to model 1 except BC-CPY, which showed an additional phase (model 1.2). Residuals from the fits are depicted in the bottom panels. Kinetics were recorded by following fluorescence polarization changes over time using a plate reader. Labeling was performed at different concentrations of CLIP and CLIPf protein. Substrate concentrations were aimed at 20 nM based on the dyes extinction coefficient but fitted in the model since significant deviations from the expected stoichiometry were observed. For structures of BC substrates see **Fig. S1**.

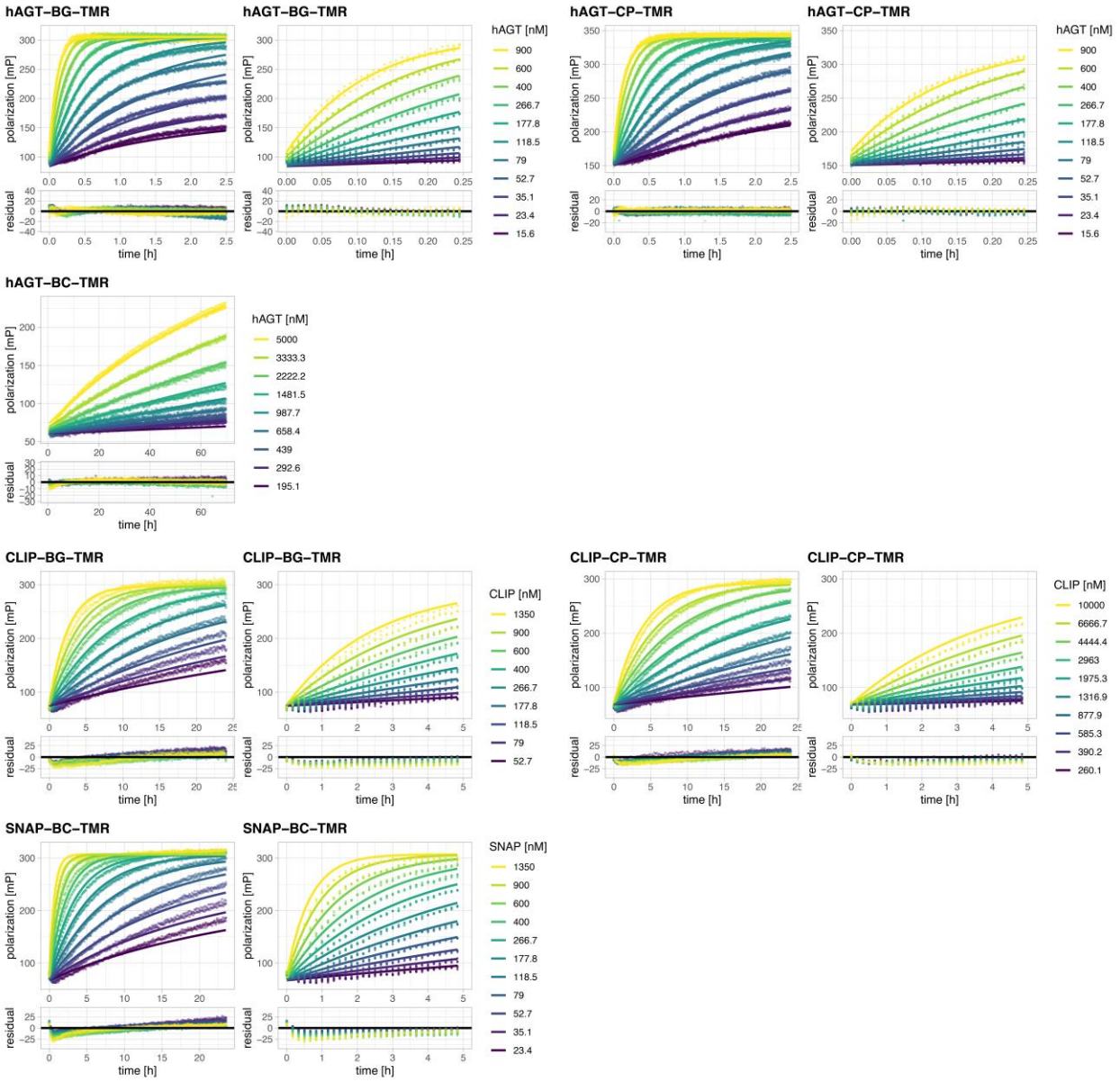

Figure S20: Labeling kinetics of hAGT, SNAP and CLIP with the non-respective BG-, CP- and BC-TMR substrates.

Full fluorescence polarization traces (points) and predications of fits based on model 1 along with zoom on the initial part (except for BC-TMR and hAGT) are represented on the top panels. Residuals from the fits are depicted in the bottom panels. Kinetics were recorded by following fluorescence polarization changes over time using a plate reader. Labeling was performed at different concentrations of hAGT, SNAP and CLIP proteins. Substrate concentrations were aimed at 20 nM based on the dyes extinction coefficient but fitted in the model since significant deviations from the expected stoichiometry were observed. For structures of BG, CP and BC substrates see **Fig. S1**.

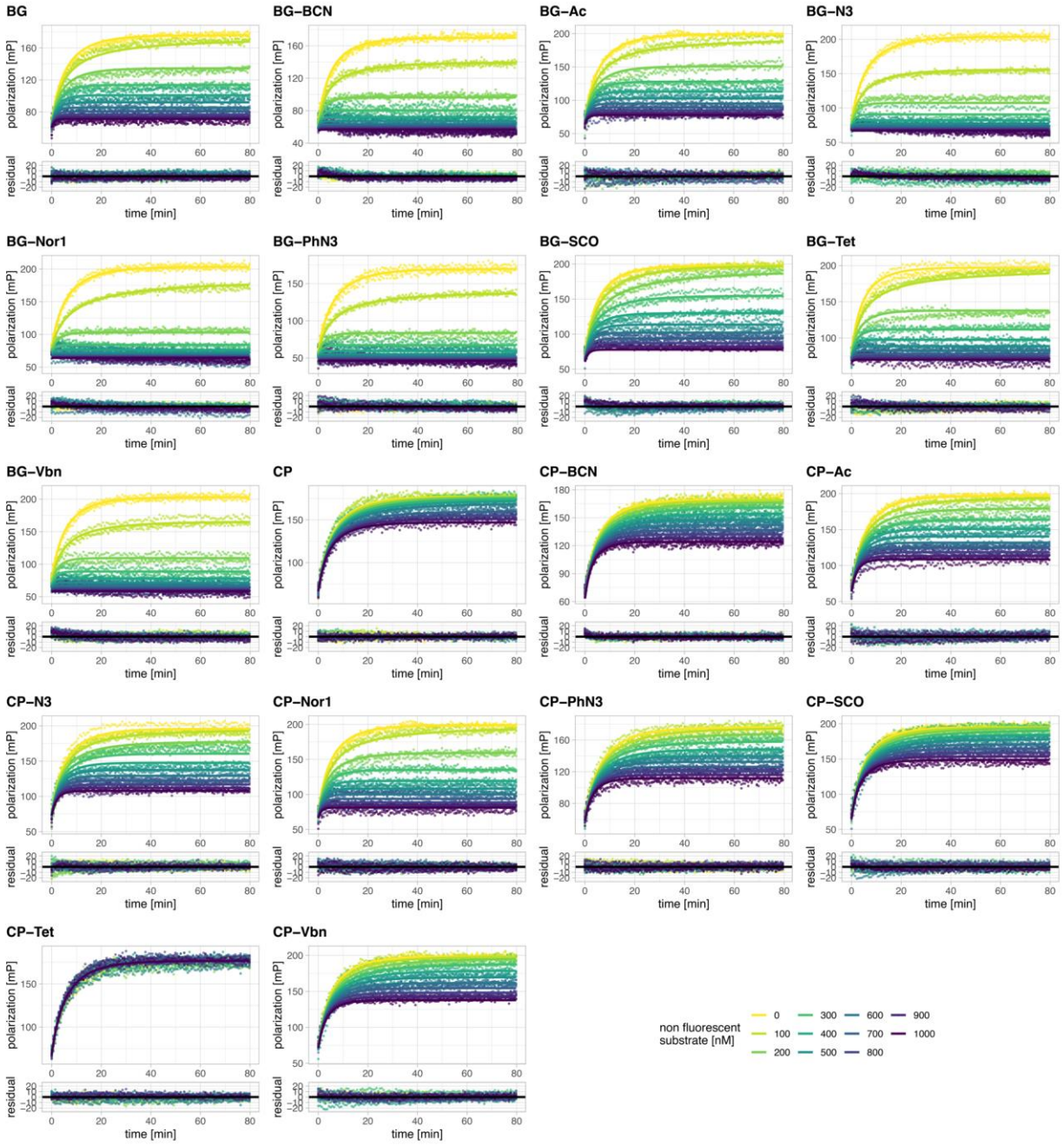

Figure S21: Labeling kinetics of SNAP with non-fluorescent BG and CP substrates.

Fluorescence polarization traces (points) of kinetic competition assays and predications of fits based on a simple competitive model (lines, see methods section for details) of SNAP labeling with BG-Alexa488 in the presence of different concentrations of non-fluorescent BG/CP substrates are represented on the top panels. Residuals from the fits are depicted in the bottom panels. Kinetics were recorded by following fluorescence polarization changes over time using a plate reader. For structures of BG and CP substrates see **Fig. S1.**

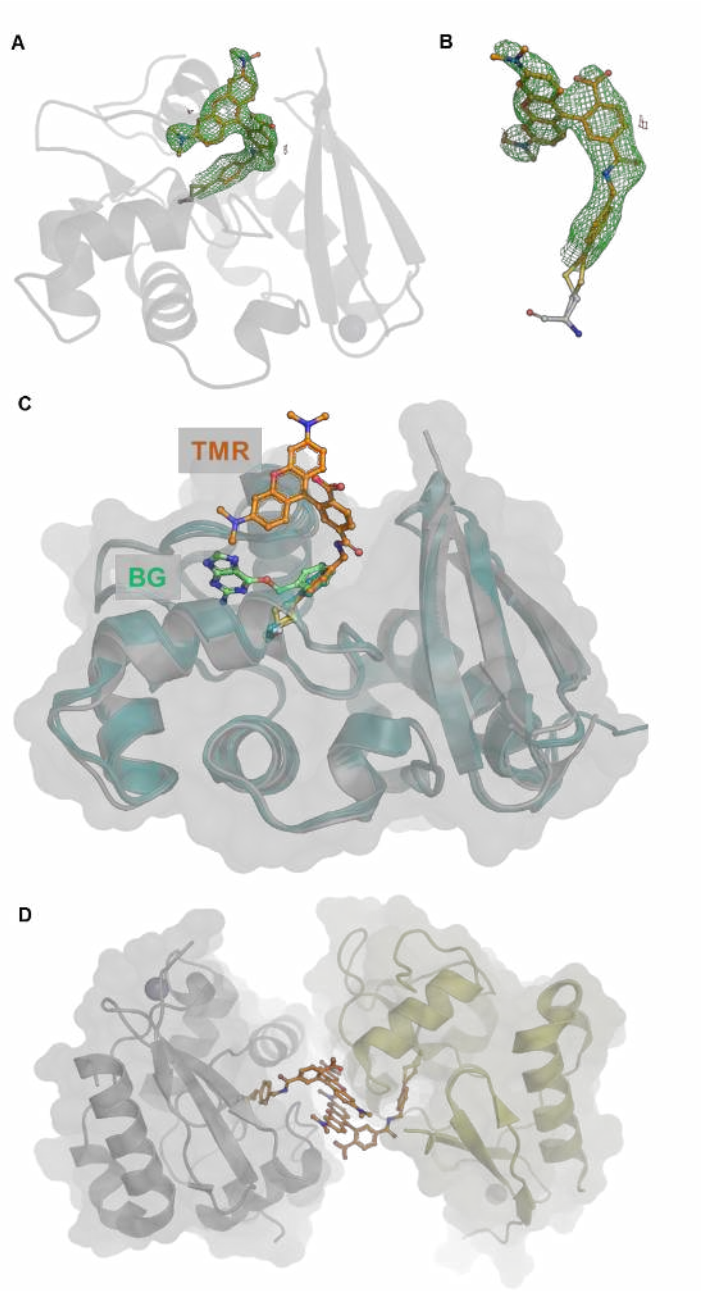

Figure S22: Validation and analysis of the SNAP-TMR X-ray structure.

A. Omit-map of the TMR ligand of the SNAP-TMR structure. The protein is represented as grey cartoon, TMR fluorophore-substrate as orange sticks and the catalytic cysteine as grey sticks. **B.** Zoom on the isolated labeled catalytic cysteine of SNAP-TMR. Omit-map contoured at 3 σ, represented as green and red mesh for missing and extra density, respectively. **C**. Comparison of the SNAP structure with available SNAP structures. SNAP-TMR is represented as previously explained. Apo SNAP (PDB ID 3KZY), benzylated SNAP PDB ID 3L00) and the BG bound dead mutant $SNAP^{C145A}$ (PDB ID 3KZZ) are represented as cartoon with different shades of blue-green. No major structural differences are observed with SNAP-TMR. **D.** Benzyl-TMR constraints by the crystal packing. Two monomers of SNAP-TMR are represented as grey and yellow cartoons. The conformation of the benzyl-TMR (orange sticks) of both monomers is constrained by the other monomer. Symmetry mates were generated within 4 Å radius and selected to highlight the packing constraints.

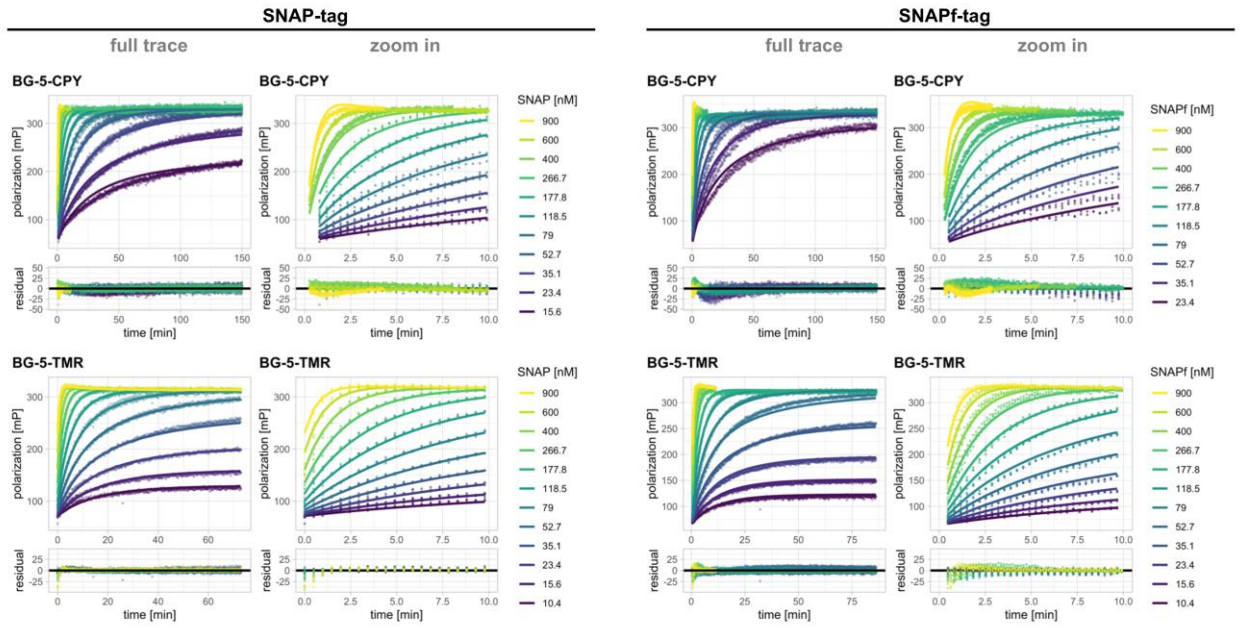

Figure S23: Labeling kinetics of SNAP and SNAPf with BG-5-TMR and BG-5-CPY.

Full fluorescence polarization traces (points) and predications of fits based on model 1.2 (lines) along with zoom on the initial 10 minutes are represented on the top panels. Residuals from the fits are depicted in the bottom panels. Kinetics were recorded by following fluorescence polarization changes over time using a plate reader. Labeling was performed at different concentrations of SNAP and SNAPf protein. Substrate concentrations were aimed at 20 nM based on the dyes extinction coefficient but fitted in the model since significant deviations from the expected stoichiometry were observed. For structures of BG substrates see **Fig. S1**.

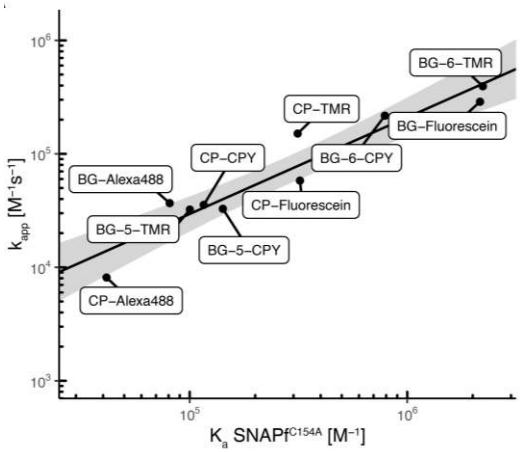

Figure S24: SNAPf kinetic and affinity correlations.

Correlation between SNAPf labeling kinetics (k_{app}) and affinity ($K_a = 1/K_d$) for different fluorophore substrates. Affinities were obtained with the catalytically dead mutant $SNAPf^{C145A}$. Log transformed values were fitted to a linear model (black line, $\log(k_{app}) = 0.2568 + \log(K_a) * 1.0697$, 95% confidence bands in grey, depicting the area in which the true regression line lies with 95% confidence). The linear correlation in logarithmic space suggests that the K_d of fluorescent SNAP substrates towards $SNAPf^{C145A}$ could represent a valid proxy to estimate their K_{app} towards native SNAPf.

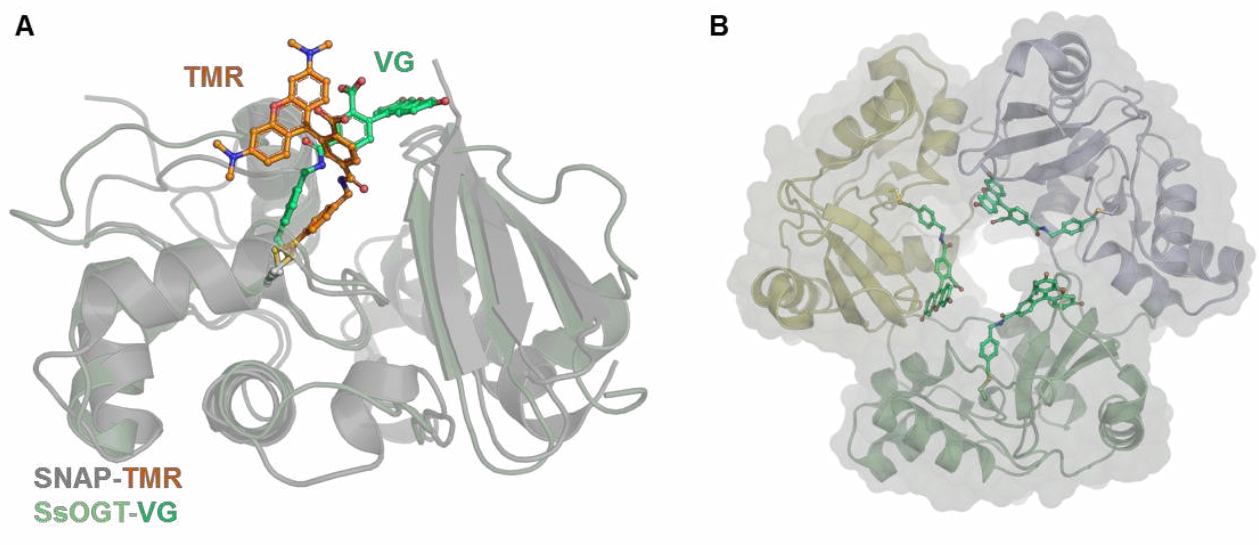

Figure S25: *Ss*OGT-H^5-VistaGreen alternative fluorophore conformation.

A. Structural alignment of SNAP-TMR with *Ss*OGT-H^5-VG structure (PDB ID 6GA0) (17). **B**. Benzyl-VG constraints by the crystal packing. Three monomers of *Ss*OGT-H^5-VG are represented as blue, green and yellow cartoons. The conformation of the benzyl-VG (green sticks) of all monomers is constrained by the neighboring monomer. Symmetry mates were generated within 4 Å radius and selected to highlight the packing constraints.

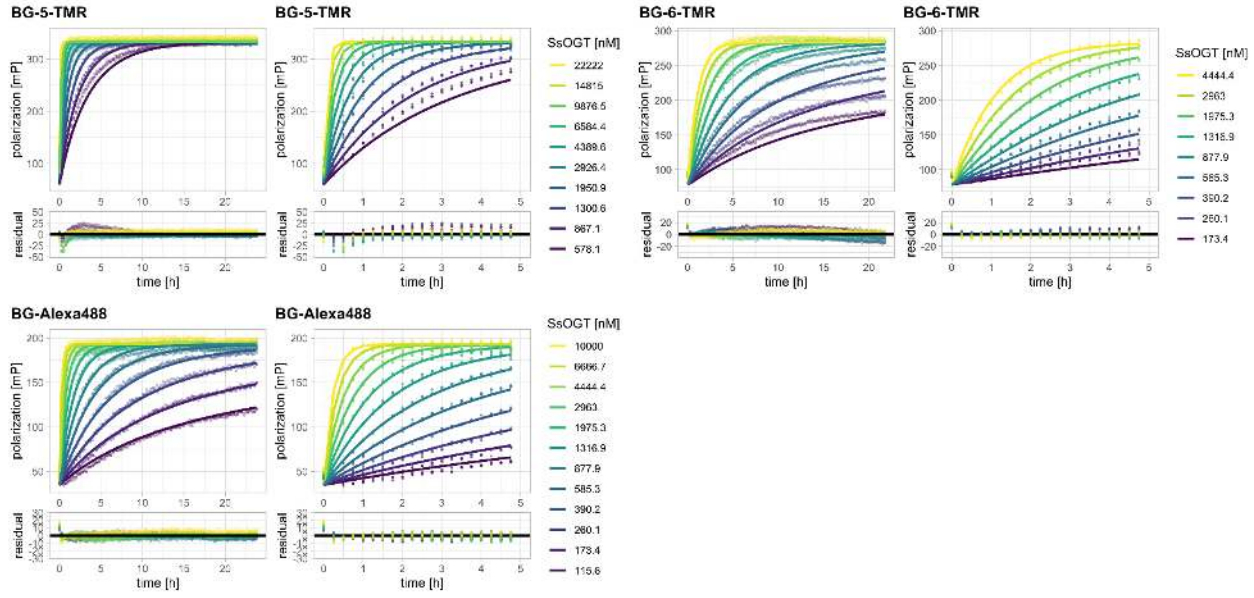

Figure S26: Labeling kinetics of *Ss*OGT-H^5 with BG-Alexa488 and BG-TMR.

Full fluorescence polarization traces (points) and predications of fits based on model 1 (lines) along with zoom on the initial 5 hours are represented on the top panels. Residuals from the fits are depicted in the bottom panels. Kinetics were recorded by following fluorescence polarization changes over time using a plate reader. Labeling was performed at different concentrations of *Ss*OGT-H^5 protein. Substrate concentrations were aimed at 20 nM based on the dyes extinction coefficient but fitted in the model since significant deviations from the expected stoichiometry were observed. For structures of BG substrates see **Fig. S1**.

Table S1: Kinetic parameters of HT7 labeling with fluorescent CA substrates.

Substrate	k_1 (± S.D.) [M^{-1} s^{-1}]	k_{-1} (± S.D.) [s^{-1}]	k_2 (± S.D.) [s^{-1}]	k_{app} (± S.D.) [M^{-1} s^{-1}]
CA-TMR	7.84 (± 0.76) × 10^7	2.56 (± 0.38) × 10^1	8.06 (± 0.29)	1.88 (± 0.01) × 10^7
CA-JF549	1.60 (± 0.16) × 10^8	9.83 (± 2.04) × 10^1	1.82 (± 0.07) × 10^1	1.66 (± 0.01) × 10^7
CA-JF669	2.35 (± 0.75) × 10^7	3.39 (± 1.49) × 10^1	6.94 (± 0.47)	4.03 (± 0.02) × 10^6
CA-CPY	1.6.7 (± 0.067) × 10^8	7.60 (± 0.98)	9.86 (± 0.73)	9.44 (± 0.18) × 10^7
CA-LIVE580	1.74 (± 0.05) × 10^8	1.75 (± 0.28)	6.77 (± 0.77)	1.39 (± 0.03) × 10^8
CA-TMR-biotin	3.69 (± 0.25) × 10^7	2.10 (± 0.25) × 10^1	8.24 (± 0.28)	1.04 (± 0.01) × 10^7

Data analyzed using model 2.

Table S2: Comparison k_{app} of HT7 labeling kinetics analyzed using models 1 and 2.

Substrate	k_{app} (± S.D.) [M^{-1} s^{-1}]	
	Model 1	Model 2
CA-TMR	1.79 (± 0.01) × 10^7	1.88 (± 0.01) × 10^7
CA-JF549	1.46 (± 0.01) × 10^7	1.66 (± 0.01) × 10^7
CA-JF669	3.95 (± 0.02) × 10^6	4.03 (± 0.02) × 10^6
CA-CPY	1.10 (± 0.02) × 10^8	9.44 (± 0.18) × 10^7
CA-LIVE580	1.58 (± 0.02) × 10^8	1.39 (± 0.03) × 10^8
CA-TMR-biotin	9.00 (± 0.04) × 10^6	1.04 (± 0.01) × 10^7

Table S3: Comparison of HT7 and HOB labeling kinetics with fluorescent CA substrates.

Protein	Substrate	k_1 (± S.D.) [M^{-1} s^{-1}]	k_{-1} (± S.D.) [s^{-1}]	k_2 (± S.D.) [s^{-1}]	k_{app} (± S.D.) [M^{-1} s^{-1}]
HT7	CA-TMR	7.84 (± 0.76) × 10^7	2.56 (± 0.38) × 10^1	8.06 (± 0.29)	1.88 (± 0.01) × 10^7
	CA-Alexa488	-	-	-	2.57 (± 0.01) × 10^4
HOB	CA-TMR	4.15 (± 0.26) × 10^7	1.83 (± 0.17) × 10^1	5.05 (± 0.13)	8.99 (± 0.04) × 10^6
	CA-Alexa488	-	-	-	8.04 (± 0.02) × 10^7

Table S4: Data collection and refinement statistics the X-ray crystal structures.

Data collections	**SNAP-TMR**	**HT7-TMR**	**HT7-CPY**	**HOB-TMR**
PDB ID	6Y8P	6Y7A	6Y7B	6ZCC
Beamline	ESRF ID29	PXII-X10SA, SLS	PXII-X10SA, SLS	PXII-X10SA, SLS
Wavelength (A°)	0.976	1.00001	1.00006	0.99984
Resolution (A°) **(last bin)**	36.88 - 2.3 (2.382 - 2.3)	50-1.40 (1.50-1.40)	50-3.10 (3.20-3.10)	50-1.50 (1.60-1.50)
Space group	$P3_221$	$P12_11$	$P321$	$P2_12_12_1$
Unit cell dimensions				
a (A°)	65.5148	44.00	161.27	52.21
b (A°)	65.5148	78.14	161.27	64.77
c (A°)	97.067	45.24	124.66	78.85
No. observed reflections	119190 (12210)	160637 (29978)	231609 (21528)	228695 (8515)
No. unique reflections	11152 (1087)	50448 (9451)	34294 (3081)	38699 (3579)
Completeness (%)	99.94 (100.00)	96.5 (97.1)	99.8 (99.9)	88.9 (47.5)
Rmerge	0.1015 (0.8636)	0.063 (0.410)	0.196 (0.596)	0.042 (0.241)
I/σ(I)	13.48 (2.82)	9.59 (2.83)	8.53 (3.10)	18.87 (2.39)
CC ½ (%)	99.9 (19.3)	99.7 (86.4)	98.8 (85.7)	99.9 (93.4)
Redundancy	10.7 (11.2)	3.18 (3.17)	6.75 (6.99)	5.91 (2.38)
Wilson B	47.75	21.39	37.99	32.28
Refinement statistics				
Resolution range (A)	36.88-2.3	39.19-1.40	49.32-3.10	43.53-1.52
No. Reflections	8878	50435	34290	38697
Rwork (%)	0.2385	0.1558	0.2074	0.1887
Rfree (%)	0.2694	0.1868	0.2594	0.2238
No. protein atoms	1231	2397	11750	2348
No. water atoms	50	348	0	312
No. ligand atoms	45	51	235	52
Average B factor (A°2)	73.06	18.93	51.23	31.74
RMSD from ideal				
Bond lengths (A°)	0.007	0.013	0.004	0.009
Bond angles (°)	1.24	1.247	0.788	1.014

Table S5: Kinetic parameters of SNAP and CLIP labeling with fluorescent substrates analyzed using model 1.2.

Substrate	k_{app} (± S.D.) [$s^{-1}M^{-1}$]	k_3 (± S.D.) [s^{-1}]	k_{app} (± S.D.) [$s^{-1}M^{-1}$]	k_3 (± S.D.) [s^{-1}]
SNAP CP-Fluorescein	1.42 (± 0.01) × 10^4	1.61 (± 0.04) × 10^{-3}	-	-
SNAP CP-CPY	1.59 (± 0.01) × 10^4	1.26 (± 0.01) × 10^{-2}	3.55 (± 0.02) × 10^4	6.22 (± 0.13) × 10^{-3}
CLIP BC-CPY	1.26 (± 0.01) × 10^4	2.16 (± 0.09) × 10^{-4}	2.65 (± 0.01) × 10^4	9.02 (± 0.48) × 10^{-7}

Table S6: Kinetic parameters of SNAP labeling with TMR substrates measured via stopped flow.

Substrate	k_1 (± S.D.) [M^{-1} s^{-1}]	k_{-1} (± S.D.) [s^{-1}]	k_2 (± S.D.) [s^{-1}]	k_{app} (± S.D.) [M^{-1} s^{-1}]
BG-TMR	4.93 (± 0.04) × 10^5	1.02 (± 0.03)	1.24 (± 0.02)	2.71 (± 0.01) × 10^5
CP-TMR	5.36 (± 0.30) × 10^5	8.96 (± 0.71)	1.58 (± 0.04)	0.81 (± 0.01) × 10^5

Data analyzed using model 2

Table S7: Comparison of SNAP/CLIP with SNAPf/CLIPf labeling kinetics with fluorescent substrates.

Substrate		k_{app} (± S.D.) [$s^{-1}M^{-1}$]	
		Original	Fast variant
SNAP BG substrates	BG-Alexa488	1.22 (± 0.01) × 10^4	3.68 (± 0.64) × 10^4
	BG-Fluorescein	1.17 (± 0.01) × 10^5	2.88 (± 0.01) × 10^5
	BG-CPY	2.17 (± 0.01) × 10^5	2.17 (± 0.02) × 10^5
	BG-TMR	4.29 (± 0.01) × 10^5	3.94 (± 0.01) × 10^5
SNAP CP substrates	CP-Alexa488	3.12 (± 0.003) × 10^3	8.13 (± 0.01) × 10^3
	CP-Fluorescein	1.42 (± 0.01) × 10^4 (*)	5.81 (± 0.01) × 10^4
	CP-CPY*	1.59 (± 0.01) × 10^4 (*)	3.55 (± 0.02) × 10^4 (*)
	CP-TMR	7.69 (± 0.01) × 10^4	1.51 (± 0.01) × 10^5
CLIP BC substrates	BC-Alexa488	1.26 (± 0.01) × 10^3	3.10 (±0.02) × 10^3
	BC-Fluorescein	4.36 (± 0.01) × 10^3	1.62 (± 0.01) × 10^4
	BC-TMR	1.85 (± 0.01) × 10^4	3.37 (± 0.01) × 10^4
	BC-CPY*	1.26 (± 0.01) × 10^4 (*)	2.65 (± 0.01) × 10^4 (*)

Data analyzed using model 1 or 1.2 (*) which included an additional phase (see Table S5).

Table S8: Comparison of SNAP labeling kinetics with 5- and 6-fluorophores.

Substrate	SNAP		SNAPf	
	k_{app} (± S.D.) [$s^{-1}M^{-1}$]	k_3 (± S.D.) [s^{-1}]	k_{app} (± S.D.) [$s^{-1}M^{-1}$]	k_3 (± S.D.) [s^{-1}]
BG-6-TMR	4.29 (± 0.01) × 10^5	-	3.94 (± 0.01) × 10^5	-
BG-5-TMR (*)	2.67 (± 0.01) x 10^4	1.53 (± 0.12) x 10^{-3}	3.23 (± 0.01) x 10^4	2.18 (± 0.18) x 10^{-3}
BG-6-CPY	2.17 (± 0.01) × 10^5	-	2.17 (± 0.02) × 10^5	-
BG-5-CPY (*)	2.51(± 0.01) x 10^4	2.11 (± 0.04) x 10^{-2}	3.28 (± 0.01) x 10^4	1.42 (± 0.03) x 10^{-2}

Data analyzed using model 1 or 1.2 (*) which included an additional phase.

Table S9: Kinetic parameters of *Ss*OGT-H[5] labeling.

Substrate	k_{app} (± S.D.) [$s^{-1}M^{-1}$]
BG-6-TMR	6.78 (± 0.67) x 10^1
BG-5-TMR	1.45 (± 0.92) x 10^2
BG-6-Alexa488	1.24 (± 0.01) x 10^2

Data analyzed using model 1.

Protein sequences:

General color code: Hisx10-tag – TEV cleavage site – Protein sequence – **Fast mutation** – **Catalytic residue**

>HT7

MHHHHHHHHHHENLYFQ|GIGTGFPFDPHYVEVLGERMHYVDVGPRDGTPVLFLHGNPTSSYVWRNIIPHVAPTHRCIAPDLIGMGKS
DKPDLGYFFDDHVRFMDAFIEALGLEEVVLVIH**D**WGSALGFHWAKRNPERVKGIAFMEFIRPIPTWDEWPEFARETFQAFRTTDVGRK
LIIDQNVFIEGTLPMGVVRPLTEVEMDHYREPFLNPVDREPLWRFPNELPIAGEPANIVALVEEYMDWLHQSPVPKLLFWGTPGVLIPP
AEAARLAKSLPNCKAVDIGPGLNLLQEDNPDLIGSEIARWLSTLEI

>HOB

MHHHHHHHHHHENLYFQ|GIGTGFPFDPHYVEVLGERMHYVDVGPRDGTPVLFLHGNPTSSYVWRNIIPHVAPTHRCIAPDLIGMGKS
DKPDLGYFFDDHVRFMDAFIEALGLEEVVLVIH**D**WGSALGFHWAKRNPERVKGIAFMEFIRPIPTWDEWP**K**FAR**K**TFQAFRT**KK**VGR
KLIIDQNVFIEGTLPMGVVRPLTEVEMDHYREPFLNPVDREPLWRFPNELPIAGEPANIVALVEEYMDWLHQSPVPKLLFWGTPGVLIP
PAEAARLAKSLPNCKAVDIGPGLNLLQEDNPDLIGSEIARWLSTLEISG

Color code: **mutations as compared to HT7**

>SNAP

MHHHHHHHHHHENLYFQ|GMDKDCEMKRTTLDSPLGKLELSGCEQGLHEIIFLGKGTSAADAVEVPAPAAVLGGPEPLMQATAWLNA
YFHQPEAIEEFPVPALHHPVFQQESFTRQVLWKLLKVVKFGEVISYSHLAALAGNPAATAAVKTALSGNPVPILIP**C**HRVVQGDLDVGG
YEGGLAVKEWLLAHEGHRLGKPGLG

>SNAPf

MHHHHHHHHHHENLYFQ|GMDKDCEMKRTTLDSPLGKLELSGCEQGLH**R**IIFLGKGTSAADAVEVPAPAAVLGGPEPLMQATAWLNA
YFHQPEAIEEFPVPALHHPVFQQESFTRQVLWKLLKVVKFGEVISYSHLAALAGNPAATAAVKTALSGNPVPILIP**C**HRVVQGDLDVGG
YEGGLAVKEWLLAHEGHRLGKPGLG

>SNAP^{cx}

MHHHHHHHHHHENLYFQ|GDCEMKRTTLDSPLGKLELSGCEQGLHEIIFLGKGTSAADAVEVPAPAAVLGGPEPLMQATAWLNAYFH
QPEAIEEFPVPALHHPVFQQESFTRQVLWKLLKVVKFGEVISYSHLAALAGNPAATAAVKTALSGNPVPILIP**C**HRVVQGDLDVGGYEG
GLAVKEWLLAHEGHRLGKR

>CLIP

MHHHHHHHHHHENLYFQ|GMDKDCEMKRTTLDSPLGKLELSGCEQGLHEIIFLGKGTSAADAVEVPAPAAVLGGPEPLIQATAWLNAY
FHQPEAIEEFPVPALHHPVFQQESFTRQVLWKLLKVVKFGEVISESHLAALVGNPAATAAVNTALDGNPVPILIP**C**HRVVQGDSDVGPY
LGGLAVKEWLLAHEGHRLGKPGLGG

>CLIPf

MHHHHHHHHHHENLYFQ|GMDKDCEMKRTTLDSPLGKLELSGCEQGLH**R**IIFLGKGTSAADAVEVPAPAAVLGGPEPLIQATAWLNA
YFHQPEAIEEFPVPALHHPVFQQESFTRQVLWKLLKVVKFGEVISESHLAALVGNPAATAAVNTALDGNPVPILIP**C**HRVVQGDSDVGP
YLGGLAVKEWLLAHEGHRLGKPGLGG

>hAGT

*MAS*WSHPQFEK*GA*DDDDK*VPH*MDKDCEMKRTTLDSPLGKLELSGCEQGLHEIKLLGKGTSAADAVEVPAPAAVLGGPEPLMQCTA
WLNAYFHQPEAIEEFPVPALHHPVFQQESFTRQVLWKLLKVVKFGEVISYQQLAALAGNPKAARAVGGAMRGNPVPILIPCHRVVCSS
GAVGNYSGGLAVKEWLLAHEGHRLGKPGLGGSSGLAGAWLKGAGATSGSPPAGRN*APGFSSISA*HHHHHHHHHH

Color code: Strep-Tag II, Enterokinase cleavage site, *linkers*

1 >*Ss*OGT-H[5]

2 *MAS*WSHPQFEK*GA*DDDDK*VPH*MLVYGLYKSPLGYITVAKDDKGFIMLDFCDCVEGNSRDDSSFTEFFHKLDLYFEGKPINLREPINLK

3 TYPFRLSVFKEVMKIPWGKVMTYKQIADSLGTAPAAVKTALSENPILLIIPCHRVIAENGIGGYERGVKLKRALLELEGVKIPEL*APGFSSI*

4 *SA*HHHHHHHHHH

5 Color code: Strep-Tag II, Enterokinase cleavage site, *linkers*

Example DynaFit scripts:

HT7 stopped flow labeling kinetics model 2

```
[task]
   data  = progress
   task  = fit
   confidence  = monte-carlo

[mechanism]
   P + S <===> P.S       :   k1   k-1
   P.S ----> Z           :   k2

[constants]  ; units: uM, sec
   k1   = 10 ?
   k-1  = 10 ?
   k2   = 10 ?

[parameters]
   R    = 0.2 ?

[data]
   Delay       0.022
   offset      0.0262
   directory   path/to/data
   sheet       data.csv
   column 6   | conc P =   1     | conc S =   1     | response Z = 1     * R  |
response P.S = 1     * R |  label c=1
   column 5   | conc P =   0.75  | conc S =   0.75  | response Z = 1.333 * R  |
response P.S = 1.333 * R |  label c=0.75
   column 4   | conc P =   0.5   | conc S =   0.5   | response Z = 2     * R  |
response P.S = 2     * R |  label c=0.5
   column 3   | conc P =   0.25  | conc S =   0.25  | response Z = 4     * R  |
response P.S = 4     * R |  label c=0.25
   column 2   | conc P =   0.1   | conc S =   0.1   | response Z = 10    * R  |
response P.S = 10    * R |  label c=0.1

[output]
   directory path/to/output/folder

[settings]
   {ConfidenceIntervals}
      LevelPercent = 95
   {Output}
      XAxisLabel = time [s]
      YAxisLabel = anisotropy

[end]
```

SNAP stopped flow labeling kinetics model 2

```
[task]
   data  = progress
   task  = fit
   confidence  = monte-carlo

[mechanism]
   P + S <===> P.S       :   k1   k-1
   P.S ----> Z           :   k2

[constants]  ; units: uM, sec
   k1   = 1 ?
   k-1  = 1 ?
   k2   = 1 ?

[concentrations]  ; units: uM
   S    = 2 ?

[responses]
   Z    = 0.07 ?
   P.S  = 1 * Z

[data]
   delay       0.022
   offset      0
   directory   path/to/data
   sheet       data.csv
   column  2   | conc P =   50     | label c=50
   column  3   | conc P =   37.5   | label c=37.5
   column  4   | conc P =   25     | label c=25
   column  5   | conc P =   12.5   | label c=12.5
   column  6   | conc P =   5      | label c=5
   column  7   | conc P =   2.5    | label c=2.5
   column  8   | conc P =   1.25   | label c=1.25

[output]
   directory  path/to/output/folder

[settings]
   {ConfidenceIntervals}
      LevelPercent  = 95
   {Output}
      XAxisLabel = time [s]
      YAxisLabel = anisotropy

[end]
```

HT7 microplate reader labeling kinetics model 1

(Time series of each condition were not averaged before DynaFit analysis since the TECAN plate reader has small inconsistencies in measurement intervals)

```
[task]
   data  = progress
   task  = fit
   confidence  = monte-carlo

[mechanism]
   P + S ----> Z     :   k_app

[constants]  ; units: uM, sec
   k_app = 1 ?

[concentrations]  ; units: uM
   S   = 0.05

[responses]
   Z   = 4000 ?

[data]
   delay      1
   offset     87.118
   directory  path/to/data
   sheet      data.csv

   column  2 |  conc P =  0     |  label 0
   column  3 |  conc P =  0     |  label 0
   column  4 |  conc P =  0     |  label 0

   column  5 |  conc P =  0.4   |  label 400
   column  6 |  conc P =  0.4   |  label 400
   column  7 |  conc P =  0.4   |  label 400

   column  8 |  conc P =  0.8   |  label 800
   column  9 |  conc P =  0.8   |  label 800
   column 10 |  conc P =  0.8   |  label 800

   column 11 |  conc P =  1.6   |  label 1600
   column 12 |  conc P =  1.6   |  label 1600
   column 13 |  conc P =  1.6   |  label 1600

   column 14 |  conc P =  3.2   |  label 3200
   column 15 |  conc P =  3.2   |  label 3200
   column 16 |  conc P =  3.2   |  label 3200

   column 17 |  conc P =  6.4   |  label 6400
   column 18 |  conc P =  6.4   |  label 6400
   column 19 |  conc P =  6.4   |  label 6400

   column 20 |  conc P =  12.8  |  label 12800
   column 21 |  conc P =  12.8  |  label 12800
   column 22 |  conc P =  12.8  |  label 12800

   column 23 |  conc P =  25.6  |  label 25600
   column 24 |  conc P =  25.6  |  label 25600
   column 25 |  conc P =  25.6  |  label 25600

   column 26 |  conc P =  51.2  |  label 51200
   column 27 |  conc P =  51.2  |  label 51200
   column 28 |  conc P =  51.2  |  label 51200

[output]
   directory  path/to/output/folder

[settings]
   {ConfidenceIntervals}
      LevelPercent  = 95
   {Output}
      XAxisLabel = time [s]
      YAxisLabel = anisotropy

[end]
```

SNAP-/CLIP microplate reader labeling kinetics model 1

(Time series of each condition were not averaged before DynaFit analysis since the TECAN plate reader has small inconsistencies in measurement intervals)

```
[task]
   data  = progress
   task  = fit
   confidence  = monte-carlo

[mechanism]
   P + S ----> Z        :  k_app

[constants]  ; units: nM, sec
   k_app = 0.0001  ?

[concentrations]  ; units: nM
   S = 50  ?

[responses]
   Z = 2  ?

[data]
   delay      2.7
   offset     73.46
   directory  path/to/data
   sheet      data.csv

   column  2  | conc P =  52     | label 52
   column  3  | conc P =  52     | label 52
   column  4  | conc P =  52     | label 52

   column  5  | conc P =  79     | label 79
   column  6  | conc P =  79     | label 79
   column  7  | conc P =  79     | label 79

   column  8  | conc P =  118.5  | label 118.5
   column  9  | conc P =  118.5  | label 118.5
   column 10  | conc P =  118.5  | label 118.5

   column 11  | conc P =  177.7  | label 177.7
   column 12  | conc P =  177.7  | label 177.7
   column 13  | conc P =  177.7  | label 177.7

   column 14  | conc P =  266.6  | label 266.6
   column 15  | conc P =  266.6  | label 266.6
   column 16  | conc P =  266.6  | label 266.6

   column 17  | conc P =  400    | label 400
   column 18  | conc P =  400    | label 400
   column 19  | conc P =  400    | label 400

   column 20  | conc P =  600    | label 600
   column 21  | conc P =  600    | label 600
   column 22  | conc P =  600    | label 600

   column 23  | conc P =  900    | label 900
   column 24  | conc P =  900    | label 900
   column 25  | conc P =  900    | label 900

[output]
  directory  path/to/output/folder

[settings]
   {ConfidenceIntervals}
      LevelPercent  = 95
   {Output}
      XAxisLabel = time [s]
      YAxisLabel = anisotropy

[end]
```

SNAP-/CLIP microplate reader labeling kinetics model 1.2

(Time series of each condition were not averaged before DynaFit analysis since the TECAN plate reader has small inconsistencies in measurement intervals)

```
[task]
   data  = progress
   task  = fit
   confidence  = monte-carlo

[mechanism]
   P + S ----> Z        :  k_app
   Z     ----> Z2       :  k_app_2

[constants]  ; units: nM, sec
   k_app   = 0.0001 ?
   k_app_2 = 0.0001 ?

[concentrations]  ; units: nM
   S = 50 ?

[responses]
   Z  = 2 ?
   Z2 = 2 ?

[data]
   delay       2.7
   offset      73.46
   directory   path/to/data
   sheet       data.csv

   column  2   | conc P =  52      | label 52
   column  3   | conc P =  52      | label 52
   column  4   | conc P =  52      | label 52

   column  5   | conc P =  79      | label 79
   column  6   | conc P =  79      | label 79
   column  7   | conc P =  79      | label 79

   column  8   | conc P =  118.5   | label 118.5
   column  9   | conc P =  118.5   | label 118.5
   column 10   | conc P =  118.5   | label 118.5

   column 11   | conc P =  177.7   | label 177.7
   column 12   | conc P =  177.7   | label 177.7
   column 13   | conc P =  177.7   | label 177.7

   column 14   | conc P =  266.6   | label 266.6
   column 15   | conc P =  266.6   | label 266.6
   column 16   | conc P =  266.6   | label 266.6

   column 17   | conc P =  400     | label 400
   column 18   | conc P =  400     | label 400
   column 19   | conc P =  400     | label 400

   column 20   | conc P =  600     | label 600
   column 21   | conc P =  600     | label 600
   column 22   | conc P =  600     | label 600

   column 23   | conc P =  900     | label 900
   column 24   | conc P =  900     | label 900
   column 25   | conc P =  900     | label 900

[output]
  directory  path/to/output/folder

[settings]
   {ConfidenceIntervals}
      LevelPercent  = 95
   {Output}
      XAxisLabel = time [s]
      YAxisLabel = anisotropy

[end]
```

References:

1. Butkevich AN, Mitronova GY, Sidenstein SC, Klocke JL, Kamin D, Meineke DN, et al. Fluorescent Rhodamines and Fluorogenic Carbopyronines for Super-Resolution STED Microscopy in Living Cells. Angew Chem Int Ed Engl. 2016;55(10):3290-4.
2. Mudd G, Pi IP, Fethers N, Dodd PG, Barbeau OR, Auer M. A general synthetic route to isomerically pure functionalized rhodamine dyes. Methods and Applications in Fluorescence. 2015;3(4).
3. Ueno Y, Jose J, Loudet A, Pérez-Bolívar Cs, Anzenbacher P, Burgess K. Encapsulated Energy-Transfer Cassettes with Extremely Well Resolved Fluorescent Outputs. Journal of the American Chemical Society. 2011;133(1):51-5.
4. Lukinavicius G, Umezawa K, Olivier N, Honigmann A, Yang G, Plass T, et al. A near-infrared fluorophore for live-cell super-resolution microscopy of cellular proteins. Nat Chem. 2013;5(2):132-9.
5. Wang L, Tran M, D'Este E, Roberti J, Koch B, Xue L, et al. A general strategy to develop cell permeable and fluorogenic probes for multicolour nanoscopy. Nat Chem. 2020;12(2):165-72.
6. Keppler A, Gendreizig S, Gronemeyer T, Pick H, Vogel H, Johnsson K. A general method for the covalent labeling of fusion proteins with small molecules in vivo. Nature biotechnology. 2003;21(1):86-9.
7. Srikun D, Albers AE, Nam CI, Iavarone AT, Chang CJ. Organelle-Targetable Fluorescent Probes for Imaging Hydrogen Peroxide in Living Cells via SNAP-Tag Protein Labeling. Journal of the American Chemical Society. 2010;132(12):4455-65.
8. Keppler A, Pick H, Arrivoli C, Vogel H, Johnsson K. Labeling of fusion proteins with synthetic fluorophores in live cells. Proceedings of the National Academy of Sciences. 2004;101(27):9955-9.
9. Correa I, Baker B, Zhang A, Sun L, Provost C, Lukinavic.ius Gz, et al. Substrates for Improved Live-Cell Fluorescence Labeling of SNAP-tag. Current Pharmaceutical Design. 2013;19(30):5414-20.
10. Hiblot J, Yu Q, Sabbadini MDB, Reymond L, Xue L, Schena A, et al. Luciferases with Tunable Emission Wavelengths. Angew Chem Int Ed Engl. 2017;56(46):14556-60.
11. Grimm JB, English BP, Chen J, Slaughter JP, Zhang Z, Revyakin A, et al. A general method to improve fluorophores for live-cell and single-molecule microscopy. Nat Methods. 2015;12(3):244-50, 3 p following 50.
12. Gautier A, Juillerat A, Heinis C, Correa IR, Jr., Kindermann M, Beaufils F, et al. An engineered protein tag for multiprotein labeling in living cells. Chem Biol. 2008;15(2):128-36.
13. Bottanelli F, Kromann EB, Allgeyer ES, Erdmann RS, Wood Baguley S, Sirinakis G, et al. Two-colour live-cell nanoscale imaging of intracellular targets. Nature communications. 2016;7(1).
14. Zhang Y, So M-k, Loening AM, Yao H, Gambhir SS, Rao J. HaloTag Protein-Mediated Site-Specific Conjugation of Bioluminescent Proteins to Quantum Dots. Angewandte Chemie International Edition. 2006;45(30):4936-40.
15. Masharina A, Reymond L, Maurel D, Umezawa K, Johnsson K. A fluorescent sensor for GABA and synthetic GABA(B) receptor ligands. Journal of the American Chemical Society. 2012;134(46):19026-34.
16. Deo C, Abdelfattah AS, Bhargava HK, Berro AJ, Falco N, Farrants H, et al. The HaloTag as a general scaffold for far-red tunable chemigenetic indicators. Nature chemical biology. 2021.
17. Rossi F, Morrone C, Massarotti A, Ferraris DM, Valenti A, Perugino G, et al. Crystal structure of a thermophilic O6-alkylguanine-DNA alkyltransferase-derived self-labeling protein-tag in covalent complex with a fluorescent probe. Biochemical and Biophysical Research Communications. 2018;500(3):698-703.